Magnus Skinlo Thomassen

Hydrogen–Chlorine Fuel Cell for Production of Hydrochloric Acid and Electric Power

Chlorine Kinetics and Cell Design

Thesis submitted for
the degree of doktor ingeniør

Trondheim, May 2005

Norwegian University of Science and Technology
Faculty of Natural Sciences and Technology
Department of Materials Technology

NTNU
Innovation and Creativity

IMT-report 2005:70

Acknowledgements

I would like to thank professor Reidar Tunold and associate professor Børre Børresen for inspiering me to take on the the challenge that led to this thesis. You have been a good source of motivation and help throughout my PhD study and always had time for discussions and consultations. I would also like to thank Dr. Steffen Møller-Holst for giving me the opportunity to work other interesting activities such as arranging national hydrogen symposia. You are all my ideals, each in your own way.

Professor Keith Scott, Christopher Jackson, Georgios "Aris" Vlachogiannopoulos, Stephen Pilditch, Dave Hall and all my other friends at the School of Chemical Engineering and Advanced Materials at the University of Newcastle upon Tyne for taking so good care of me during my 8 month stay in 2003. I had a super time and look back on it with fond memories.

I would further like to thank all my colleagues at NTNU and SINTEF working with electrochemical energy technology and all the other people at the Electrochemistry group for the excellent working environment. A special thanks to Martha Bjerknes and Kjell Røkke for all the help with day to day administrative and practical tasks, allowing me to focus on my research. I also had the pleasure of having M.Sc. student Camilla Karlsen working with me on this project, contributing to the experimental work.

The Research Council of Norway (NFR) and Norsk Hydro ASA funded my work at NTNU. Professor Reidar Tunold, Associate professor Børre Børresen and Dr. Steffen Møller-Holst deserves recognition together with representatives from NFR and Norsk Hydro for initiating and starting the project.

To my friends, especially Sigmund Brabrand, Andreas Evensen, Tore Halvorsen and David Lockert Lie. As you probably have discovered, embarking on a PhD makes it hard to separate work and spare time. Especially in the latter phases,

when it seems as if the PhD has an inate ability to become the predominant factor in ones life. Thank you for helping me remember the life outside the office and showing understanding for my periodical absent behaviour.

One beautiful summer day in 2003, in Reykjavik, Iceland of all places, I met the most wonderfull person in the world. Since Maria entered my life she has been a perfect life companion, broadening my view on life and offering support, comfort and understanding. I am looking forward to our future together.

Finally, I would like to thank my parents for always being there for me and for giving me an excellent learning-environment in my early days. Thank you for supporting me in my choices and for the warmth you always have given me.

Summary

This thesis work is the continuation and final part of a joint project between the Department of Materials Technology, NTNU and Norsk Hydro Research Center in Porsgrunn, looking at the possibility of using fuel cells for production of hydrogen chloride and electric power. The experimental work encompass an evaluation of three hydrogen - chlorine fuel cell design concepts, development and implementation of a mathematical fuel cell model and a kinetic study of the chlorine reduction reaction.

The evaluated fuel cell designs consisted of *a)* a conventional PEM fuel cell applying a Nafion membrane, *b)* a composite system applying an aqueous HCl electrolyte and Nafion membrane and *c)* a phosphoric acid doped PBI membrane fuel cell operating at intermediate temperatures of 150 - 175 °C. From the evaluation it was found that the chlorine reduction kinetics are much faster than the corresponding oxygen reduction reaction, leading to low activation losses on the fuel cell cathode. However, the nature of the reactant, chlorine, and the product, HCl, places strict demands on the corrosion resistance of the construction materials and drastically increases the difficulties related to water management in the cells. Due to these effects, none of the investigated systems were able to demonstrate stable operation under the conditions used in this study. The PBI cell showed best potential and seems to be the system in which the humidification and corrosion difficulties easiest can be remedied. The first design criteria for such a system should be the minimisation of the existence of liquid water, ideally a hydrogen - chlorine fuel cell system should operate in totally water free environment and consist of a high temperature proton conductor.

A two dimensional, isothermal mathematical model of a hydrogen - chlorine single fuel cell with an aqueous HCl electrolyte is presented. The model focuses on the electrode reactions in the chlorine cathode and also includes the

mass and momentum balances for the electrolyte and cathode gas diffusion layer. There is good agreement between the model predictions and experimental results. Distributions of physical parameters such as reactant and product concentrations, solution and solid phase potentials and local current densities and overpotentials as a function of cell voltage are presented. Effects of varying the initial electrolyte concentration and operating pressure are analysed. It was found that an electrolyte inlet concentration of 6 mol dm^{-3} gave the best cell performance and that an increase of operating pressure gave a steady increase of the fuel cell performance.

The rate and mechanism of the electroreduction of chlorine on electrochemically oxidised Pt and Ru electrodes has been investigated relative to the state of oxide formation. Current/potential curves for the reduction process in 1 mol dm^{-3} HCl solution saturated with Cl$_2$ have been obtained for electrode surfaces in various states of preoxidation with the use of the rotating disc electrode technique (RDE). In the case of chlorine reduction on platinum, the results indicate that adsorption of chlorine molecules with a subsequent rate determining electrochemical adsorption step is the dominant mechanism. The exchange current density seems to decrease linearly with the logarithm of the amount of surface oxide.

Chlorine reduction on ruthenium is best described by a Heyrovsky-Volmer mechanism with the first charge transfer reaction as the rate determining step. The Krishtalik mechanism incorporating adsorbed O$^{\bullet}$Cl^{+} intermediates is also able to describe the reaction successfully. The reaction order is constant for all oxide coverages while the exchange current density apparently moves through a maximum at intermediate oxide coverages ($\sim$100 mC cm^{-2}). The results show that the electrocatalysis of the cathodic reduction of chlorine is very sensitive to the state of the oxidation of the electrode surface.

The rate and mechanism of the electroreduction of chlorine on electrooxidised ruthenium has further been investigated with focus on the effect of solution pH. Current/potential curves for the reduction process in solutions with constant chloride concentration of 1.0 mol dm^{-3} and varying H^{+} concentration have been obtained with the use of the rotating disk electrode technique (RDE). It was found that the chlorine reduction rate is highly inhibited in solutions with high H^{+} concentrations and that it can be satisfactorily described by the Erenburgh mechanism, previously suggested for the chlorine evolution on RuO$_2$ and ruthenium titanium oxides (RTO). The expression of the kinetic current as a function of chlorine and H^{+} concentration was obtained by solving the elementary rate equations of the kinetic mechanism. The kinetic constants obtained

from the correlation of the kinetic current expression to the experimental data were used to simulate the dependence of the surface coverages and elementary reaction rates on overpotential.

Contents

List of Figures

List of Tables

Nomenclature

Roman Letters

A_{cat}	Catalyst surface area	$cm^2\,g^{-1}$
A	Electrode Area	cm^2
a^g	Specific area of the gas-electrolyte interface	$cm^2\,cm^{-3}$
a_i^A	Activity of species i, adsorbed on electrode surface	
a_i^b	Activity of species i, in bulk solution	
B	Factor in Eq. (6.16)	
C_i	Concentration of species i	$mol\,dm^{-3}$
c_e	Electrolyte concentration	$mol\,cm^{-3}$
c_e	Electrolyte concentration	$mol\,cm^{-3}$
c_i	Concentration of species i	$mol\,cm^{-3}$
c_i^0	Concentration of species i at a reference condition	$mol\,cm^{-3}$
D_i	Free stream diffusivity of species i	$cm^{-2}\,s^{-1}$
$D_i^{'g}$	Effective gas diffusivity of species i	$cm^{-2}\,s^{-1}$
$D_i^{'l}$	Effective liquid phase diffusivity of species i	$cm^{-2}\,s^{-1}$
d_{cat}	Electrode catalyst loading	$mg\,cm^{-2}$
E	Electrode potential	V
E^{rev}	Theoretical open circuit potential at the given conditions	V
E^0	Theoretical open circuit potential at standard conditions	V
F	Faraday's constant 96485.309	$C\,mol^{-1}$
f	$F/(RT)$	
f	Frequency	s^{-1}
$\Delta G_a^{\ddagger}$	Activation energy for anodic reaction	$kJ\,mol^{-1}$
$\Delta G_c^{\ddagger}$	Activation energy for cathodic reaction	$kJ\,mol^{-1}$

H_i	Henry's law constant for species i	$mol\,cm^{-3}atm$
I	Total current density of single cell	$A\,cm^{-2}$
i	Local current density	$A\,cm^{-2}$
i_d	Diffusion controlled current density	$A\,cm^{-2}$
i_k	Kinetically controlled current density	$A\,cm^{-2}$
k	Potential-dependent rate constant	$mol\,s^{-1}\,cm^{-2}$
k_n	Rate constant for n-th step in a multistep reaction mechanism	$mol\,s^{-1}\,cm^{-2}$
L_i	Length of layer i	cm
M_i	Symbol for the chemical formula of species i	
m_i	Reaction order of species i	
N_i	Molar flux of species i	$mol\,cm^{-2}\,s^{-1}$
n	Number of electrons transferred	
p	Reaction order	
p_i	Partial pressure of species i	bar
p_i^v	Vapour pressure of species i	bar
Q_{ox}	Quantity of charge to reduce surface oxide	$mC\,cm^{-2},\,\mu C\,cm^{-2}$
R	Ideal gas constant, 8.31451	$J\,K^{-1}\,mol^{-1}$
R_{cell}	Total cell resistance	Ω
R_i^e	Electrochemical reaction rate per unit volume species i	$mol\,cm^{-3}\,s^{-1}$
R_i^p	Mass transfer rate over phase boundary species i	$mol\,cm^{-3}\,s^{-1}$
s_i	Stoichiometric coefficient of species i	
T	Absolute temperature	K
t	Time	s
U	Electrical potential of an electronically conductive solid phase	V
U_{cell}	Cell voltage	V
u_i	Free stream mobility, species i	$mol\,cm^2\,J^{-1}\,s^{-1}$
$u_i^{'}$	Effective mobility, species i	$mol\,cm^2\,J^{-1}\,s^{-1}$
V_{cat}	Specific catalyst volume	cm^{-1}
v	Volume average velocity	$cm\,s^{-1}$
v_n	Reaction rate of step n in a multistep reaction mechanism	
z_i	Charge number, species i	

Greek Letters

α_a	Anodic transfer coefficient	
α_c	Cathodic transfer coefficient	
δ	Thickness of electrolyte film	cm
ϵ	Porousity	
Φ	Solution phase potential	V
γ	Anodic transfer coefficient for second step in a multistep reaction mechanism	
η	Electrode overvoltage	V
κ	Effective electrical conductivity	$S\,cm^{-1}$
ν	Kinematic viscosity	$cm^2\,s^{-1}$
θ_i	Surface coverage of species i	
ω	Rotation rate	rpm
ξ	Dimensionless spatial coordinate	

Superscripts

e	Electrochemical reaction
g	Gas phase
l	Liquid phase
p	Mass transport across phase boundary
v	Vapour pressure
0	Reference condition

Subscripts

(ads)	Adsorbed specie
AN	Anode
CCL	Cathode catalyst layer
c	Cathode
cat	Catalyst (RuO_2)
$DIFF$	Cathode diffusion layer
i	Species i
j	Species j
MEM	Membrane
m	Membrane
SEP	Separator
(l)	Liquid phase

(aq)	Solvated
$+$	Cations (H^+)
$-$	Anions (Cl^-)

Abbreviations

AFC	Alkaline Fuel Cell
ClER	Chlorine Electrode Reaction
ClRR	Chlorine Reduction Reaction
DEMS	Differential Electrochemical Mass Spectroscopy
DSA	Dimensionally Stable Anode
EIS	Electrochemical Impedance Spectroscopy
EQCM	Electrochemical Quartz Crystal Micro Balance
FTIR	Fourier Transform Infrared Spectroscopy
HCAFC	HydroChloric Acid Fuel Cell
HER	Hydrogen Evolution Reaction
MEA	Membrane Electrode Assembly
NEMCA	Non-Faradaic Electrochemical Modification of Catalytic Activity
OCV	Open Circuit Voltage
ORR	Oxygen Reduction Reaction
PAFC	Phosphoric Acid Fuel Cell
PBI	Polybenzimidazole
PEEK	Poly Ether Ether Ketone
PEFC	Polymer Electrolyte Fuel Cell
PEMFC	Polymer Electrolyte Membrane Fuel Cell
PEM	Proton Exchange Membrane
PFSA	PerFluorSulphonic Acid
PPS	PolyPhenylSulphone
PTFE	PolyTetraFluorEthylene
RDE	Rotating Disk Electrode
RTO	Ruthenium Titanium Oxide
SEM	Scanning Electron Microscope
SOFC	Solid Oxide Fuel Cell

Chapter 1

Introduction

1.1 Background

Energy is one of the most important commodities of the modern society and the industrialised world is totally dependent on the access of cost effective energy, usually in the form of fossil fuels. The modern society's activity and subsequent energy use have a substantial impact on the global environment as comprehensively documented in reports from i.a. the Intergovernmental Panel on Climate Change (IPCC) and the World Watch Institute. The main contribution to the global environmental impact is the burning of fossil fuels, but also deforestation and regulation of waterways does impact, although on a more local scale. In addition to having an impact on the environment, fossiled fuels, the largest energy source of today, also has the shortcoming of being available in limited reserves, being reduced by environmental intrusion, geopolitical instabilities and competing energy technologies [1]. Thus a transition from fossil fuels to renewable energy sources is both required and inevitable. To alleviate the move from concentrated, reliable energy sources to the more diffuse and irregular availability and scattered occurrence of renewable energy, an energy efficiency increase and a decrease in energy usage is vital.

Hydrogen has repeatedly been suggested as the ultimate energy carrier of the future, being relatively easy to produce from all energy sources and, although with some difficulties, storable. One technology able to efficiently convert hydrogen to electric energy when needed is fuel cells. The interest for developing fuel cell technology is partly motivated by efficiency considerations. The fact

that chemical energy can be transformed directly into electrical energy without going via combustion and mechanical steps, makes the fuel cell potentially more efficient than practical combustion processes. Furthermore, emissions of local pollutants are minimized by the use of fuel cells vs internal combustion engines. Fuel cells and fuel cell technology can also be utilized in modifications of existing industrial processes to reduce the total power consumption of the process or to produce net high value electric energy.

1.1.1   Fuel cells, a brief history

The *fuel cell effect* was first reported in January 1839 by Christian Friedrich Scönbein in the paper *"On the Voltaic Polarization of certain Solid and Fluid Substances"* and by Sir William Robert Grove in February 1839 *"On Voltaic Series and the Combination of Gases by Platinum"* . Grove later constructed a series of fuel cells, referred to as the *"Gaseous Voltaic Battery"* and described in several papers in the period 1842-1845 [2]. The 1950s and 1960s saw a renewed technological interest in fuel cells and most of the concepts used today were developed in this period. The alkaline fuel cell (AFC) was invented by Francis T. Bacon in 1932, used in the Apollo space program and later in NASAs Space Shuttle. The polymer electrolyte fuel cell (PEFC), also known as the proton exchange membrane fuel cell or the polymer electrolyte membrane fuel cell (PEMFC), was invented in 1957 by Willard T. Grubb and further developed in the 1960s by General Electric for space applications [3]. It was used in the Gemini Earth-orbiting missions, but was not used in the Apollo program due to stability problems with the membrane. Later, PerFluorSulphonic Acid (PFSA) membranes, which Nafion$^{\textcircled{R}}$ is an example of, were developed, making PEFC more competitive. In the late 1950s, researchers at Westinghouse Electric Cooperation (now Siemens Westinghouse) began experimenting with zirconia compounds and developed the Solid Oxide Fuel Cell (SOFC) [4]. The Phosphoric Acid Fuel Cell (PAFC) was also developed in the late 1960s seeing a drastic technological development through *"The Moonlight Program"* in Japan during the 1970s, culminating with the construction of a 11 MW PAFC power plant in the 1980s [3].

1.1.2   Fuel cells as electrochemical reactors

Since the time of Scönbein and Grove the focus of fuel cell development and use has solely been on efficient energy conversion. Applications such as road

and maritime transportation, distributed power generation, stand-alone power systems, combined FC and gas turbine power generation and premium power for portable electronics have received much attention.

The use of fuel cells or fuel cell technologies in industrial processes however, has received relatively little interest. Industrial reactors incorporating fuel cells directly or derivatives of fuel cell technologies would have several advantageous properties.

Fuel cell integration

The integration of conventional fuel cells or fuel cells operating on other, more unconventional reactants, can primarily replace combustion processes. Chemical and electrochemical processes such as plastic production, steam reforming of natural gas and chlor-alkali electrolysis produce surplus hydrogen which can be used in fuel cells for power production. The Dow Chemical company and GM installed a 75 kW PEM fuel cell as a part of the chlor alkali electrolysis process at the Dow's chemical plant in Freeport Texas in 2004 and have plans for increasing the installed efficiency to 35 MW [5].

Electrogenerative chemical reactors

The term *"Electrogenerative processes"* was introduced by Langer in 1963 [6, 7] for processes involving partial recovery of the energy of exothermic chemical reactions as electric power rather than low-grade heat and where the product from the chemical process is the main objective [8]. Reactions such as partial oxidation, hydrogenation and halogenation have received most attention as these encompass large, important industrial processes. In addition, removal of pollutants such as sulphur dioxide, hydrogen sulphide, nitrous oxides and halogens [9] are environmentally significant reactions which would yield power while consuming the pollutants. Under some conditions, the use of fuel cell technologies may give further advantages other than the production of electric energy. Since the reactants are physically separated by a solid or liquid electrolyte, unwanted side reactions can be reduced to a minimum, leading to the possibility of a product yield increase and a decrease of the amount of pollutants generated. The ability to control the voltage of the cell can improve the selectivity of certain reactions and thus contribute to an increase of the yield of the desired product.

Energy conserving processes

Fuel cell technologies may be applied to well known electrochemical electrolysis processes such as water and brine electrolysis to reduce the overall energy consumption. Especially the replacement of the hydrogen evolving cathode in the chlor-alkali membrane electrolysis cell by an oxygen reducing electrode has received considerable attention of researchers. It has been demonstrated that oxygen-reducing cathodes can save about 0.9 V out of the 3.1-3.3 V required for the operation of state of the art membrane chlor-alkali cells [10]. Replacement of the hydrogen cathode in the water electrolysis process has also been suggested to reduce the energy consumption for production of high purity oxygen [8].

The NEMCA effect

The non-Faradic electrochemical modification of catalytic activity (NEMCA) effect designates the possibility of altering the catalytic activity and selectivity of catalysts deposited on solid electrolytes by electrochemical polarisation. It has been observed catalytic rates 3×10^5 higher than the steady state transfer of ions through the electrolyte. Furthermore, the net catalytic rate increase under polarisation has been measured to be up to 70 times higher than at open circuit and significant changes in selectivity has been observed [11]. More than 50 heterogeneous catalytic reactions have been shown to exhibit this effect [12] and it has been demonstrated on several catalyst materials deposited on different solid electrolytes [13]. However, although the phenomenon has been studied for over a decade, further research is needed to fully understand the technical potential of electrochemical promotion and to establish the basis for its technological utilization.

1.2   Motivation for the Thesis

An important step in the magnesium electrowinning process is the production of anhydrous magnesium chloride. Norsk Hydro ASA has developed a process in which magnesium chloride is produced from magnesium carbonate and hydrogen chloride. Today, HCl is produced by combustion of hydrogen and chlorine in a chlorine incinerator. The chlorine is supplied from the electrolysis of magnesium chloride while the hydrogen is produced by reformation of hydrocarbons. The combustion reaction is strongly exothermic and occurs at

temperatures around 2300 °C. In addition to being used in the production of magnesium chloride, parts of the produced HCl gas is also used for the final drying step of the produced magnesium chloride before it is introduced into the electrolysis bath. The removal of water is vital for achieving high current efficiencies in the process.

This thesis work is the continuation and final part of a joint project between the Department of Materials Technology, NTNU and Norsk Hydro Research Center in Porsgrunn, looking at the possibility of replacing the combustion of chlorine and hydrogen with direct production of electric energy using fuel cells. The use of fuel cells in this process would increase the utilization of the chemical energy in the produced chlorine and thus contribute to the reduction of the overall energy consumption of the electrowinning process. In addition to the production of high value electric energy, the introduction of fuel cells would also reduce the emissions of chlorinated hydrocarbons due to the physical separation of the reactant gases by the fuel cell electrolyte.

Only a few papers on hydrogen - chlorine fuel cells are available together with a handful of registered patents [14–25]. In the available literature, such fuel cells are proposed used in regenerative energy storage systems, as an energy source for space applications or for use in the chlor-alkali electrolysis. None of the published results present any indications of long term stability, technological difficulties encountered or descriptions of operational experience.

1.3 Problem statement

The main objective of the thesis work was to investigate the possibility of including a hydrogen - chlorine fuel cell in the magnesium electrowinning process. The focus of the work should be on looking at different fuel cell concepts and evaluate their feasibility as electrochemical reactors for co-production of hydrochloric acid and electric power. It is also of interest to study the chlorine reduction reaction on potential catalyst materials.

1.3.1 Fuel cell water management

Earlier work at the department focused on a standard PEM fuel cell with a Nafion membrane and found that the water management of the system was

extremely complex [26,27]. The reduction of water content in the Nafion membrane leads to lower conductivity of the polymer electrolyte and thus either a drastic reduction in cell performance or a total breakdown of the cell. Evaluations of fuel cell designs with higher water-management robustness was identified as a key activity.

1.3.2   Electrode kinetics

The chlorine electrode is a well studied reaction, due to the industrial importance of chlorine production. However, only a handful of published papers deals with the reduction of chlorine. To optimise the yield from the potential hydrogen - chlorine fuel cell it is important to have a good, stable electrocatalyst for the chlorine reduction. It is therefore of interest to investigate the chlorine reduction kinetics on different possible catalyst materials such as platinum, ruthenium and ruthenium oxides.

1.4   Methodology

A fuel cell is a complex system, even when using a laboratory scale single cell unit. Several operating parameters have to be controlled, such as gas supply and distribution, gas humidification, temperature control and current/potential distribution as well as manufacture and assembly techniques for electrodes and electrocatalysts. This makes fuel cells unsuited for studying the fundamentals of processes occuring in such systems, since it is a challenging task to perform FC measurements that are reproducible and stable, and where all operational parameters are under control simultaneously. Thus, in this work, fuel cell measurements have been used only to qualitatively investigate different fuel cell designs for operation on hydrogen and chlorine.

Similarly, investigations of fundamental electrode kinetics on nanostructured electrocatalysts are not straightforward, the complex geometric structure of these particles makes it difficult to control the distribution of parameters such as potential, current and reactant concentrations at the surface. Thus, the chlorine reduction measurements were performed on well defined, polished planar electrodes.

1.4.1 Fuel cell design evaluation

Not much is known of fuel cells operating on chlorine. To increase the knowledge of the technological challenges facing the design of hydrogen/chlorine fuel cell systems, three different fuel cell designs were evaluated. Effects of the highly corrosive and hygroscopic nature of Cl_2 and HCl on the cell performance and stability was monitored. A mathematical model of one of the fuel cell designs were developed and implemented in a numerical modelling program (FEMLAB). This model was used as a tool to better understand the processes occuring in the fuel cell.

1.4.2 Chlorine electrode kinetics

The reduction of chlorine dissolved in hydrochloric acid was investigated using the Rotating Disk Electrode (RDE) technique. Electrodes of platinum and ruthenium were used and effects of the surface oxidation state and solution pH were studied. This method gives excellent control over the mass transport of reactants and products to and from the electrode surface and facilitates the determination of kinetic parameters. To interpret the experimental results, rate equations for several reaction mechanisms were developed and evaluated by numerical non-linear curve fitting methods.

1.5   Outline of Thesis

The contents of this thesis is organised as a series of individual chapters built up as scientific papers. This format is chosen since some of the work already is published or otherwise planned for publication. This structure inevitably leads to some repetition of introductory information, but hopefully divides the work into more apprehensible sections for the reader. Chapters 2-4 deals with the evaluation of different hydrogen - chlorine fuel cell concepts through experimental work and the development of a mathematical fuel cell model. Since it was difficult to achieve stable, reproducible experiments with the fuel cells it was decided to perform a more fundamental study of the chlorine reduction reaction. This study is treated in chapters 6 and 7.

Chapter 1:   *Introduction.* Gives a brief summary of the history of fuel cells and the use of fuel cells as electrochemical reactors. The motivation for the project as well as a problem statement and methodology is presented.

Chapter 2:   *H_2 - Cl_2 fuel cell for co-generation of electricity and HCl.* A hydrogen - chlorine fuel cell with an aqueous hydrochloric acid electrolyte is presented. Effects of electrolyte concentration and temperature on the open circuit voltage and cell performance are evaluated. Most of the experimental work was performed as a part of a Masters degree in electrochemical engineering, leading up to and forming the basis for this thesis work. This chapter has been published in Journal of Applied Electrochemistry [28]

Chapter 3:   *Evaluation of fuel cell concepts for hydrogen - chlorine fuel cells.* Three low temperature fuel cell designs have been evaluated for use as a hydrogen - chlorine fuel cell. A standard Nafion fuel cell, a composite cell with both Nafion and aqueous hydrochloric acid as electrolyte and a phosphoric acid doped PBI-membrane fuel cell. The characteristics and performances of the different designs were studied. All designs had problems with stability and the cause for these difficulties were investigated. The experiments with and the initial interpretation of the results from the standard Nafion fuel cell was performed by Espen Sandnes [26, 27].

Chapter 4:   *Computational model of a hydrogen - chlorine fuel cell.* A two dimensional, isothermal mathematical model of a H_2 - Cl_2 single

fuel cell with an aqueous HCl electrolyte similar to the composite fuel cell in chapter 3 is presented. The model focuses on the electrode reactions in the chlorine cathode and also includes the mass and momentum balances for the electrolyte and cathode gas diffusion layer. The work was performed at the School of Chemical Engineering and Advanced Materials at the University of Newcastle, UK under supervision of professor Keith Scott. Preliminary results were presented at the Electrochem 2003 conference in Southampton, UK, 14-17 September 2003. This chapter was submitted for publication in Journal of Power Sources in November 2004.

Chapter 5: *Background theory.* This chapter gives a brief overview of the theories for electron transfer at the solid/electrolyte interface, a summary of the derivation of mechanistic rate equations and the theory of the rotating disk electrode. All of which is central in the two following chapters.

Chapter 6: *Chlorine reduction on platinum and ruthenium: The effect of oxide coverage.* The kinetics of chlorine reduction in hydrochloric acid on platinum and ruthenium electrodes was investigated. The influence of the oxidation state of the electrodes were the main focus of this work. Rate equations for several reaction mechanisms were developed and evaluated against the experimental results using numerical non-linear curve fitting. This chapter has been published in Electrochimica Acta [29]

Chapter 7: *Chlorine reduction on electrooxidised ruthenium.* This chapter is a continuation of the work presented in the preceding chapter. The kinetics of chlorine reduction on electrooxidised ruthenium were investigated with emphasis on the effect of solution pH. Most of the experimental work was performed by M.Sc. student Camilla Karlsen. This chapter has been submitted for publication in Electrochimica Acta in February 2005.

Chapter 2

H_2 - Cl_2 Fuel Cell for co-generation of Electricity and HCl

M. Thomassen, B. Børresen, G. Hagen, R. Tunold
Department of Materials Technology
Norwegian University of Science and Technology
NO-7491 Trondheim, Norway

2.1   Abstract

A H$_2$ - Cl$_2$ fuel cell system with an aqueous electrolyte and gas diffusion electrodes has been investigated, and the effects of electrolyte concentration and temperature on the open circuit voltage (OCV) and cell performance have been evaluated. Furthermore, the kinetics and long-term stability of Pt as electrocatalyst have been studied under various conditions. In addition, the long-term stability of Rh electrocatalyst has been evaluated. The OCV obtained showed that the Cl$_2$ reduction is more reversible than O$_2$ reduction. The ohmic drop was determining the cell performance at high current densities. An output power of about 0.5 W cm^{-2} was achieved with this system.

2.2   Introduction

Fuel cells are in general used as generators of electric energy, either for mobile or stationary applications. The fuel may either be pure hydrogen or a hydrogen rich compound like hydrocarbons or ammonia. As an oxidant oxygen is normally used, either pure or more commonly from air.

In a H$_2$ - Cl$_2$ fuel cell, oxygen is substituted by chlorine as the oxidising agent. Hence the product from this cell is not water, but hydrogen chloride. This product is potentially of more value than water and consequently the H$_2$ - Cl$_2$ fuel cell is as much a chemical reactor as an electric generator and the competitiveness of such units is dependent on both the prices of electricity, chlorine and HCl.

Although comparatively less popular than H$_2$ - O$_2$ fuel cells, early reports on H$_2$ - Cl$_2$ fuel cells from the 1920s are available [14, 15]. Catalysts such as Pt [16, 18–20], Pt-Ir alloy [21], RuO$_2$ [16, 18, 22] or Pb$_2$Ru$_2$O$_7$ [19], have been evaluated for Cl$_2$ reduction.

The use of H$_2$ - Cl$_2$ fuel cells for industrial applications has been proposed for plants having an excess of hydrogen and chlorine readily available. The chlorine-alkaline industry has a potential for energy savings with the use of H$_2$ - Cl$_2$ fuel cells [23]. The use of H$_2$ - Cl$_2$ fuel cells in industries where chlorine is produced as a by-product, e.g. in magnesium and sodium electrolysis, can also be beneficial.

H$_2$ - Cl$_2$ fuel cells have also been suggested as an alternative to H$_2$ - O$_2$ fuel

cells in space applications [19], and as regenerative systems for storage of electric energy [16, 18, 22, 24, 25].

2.3 Experimental

The experimental fuel cell consisted of a housing made of PEEK (polyetheretherketone) and current collectors made of non-porous graphite. The active surface area of the electrodes was 2.2 cm^2. A separator made of PEEK separated the electrodes, which made it possible to vary the interpolar distance by using separators with various thicknesses. A schematic illustration of the cell is given in Figure 2.1.
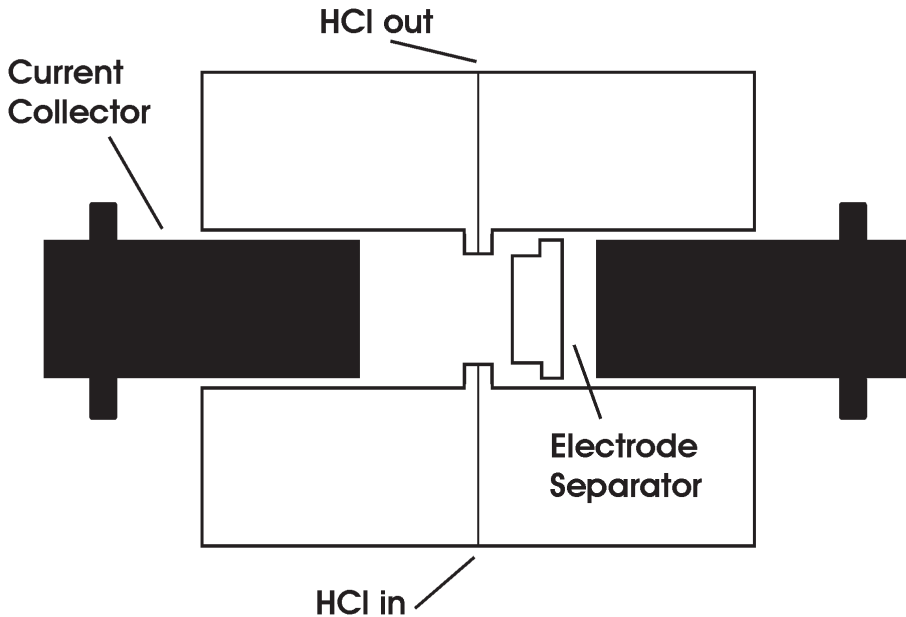
Figure 2.1: Schematic illustration of experimental cell

The electrolyte with various concentrations of HCl was made from 37 wt% aqueous HCl (p.a. MERCK), and pumped from a temperature-controlled reservoir through the cell housing and the separator by a Masterflex pump via insulated viton (iso-versinic) tubes. The single electrode potentials were studied in a cell with a similar design as the experimental fuel cell, but with a longer inter

electrode distance. One of the gas diffusion electrodes was substituted with a platinum foil and a Ag/AgCl reference electrode was positioned in close vicinity of the remaining gas diffusion electrode. The magnitude of the ohmic drop between the gas diffusion electrode and the reference electrode was determined by electrochemical impedance spectroscopy (EIS) and the measured electrode potentials were iR compensated.

Commercially available 20% Pt on carbon (Pt/C), 0.5 mg cm^{-2} Pt gas diffusion electrodes (STD/DS/V2/ELAT & STD/SS/V2/ELAT) and 30% Rh on carbon (Rh/C), 1.0 mg cm^{-2} were obtained from E-TEK Inc. The gases, hydrogen (5.0 AGA) and chlorine (2.7 Gerling Holtz), were fed to the cell without any kind of pre heating or humidification and exited the cell through a water column to create a small overpressure inside the cell (10 cm H$_2$O). The cathode exit gas was then led through a KOH solution to remove excess chlorine. The H$_2$ gas was controlled by a flow controller and the Cl$_2$ gas flow was regulated manually. Both gases had a flow rate of approx. 5 ml s^{-1}. The cell potential was controlled by a potentiostat (AUTOLAB PGSTAT 20) connected to a 20 A current booster (BSTR 10A + Extension module), both from Eco Chemie. Polarisation curves were obtained by a data acquisition unit (HP 34970A) connected to the current collectors to minimise the error from resistance in connectors and cables.

Means of preventing Cl$_2$ and H$_2$ recombination was deemed unnecessary for the present investigations due to the high OCV attained and the low solubility of H$_2$ in the electrolyte. For an industrial reactor this issue has to be addressed.

2.4   Results and Discussion

2.4.1   Effect of electrolyte concentration

The open circuit voltage as a function of HCl concentration at 20 °C for a hydrochloric acid fuel cell (HCAFC) and theoretical (calculated) values are presented in Figure 2.2. Activity coefficients for HCl solutions are taken from Lobo [30]. As can be observed from the figure, the measured and calculated values for the open circuit voltage are almost identical for HCl concentrations from 5 mol dm^{-3} to 0.1 mol dm^{-3}, as apposed to H$_2$ - O$_2$ fuel cells where the OCP is close to 1.0 V compared with the thermodynamically expected value of 1.23 V.

The low OCP of ordinary H$_2$ - O$_2$ PEM fuel cells is caused by the poor kinetics

of the oxygen reduction reaction (ORR), resulting in a mixed potential at open circuit [31, 32]. The mixed potential originates from the ORR, which may yield both water and hydrogen peroxide, and a parasitic anodic component of several possible origins, typically oxidation of traces of hydrogen in the cathode compartment. The absence of such a discrepancy between the thermodynamical and actual OCP of the HCAFC strongly indicates that the chlorine reduction reaction (ClRR) has much better kinetics than the ORR (higher exchange current density), and thus govern the electrode potential. The high OCV of the HCAFC facilitates both high energy efficiency and power density in a fuel cell system.
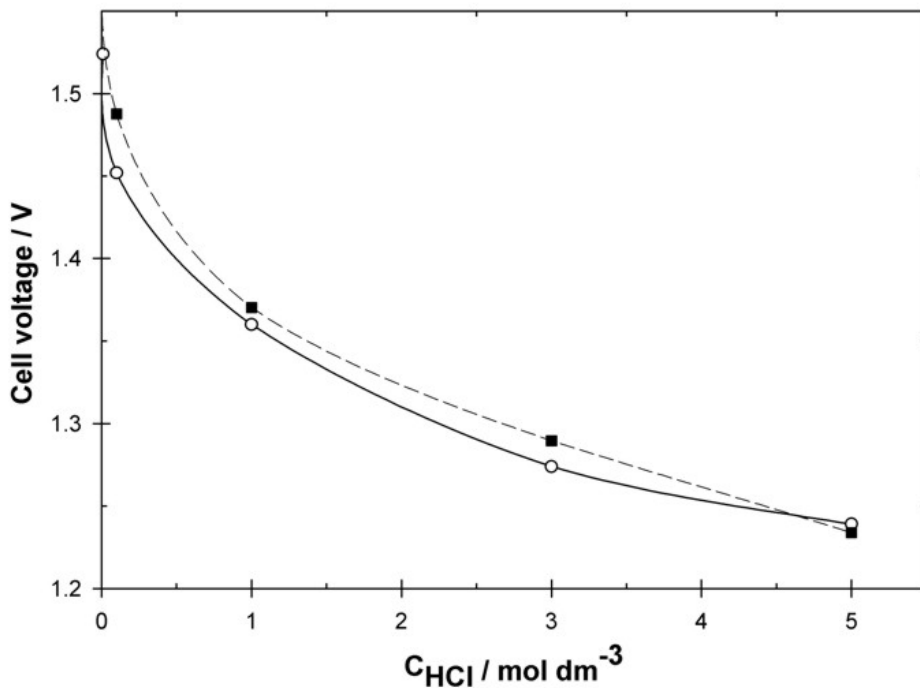
Figure 2.2: Open circuit voltage against HCl concentration at 20 °C (-) experimental values, (- - -) theoretical values, calculated with data from [30])

Steady state polarisation curves at 20 °C as a function of HCl concentration are presented in Figure 2.3. A comparison of the achieved power density at

a given potential as a function of the electrolyte concentration show that the polarisation curves does not have a linear variation with HCl concentration. The performance of the HCAFC increases with the electrolyte concentration from 0.01 mol dm^{-3} HCl to 3 mol dm^{-3} HCl. A further increase of the concentration to 5 mol dm^{-3} has an insignificant effect. The decrease in the slope of the polarisation curves with increasing concentration at current densities above 0.4-0.6 A cm^{-2} indicates that higher electrolyte conductivity in the concentrated electrolytes (3 and 5 mol dm^{-3}), and thus a lower iR drop, is the primary cause for the observed performance increase. HCl has its highest conductivity in the 5 - 6 mol dm^{-3} concentration range [30]. One of the reasons for the non-linear dependence of concentration on conductivity is that coulombic forces between the ions in the high concentration solutions retard the ion migration. This concentration effect is also reported by Shibli and Noel [21].
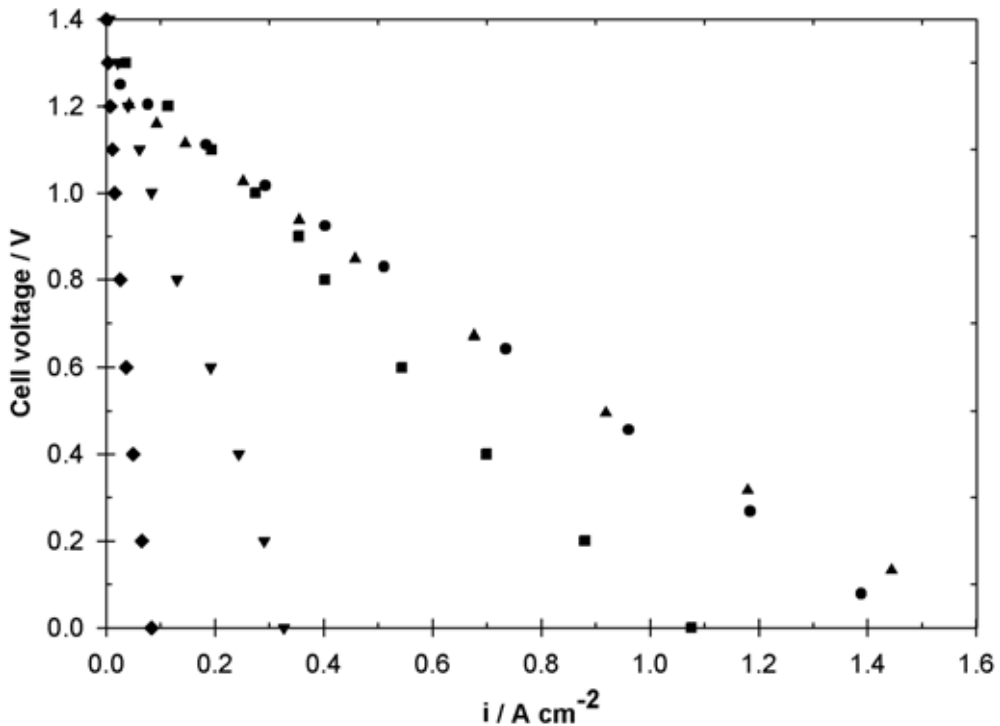
Figure 2.3: Effect of HCl concentration on HCAFC performance at 20 °C. ♦: 0.01, ▼: 0.1, ■: 1, •: 3, ▲: 5 mol dm^{-3}

2.4.2 Effect of temperature

The effects of operating temperature on the overall fuel cell performance, as well as on the individual electrode reactions are shown in Figure 2.4. An increase in temperature leads to a decrease in electrode potential for both electrode processes and the overall operating cell voltage increases with temperature at all current densities over 250 mA cm^{-2}.

The polarisation curves of H_2 oxidation and Cl_2 reduction are only to a small degree affected by the increase of temperature from 20 °C to 50 °C (Figure 2.4B). The chlorine curve is only shifted in the direction of a more negative potential, the shape of the curve is unaffected. The hydrogen curve is also shifted to a more negative potential, but in addition, the overvoltage at a given current density decreases somewhat. The shifts to more negative potentials have a small effect on the open circuit potential of the cell, as can be seen from Figure 2.4A. At current densities above 500 mA cm^{-2} the difference between the cell voltage at 20 °C and 50 °C is much higher than can be attributed to the improved hydrogen oxidation kinetics. This suggests that the main factor for the increased fuel cell performance with temperature is the increase of electrolyte conductivity and not enhanced electrode kinetics.

Operation of the fuel cell at higher temperatures might have lead to a further improvement of the fuel cell performance, but at temperatures above 50 °C, the corrosion of the cathode catalyst had reached a rate too high to attain stable polarisation curves. This is explained in more detail in section 3.4. In addition, the reduced viscosity of the electrolyte resulted in a drastic increase of electrolyte leakage through the gas diffusion electrodes and into the gas channels. The combination of these two effects made it impossible with the present cell design to achieve reproducible conditions in at temperatures above 50 °C.
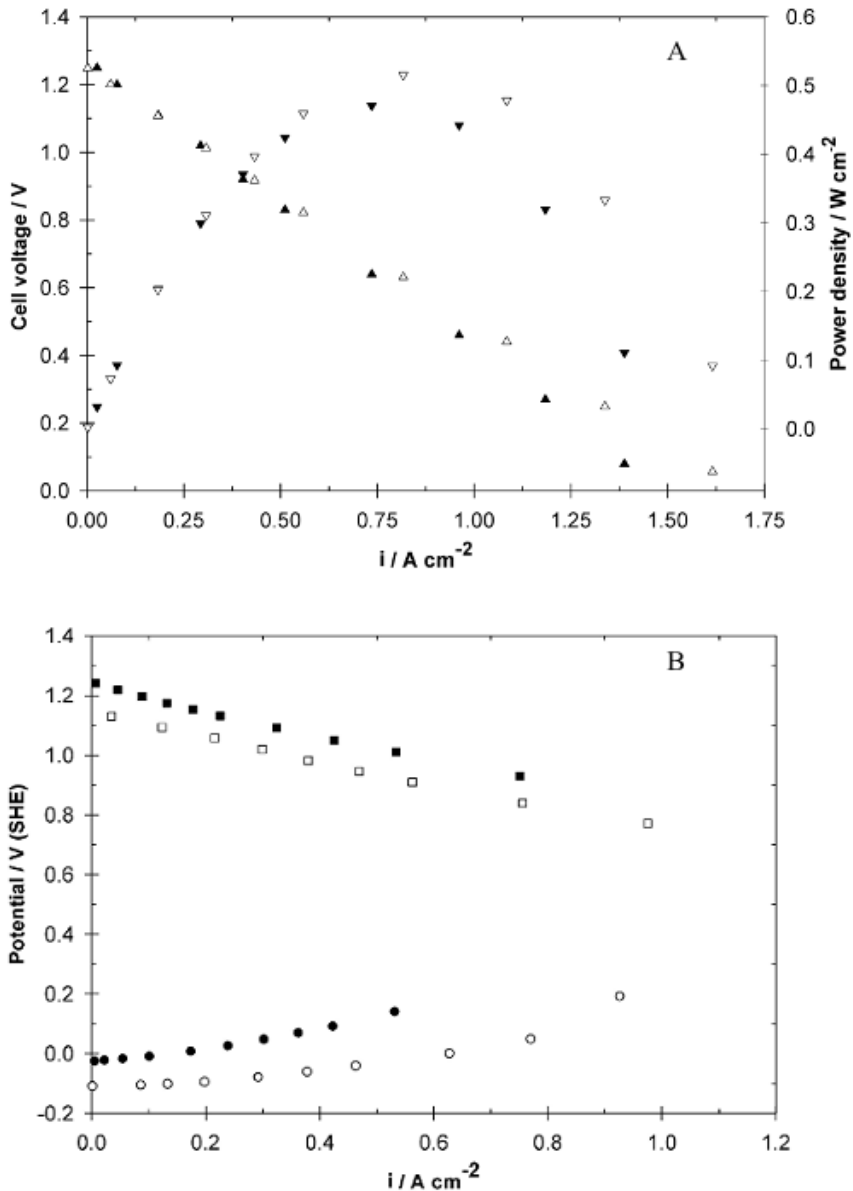
Figure 2.4: Effect of temperature on the overall fuel cell performance and the individual electrode polarization curves, 3 M HCl as electrolyte. A: (▲) cell voltage 20 °C, (△) cell voltage 50 °C, (▼) Power density 20 °C, (▽) Power density 50 °C; B: (●) H$_2$ oxidation 20 °C, (○) H$_2$ oxidation 50 °C, (■) Cl$_2$ reduction 20 °C, (□) Cl$_2$ reduction 50 °C

2.4.3 Effect of pressure

The effect of a small overpressure on the H_2-gas side is shown in Figure 2.5. The cell voltage was held at a constant value of 500 mV and at the points A and B a valve in the H_2-gas outlet was partially closed, creating a small overpressure in the anode compartment. The value of the overpressure was not recorded, due to lack of appropriate instrumentation, but was estimated to about 100mm H_2O. 10 minutes after the valve was closed for the second time a stable current about 20% higher than the current with the valve open were established. Opening the valve reduced the current back to its original level. A similar test was made on the cathode, but no change in current density was observed with the addition of a small Cl_2 overpressure.

A pressure increase leads to higher activities of the reactants and decrease the mass transport limitations of the system, but the overpressure applied was not high enough to explain the 20% current increase if only reactant activity and mass transport are considered. The electrode reactions taking place in systems where the reactants are in the gas phase can either proceed through a direct adsorption on the catalytic surface with a subsequent electrochemical reaction or through a process where the reactant is first dissolved in the electrolyte. Depending on the relevant mechanism, a wetting/flooding of the electrode structure may significantly alter the performance. The hydrogen oxidation reaction is highly dependent on the three-phase boundary due to the extremely low solubility of hydrogen in the electrolyte, which effectively limits the reaction to proceed from gas phase reactants. The solubility of chlorine is about 100 times higher than the solubility of hydrogen and the chlorine reduction reaction can with a high probability be described by the following sequence:

$$Cl_{2(g)} \rightarrow Cl_{2(aq)} \rightarrow 2Cl_{(ads)} + 2e^- \rightarrow 2Cl_{(aq)}^- \tag{2.1}$$
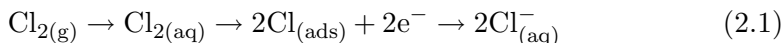
This renders the ClRR virtually independent of the three-phase boundary.

In this system, the balance between the gas-, electrolyte- and catalyst phase inside the gas diffusion electrode is extremely sensitive to changes in temperature and gas pressure due to the low viscosity of the electrolyte. Thus, a possible explanation for the current increase with a small H_2 overpressure and no increase with a small Cl_2 overpressure is a displacement of the three-phase boundary inside the gas diffusion electrode to a more beneficial position and consequently, an increase of the active electrode surface for hydrogen oxidation.
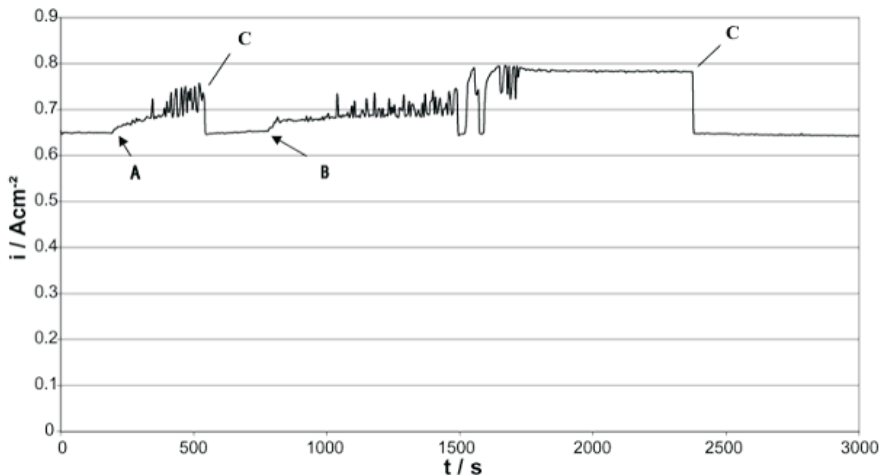
Figure 2.5: Effect of anode gas pressure. Cell voltage: 500 mV, 1 mol dm^{-3}. The gas pressure was increased at (A) and (B) and decreased at (C)

2.4.4   Fuel cell performance

A long-term stability test was performed for the fuel cell with 1 mol dm^{-3} HCl as electrolyte, 25 °C operating temperature and a 300 mA cm^{-2} discharge current. A relatively rapid decrease in fuel cell performance was observed. After 120 hours the cell voltage had dropped from 1.05 V to 0.6 V. A visual inspection of the anode after the long-term test revealed a metallic coating on the area exposed to the electrolyte that is believed to be caused by a dissolution/precipitation of Pt. Figure 2.6 shows a SEM photo of the electrode, the white region on the left has been in contact with the electrolyte and a layer of Pt has been formed. It is well known that platinum is insoluble in hydrochloric acid, but in presence of chlorine it dissolves, forming chloroplatinic acid (H$_2$PtCl$_6$). A sample of the electrolyte was tested for Pt with inductive coupled argon plasma atomic emission spectroscopy (ICP), which showed a significant concentration of Pt in the electrolyte. These observations indicate that Pt is not stable as a cathode material within the operating conditions of the HCAFC and thus dissolves into the electrolyte and precipitates on the anode by the H$_2$ present on the electrode. A long-term stability test was also conducted with Rh as chlorine reduction catalyst. The preliminary results showed that Rh has a lower initial activity towards chlorine reduction, but a lower rate of

corrosion than Pt in the system environment.
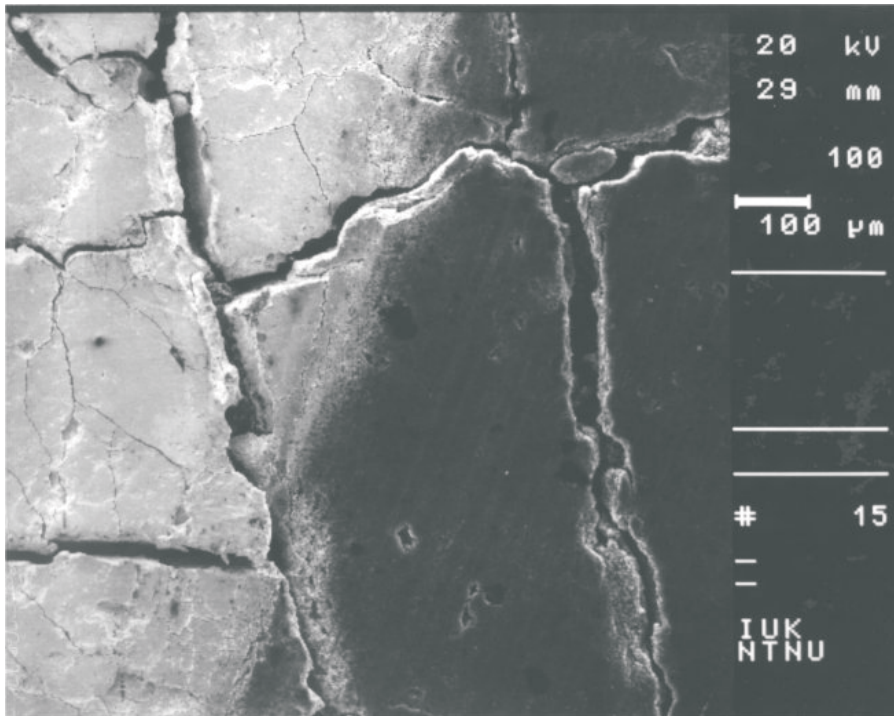
Figure 2.6: SEM photo of fuel cell anode of a HCAFC. The white region on the left has been in contact with the electrolyte and a precipitated layer of Pt has formed.

2.5   Conclusions

The performance of the HCAFC system investigated shows a strong dependence on electrolyte concentration. The optimum conditions for the system investigated are 50 °C and 3 mol dm^{-3} HCl, which gave a performance of 0.51 W cm^{-2} at 0.5 V.

Pt an Rh electrocatalysts are not stable in the system environment. Long-term stability tests showed a decrease in performance of 45% in 120 hours. Rh was found to have a lower initial activity towards chlorine reduction but showed a higher long-term stability. Chlorine reduction is considerably more reversible than oxygen reduction, leading to an open circuit voltage close to the thermodynamic value.

2.6   Acknowledgements

Chapter 3

Evaluation of Fuel Cell Concepts for Hydrogen - Chlorine Fuel Cells

3.1 Abstract

Three different concepts for H_2 - Cl_2 fuel cells have been evaluated. An ordinary PEM fuel cell based on a Nafion membrane, a fuel cell based on a combination of circulating hydrochloric acid and a Nafion membrane and a system based on a phosphoric acid doped Polybenzimidazole (PBI) membrane. None of the investigated systems were able to demonstrate stable operation under the conditions used in this study, due to electrocatalyst corrosion, membrane dehydration and/or electrode flooding. All systems studied achieved open circuit voltages close to the reversible thermodynamic value for production of aqueous hydrochloric acid, suggesting formation of dissolved HCl in the electrolyte and fast electrode kinetics.

3.2 Introduction

Fuel cells are in general used as generators for electric energy, either for mobile or stationary applications. The fuel may either be pure hydrogen, a hydrogen rich fuel or a hydrocarbon. The oxidant in all these cases is oxygen, either pure

23

or more commonly from air. In a H_2 - Cl_2 fuel cell, the oxidant (O_2) has been substituted by chlorine. Hence the product from such systems is not water, but hydrogen chloride.

The use of H_2 - Cl_2 fuel cells has been investigated both for space and ground applications [16, 18–20, 23] due to the faster electrode kinetics for the chlorine reduction compared to oxygen reduction, which implicates a possible higher energy efficiency of systems applying Cl_2 rather than O_2. For reversible energy storage systems, where HCl is split into H_2 and Cl_2 by electrolysis in periods with excess of electric energy and converted to HCl in a fuel cell during periods of demands of electric energy, the overall energy efficiency has been calculated to be about 70% [18, 25]. Corresponding systems applying oxygen as oxidant and water as the reaction medium are commonly operating at an energy efficiency of around 50% [33]. The use of H_2 - Cl_2 fuel cells for industrial applications has been proposed for plants having excess of hydrogen and chlorine readily available and where HCl is needed in the process, such as the chlor-alkali industry. Energy savings for such plants obtained by applying this technology has been estimated to be 2 % when using 5 % of the produced hydrogen and chlorine for production of HCl required for brine acidification [23]. Furthermore, the use of such units in other industries where chlorine is produced, e.g. in magnesium electrowinning, can be beneficial both with respect to economy and environmental considerations. The electrochemical conversion of hydrogen and chlorine to hydrogen chloride rather than by combustion will supply high value electric energy instead of low value heat.

From a constructional point of view, a H_2 - Cl_2 fuel cell could use any electrolyte being either proton or chloride conducting. Depending on the electrolyte, the characteristics of the system will vary. The purpose of this work was to study the possibility of developing a H_2 - Cl_2 fuel cell system for industrial applications by considering three different cell configurations, and define the characteristics of each of these systems. The three systems were: a) a conventional PEM fuel cell applying a Nafion membrane, b) a composite system applying an aqueous HCl electrolyte and Nafion membrane and c) a phosphoric acid doped PBI membrane fuel cell operating at intermediate temperatures (150-175 °C).

3.3   Experimental

3.3.1   Nafion PEM fuel cell

A 5 cm^2 fuel cell with graphite current collectors with a serpentine flow field
was used. The membrane electrode assemblies (MEA) were constructed using
ELAT gas diffusion electrodes (E-TEK) with a 20 wt% Pt/C catalyst loading
of 1 mg Pt cm^{-2} and a Nafion content of 0.8 mg cm^{-2} hot pressed at 130 °C
and a pressure of 10 MPa for 3 minutes onto a Nafion 115 membrane. The
mechanical pressure on the MEA after being loaded into the fuel cell housing
was controlled by a pneumatic piston and was set to 1 MPa. Fig. 3.1 shows a
schematic illustration of the Nafion fuel cell construction. The gases, hydrogen
(5.0 AGA) and chlorine (2.8 Gerling Holtz) were humidified by thermostatically
controlled bubble humidifiers. The humidifiers consisted of an inner saturation
tank heated by a water filled outer tank, both made of glass. Steady state
polarisation curves were recorded using a Bank HP 20-16 potentiostat connected
with Hyscan (Bank Electronics) interface. The cell was operated at 60 °C with
a humidification temperature of 90 °C.
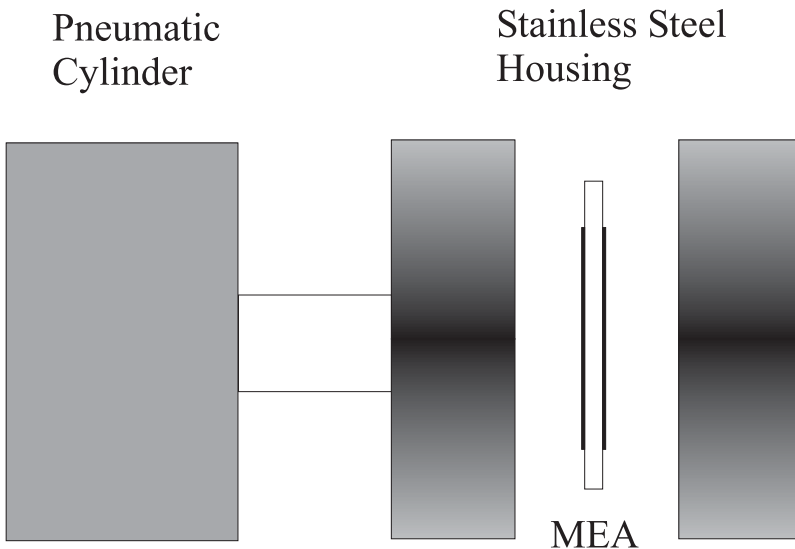
Figure 3.1: Schematic illustration of the Nafion fuel cell construction

3.3.2   Composite aqueous/Nafion electrolyte

The composite aqueous system is a further development of the cell examined in chapter 2 and a conventional Nafion PEM fuel cell. The intention behind the merging of these two technologies was to solve problems with humidification of the Nafion membrane observed in earlier work and to isolate the platinum catalyst at the anode from the corrosive, chlorine rich liquid electrolyte. The addition of a Nafion membrane to the aqueous system also fills the role as a physical separator to prevent mixing of the reactant gases, which of safety reasons most probably would be required in an industrial system. In earlier work [28] it was found that the platinum catalyst exposed to the aqueous electrolyte, especially that on the cathode, corroded and most probably dissolved as hexachloroplatinic acid (H_2PtCl_6). It was therefore decided to use ruthenium oxide as the cathode catalyst for this fuel cell.

Figure 3.2 shows a schematic illustration of the composite fuel cell construction. The fuel cell housing consisted of two graphite current collectors with double serpentine flow fields, a carbon paper anode attached to a Nafion 117 membrane, a PPS (polyphenylsulphone) cloth separator, a carbon paper cathode and a silicon gasket. The graphite current collectors included inlets and outlets for the circulating liquid HCl electrolyte. The PPS cloth acts as a spacer between the electrodes making it possible to apply a mechanical pressure to the electrodes and simultaneously supplying space for the circulating electrolyte.

Cathode preparation

The cathodes were constructed of ELAT carbon paper (E-TEK) with various amounts of Teflon impregnation (0-60 wt%). Catalyst inks were prepared using commercial unsupported RuO_2 catalyst (Alpha Aesar). The catalyst was mixed with various amounts of Teflon suspension and isopropanol to produce a range of catalysts with different degrees of wet-proofing. The mixture was stirred and ultrasonicated for several hours before application to the cathode carbon paper electrode using an air-brush (Badger), with the carbon electrode placed on a thermal-controlled heating plate. After spraying, the electrode was dried in a forced convection oven at 150 °C for one hour.
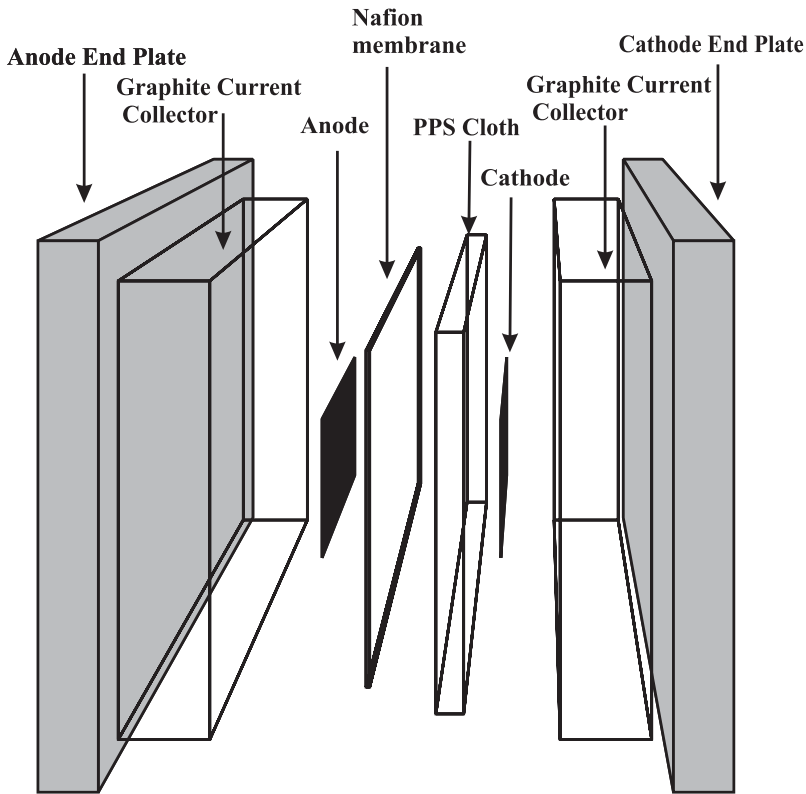
Figure 3.2: Schematic illustration of the hybrid fuel cell construction

Membrane and MEA preparation

The Nafion 117 membranes were treated by immersion in 85 °C 18.2 MΩ distilled water for 15 minutes, thereafter in 5% H_2O_2 (Merck *p.a.*) for 30 minutes and washed with distilled water and ion exchanged twice in 0.05 M H_2SO_4 (Merck *p.a.*), each time for 30 minutes. After ion exchange, the membranes were washed thoroughly by immersion in distilled water four times, each for about 15 minutes. The membranes were then cut in rectangular pieces and stored in purified water. Commercially available ELAT gas diffusion electrodes (E-TEK) with a 20 wt% Pt/C catalyst loading of 1 mg Pt cm^{-2} were used as anodes. A rectangular piece of Nafion membrane were gently dried with a lint free paper, sandwiched with a 6.5 cm^2 rectangular anode piece between two thin Teflon sheets and hot-pressed for 3 minutes at 130 °C and 10 MPa. The MEA was then cooled down and placed in purified water until mounted in the

cell.

Fuel cell testing

The cell was assembled using a torque of 0.15 Nm on the bolts. All experiments reported here were conducted at room temperature and atmospheric pressure. The gases, hydrogen (5.0 AGA) and chlorine (2.8 Gerling Holtz), were fed to the cell without any kind of pre heating or humidification and exited the cell through a water column to create a small overpressure inside the cell (10 cm H_2O). The fuel cell was controlled using a Solartron SI1287 electrochemical interface. Quasi steady-state polarisation curves were recorded at an operating temperature of 25 °C by sweeping the potential at 1 mV s^{-1} from open circuit to approx. 0.2 V and then reversed. The HCl liquid electrolyte circulated from a thermally controlled external reservoir through the cell at a rate of 2 ml s^{-1} via a peristaltic pump. The HCl electrolyte concentration was varied between 1 and 5 mol dm^{-3}.

3.3.3   PBI fuel cell

Fuel cell construction and testing

The MEA consisted of a phosphoric acid doped PBI membrane with attached gas diffusion electrodes. The catalyst loading was 0.4 mg 50 wt% Pt/C cm^{-2} on the anode and 0.6 mg 50 wt% Pt/C cm^{-2} on the cathode. Further details of the experimental cell and MEA preparation can be found in Seland et al. [34]. The MEA was mounted in a graphite fuel cell housing (Electrochem) with an active area of 6.25 cm^2. The housing was fitted with heating elements and the cell temperature was measured by a thermocouple and controlled by a PID regulator. The fuel cell was controlled using a Solartron SI1287 electrochemical interface and quasi steady-state polarisation curves were recorded by sweeping the potential at 1 mV s^{-1} from open circuit to approx. 0.2 V and then reversed to open circuit at temperatures between 125 and 175 °C and atmospheric pressure. Hydrogen (5.0 AGA) and either chlorine (2.8 Gerling Holtz) or oxygen (2.0 AGA) was humidified by passing through bubble flasks with purified water at room temperature.

Resistance measurements

The ohmic resistance in a fuel cell may be assessed either by current interrupt techniques or by high frequency impedance measurements [35, 36]. The current interrupt technique is easier to implement and requires less equipment. Current interrupt is based on breaking the electronic circuit and measuring the potential transient of the cell. The cell voltage of a fuel cell consists of various components and may be expressed as:

$$E = E^{rev} - \sum \eta - IR_{cell} \tag{3.1}$$

Where $\sum \eta$ is the sum of the overvoltages related to the electrode kinetics, IR is the potential drop due to the ohmic resistance in the electrodes and electrolyte and E^{rev} is the thermodynamical voltage of the cell. Both the overpotentials and the ohmic potential drop are dependent on the current passing in the system. The instant voltage change at the moment the circuit is broken, ΔE_{inst}, is related to the circuit resistance through Ohm's law:

$$\Delta E_{inst} = R_{cell} \Delta I \tag{3.2}$$

In a real electrochemical cell, the local current in parts of the cell might not drop instantly to zero due to electrochemical processes occuring in the electrodes. In a fuel cell, this will lead to a potential gradient through the porous electrodes and the resistance estimated from Eq.3.2 will be too high, that is, some of the polarization overvoltage is erroneously attributed to the ohmic resistance of the cell. The potential relaxation of the porous electrodes is closely connected to the exchange current density, i_0, of the electrochemical reactions and the error in the estimated ohmic resistance increases with decreasing i_0 [36].

The resistance in the PBI fuel cell was measured using the current-interrupt technique. An electric switch was installed between the counter electrode and the potentiostat and a digital oscilloscope (Pico-technologies) was used to measure the voltage transient from the interruption of the circuit. The cell was run galvanostatically at current densities of approx. 0.2 A cm^{-2} during these measurements. Figure 3.3 shows a typical voltage transient for the fuel cell at current interruption.

Right after the circuit break the voltage signal is noisy, making it impossible to select a representative value for the cell potential. Instead, the voltage change
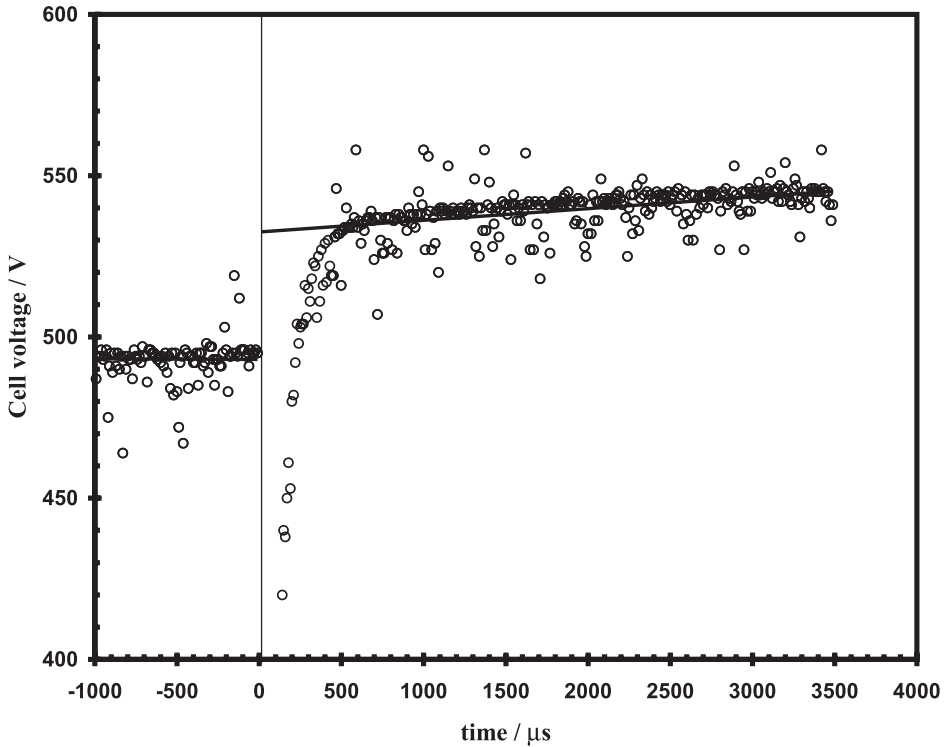
Figure 3.3: Typical cell voltage transient after current interruption

at current interrupt can be calculated by extrapolating a linear fit to the data recorded some time after the interrupt back to $t = 0$ as shown in Figure 3.3.

The cell was fed with oxygen and operated galvanostatically until a stable potential and resistance was obtained. The feed was then changed to chlorine gas ($t = 0$) and several consecutive current interrupt measurements were performed until relatively stable values of the cell voltage and resistance were observed.

3.4 Results and Discussion

3.4.1 General thermodynamics

A simple thermodynamic overview of the temperature dependence of the open circuit voltage of the hydrogen - chlorine fuel cell is presented in Figure 3.4. Thermodynamic data for the reactants and products at 25 °C [37] have been used to calculate the cell voltage dependency for an aqueous and gaseous reaction respectively.

$$1/2\,H_{2\,(aq)} + 1/2\,Cl_{2\,(aq)} \;\rightleftharpoons\; HCl_{(aq)} \tag{3.3}$$

$$1/2\,H_{2\,(g)} + 1/2\,Cl_{2\,(g)} \;\rightleftharpoons\; HCl_{(g)} \tag{3.4}$$
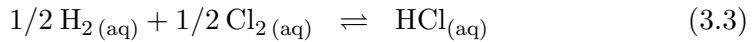
It is clearly seen that due to the strong exothermic energy associated with dissolution of hydrogen chloride in water, the theoretical cell voltage will be strongly dependent on the system in question. For a system where the product is an aqueous solution of HCl, the maximum theoretical cell voltage is 1.39 V at 25 °C at standard conditions, while a gaseous reaction would only yield an cell voltage of 0.98 V. It is also interesting that the voltage of the aqueous system decreases with increasing temperature, while the gaseous system displays a slight increase of cell voltage. This rather unexpected behaviour of the gaseous system is due to the negative entropy term in this reaction.
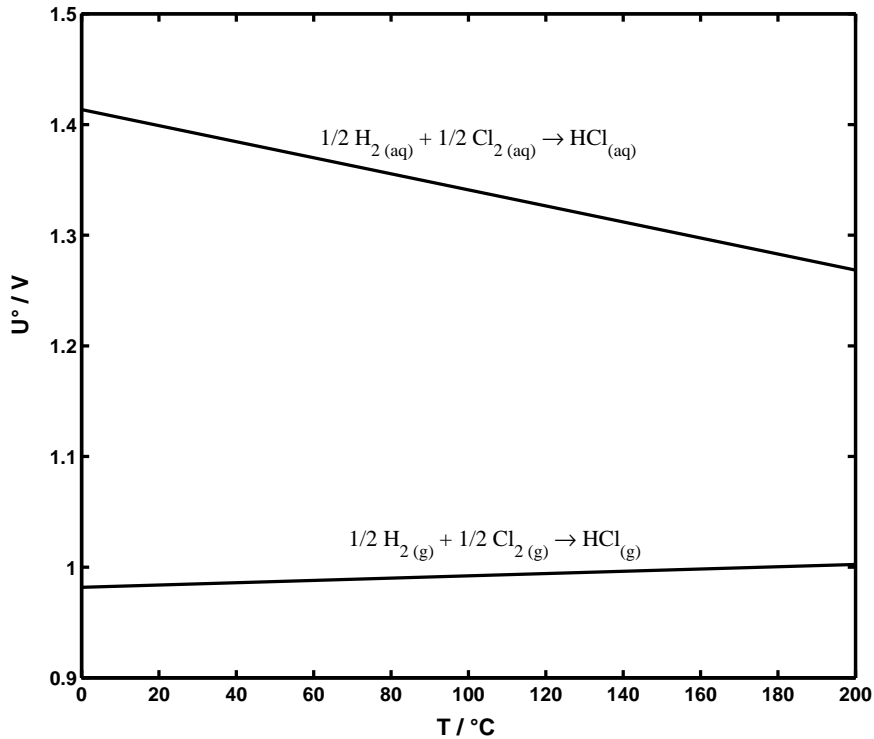
Figure 3.4: Temperature dependence of the thermodynamic cell voltages of the hydrogen - chlorine fuel cell with an aqueous or gaseous phase reaction

3.4.2 Nafion PEM fuel cell

The results of steady state polarisation of the Nafion fuel cell using oxygen and chlorine as cathode feed are given in Figure 3.5. The cells are operated at 60 °C and with gas humidification of both anode and cathode gases.

It can be observed that the open circuit voltage is drastically increased (from 0.9 V to 1.35 V) when switching from oxygen to chlorine as oxidant. However, the maximum electric power output is not increased. The data points from the polarisation of the chlorine fed cell show a much larger scatter than for the oxygen fuel cell as the current output at a given potential constantly decreases with time. This demonstrates the unstable behaviour of the system
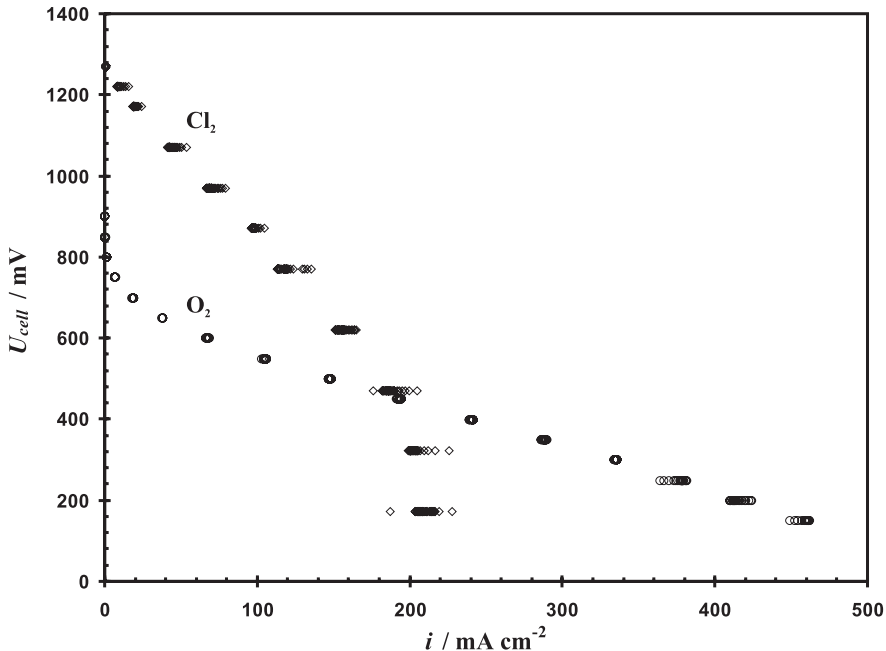
Figure 3.5: Polarisation curves obtained from Nafion fuel cell operated on oxygen and chlorine at 60 °C

compared to the oxygen fuelled cell. It is also clearly seen that the resistance of the cell fed with chlorine is much higher than that of the oxygen cell, as the slope of the Cl_2 polarisation curve is much steeper than that for oxygen. This indication of a membrane conductivity decrease was further investigated by electrochemical impedance spectroscopy at various potentials. This showed values for the cell resistance of 0.35 Ω for the oxygen cell and a value of 0.5-1.0 Ω for the chlorine fed cell. This increase of the cell resistance is most probably due to the removal of water in the membrane by the produced hydrochloric acid. A reduction of the water content in the Nafion membrane will drastically reduce the proton conductivity and thus yield a higher ohmic resistance in the cell [38]. A reduction of the electrolyte conductivity will also influence the potential and current distribution in the porous electrodes so that the utilisation of the available electrocatalyst is reduced.

From Figure 3.5 it can be seen that the overpotential for oxygen reduction

is in the order of 400 mV before any appreciable current is supplied by the cell. For the cell fuelled with chlorine however, a significant amount of current is produced after a polarisation of 50 mV. This strongly indicates that the kinetics of the chlorine reduction reaction is much better than the kinetics for oxygen reduction.

3.4.3   Composite aqueous/Nafion electrolyte

A typical steady state polarisation curve of the fuel cell with an electrolyte consisting of both a liquid circulating electrolyte and a Nafion membrane is shown in Figure 3.6. It can be observed from the linear current/potential curve at low currents that the open circuit potential is close to the thermodynamical value and that the activation overpotential appears to be small. A mass transport controlled behaviour is apparent at current densities above 0.3 A cm^{-2}.

Under operation, leakage of electrolyte through the electrodes and into the gas channels was a constant problem, especially on the cathode side. Intrusion of chlorine gas into the electrolyte was also frequently observed. Multiple electrodes with varying amounts of Teflon impregnation, both in the gas diffusion layer and the catalyst layer, was tested and a reduction of leakage was observed with high degrees of electrode wet proofing. However, no significant difference in the performance or operating stability of the fuel cell could be established. In addition to an irregular cell performance, the reproducibility between identical electrodes was poor.

The high open circuit voltage of this fuel cell indicates that the majority of the produced HCl is dissolved in the aqueous phase. At standard conditions, the thermodynamical potential of the chlorine electrode is 1.36 V for formation of aqueous HCl compared to 0.98 V for gaseous HCl. In this system, with an aqueous electrolyte in which the formed HCl is dissolved, the liquid phase has to be circulated to remove the product from the cell. A gradual increase of the concentration of HCl in the electrolyte itself would unavoidably cause an unevenness of the current distribution along the electrode and/or through the stack due to a change of the reversible voltage of the system, as shown in the mathematical model presented in chapter 4.
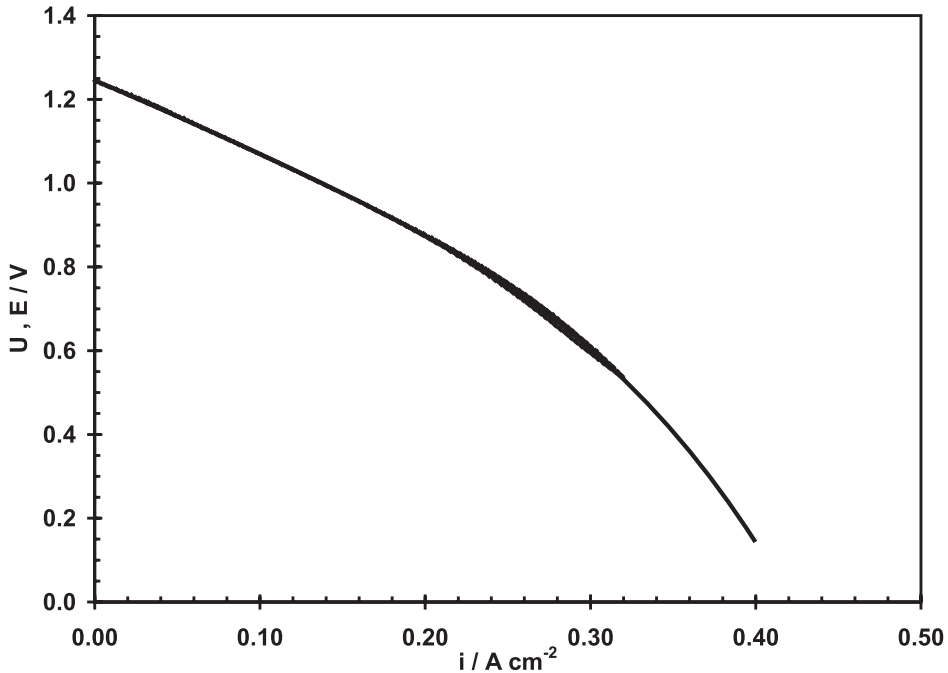
Figure 3.6: Polarisation curves obtained from the composite fuel cell operated on 3 mol dm^{-3} HCl and an operating temperature of 25 °C

3.4.4   PBI fuel cell

Polarization curves

Figure 3.7 shows polarisation curves for the PBI fuel cell running on oxygen (full lines) and chlorine (dashed lines) at 175 °C. There is a significant difference in the open circuit cell voltage when operating on either oxygen or chlorine. The OCP of the oxygen-fed cell lies several hundred millivolts below the thermo-dynamical value, while for chlorine the theoretical and actual cell voltage is nearly identical. The different lines are polarisations recorded in chronological order, from (a) to (f). The first polarisation (a) was performed using oxygen as feed. The feed was then changed to chlorine and curves (b) to (d) was recorded successively. The feed was then changed back to oxygen and curves (e) and (f) was recorded with an hour of operation at 0.4 V between the curves.
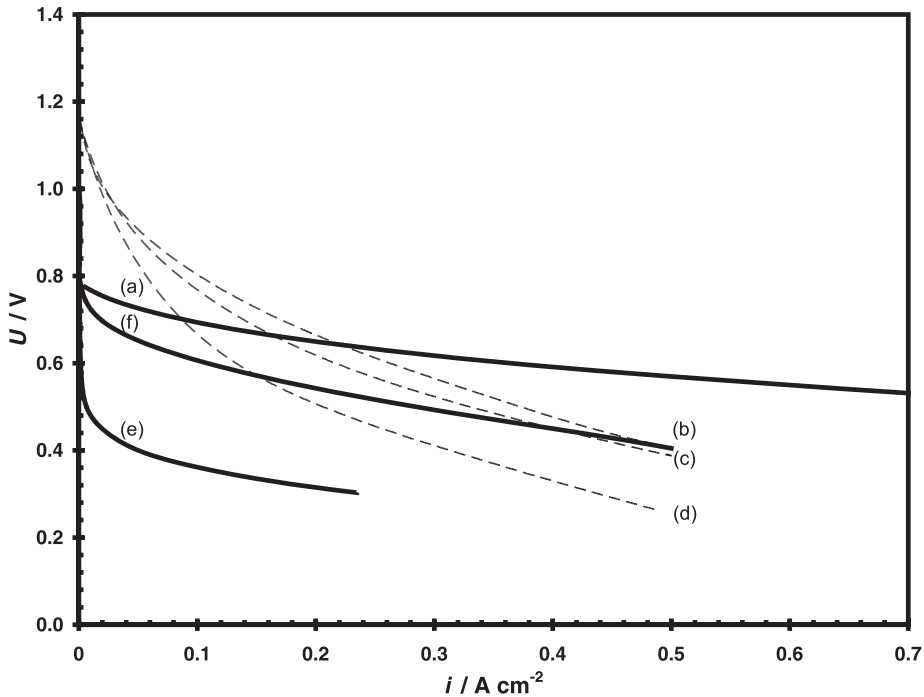
Figure 3.7: Polarisation curves obtained from PBI fuel cell operated at 175 °C on oxygen and chlorine. Curve a is the original polarisation curve of the cell fed with O_2 and H_2, curves b,c and d are polarisations (in chronological order) while the cell is fed with Cl_2. Curves e and f are cell polarisations with O_2 after Cl_2 operation

The open circuit voltage of the cell when operated on chlorine is 1.15 V, which is close the thermodynamical potential for formation of aqueous HCl. This indicates that the produced HCl is formed as a dissolved species in the immobilized phosphoric acid in the polymer matrix and not directly as gaseous HCl. Based on the high open circuit voltage it can be assumed that the kinetics for the reduction of chlorine is rapid also in this system. The three curves b, c and d are as previously stated recorded in chronological order and it is clearly seen that the performance of the fuel cell decreases rapidly with time. This decrease could be attributed to either catalyst degradation, reduction of the ionic conductivity of the polymer electrolyte or a combination of these. The cell was then switched to an oxygen feed, and a polarization curve was recorded (curve e). As can be seen, the resulting performance of the fuel cell was poor. It was,

however, observed a slight increase in the performance during the recording of the polarisation curve and after running the cell at 0.4 V for approximately one hour, another polarisation curve was recored (curve f). The curve shows that the performance of the fuel cell had improved drastically and approached the performance of the cell prior to exposing it to chlorine.

Resistance measurements

To further elucidate the cause of the reduction in cell performance when feeding the cell with chlorine, current interrupt measurements were performed on the cell while changing the feed from oxygen to chlorine. The current-interrupt resistance measurements of the PBI fuel cell can be seen in Figure 3.8. The open circles represent the cell resistance (R_{cell}) and voltage (U_c), while the open squares are the calculated iR-free cell voltage. When fed with oxygen, the value of the cell resistance was found to be close to 0.2 Ω cm^{-2}. Switching to a chlorine feed, the cell resistance increased rapidly reaching values close to 0.5 Ω cm^{-2} within 30 minutes of operation. The resistance further increased to a stable value of 0.55 Ω cm^{-2} during the next two hours. The full lines in Figure 3.8 represent a logarithmic increase/decline of the cell resistance and -voltage respectively, while the dashed curve represent a linear decrease in the iR-corrected cell voltage.

The drastic increase of the cell resistance occuring almost instantaneously after changing to chlorine shows that it is most probably a decrease in the conductivity of the polymer electrolyte that causes the reduction in cell performance and not a degradation of the catalyst. HCl is hygroscopic and is a well known drying agent used in several industrial processes. Most probably, the production of HCl in the fuel cell causes a removal of water from the system and forces the phosphoric acid in the membrane to polymerize to pyrophosphoric acid or higher oligomers [39, 40].

$$\text{H}_3\text{PO}_4 \rightarrow \text{H}_4\text{P}_2\text{O}_7 \rightarrow \text{H} - (\text{HPO}_3)_\text{n} - \text{OH} \tag{3.5}$$
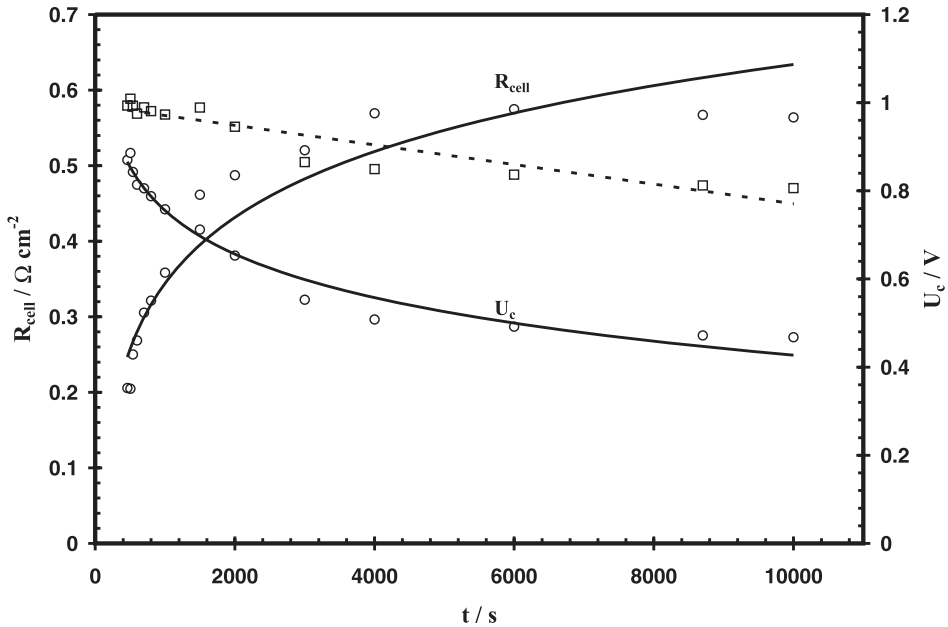
Figure 3.8: Current interrupt measurements of PBI fuel cell switched from oxygen to chlorine feed, galvanostatic operation 0.2 A cm^{-2}. Circles and full lines represent the cell voltage and cell resistance, the open squares and dashed line are the iR corrected cell voltage

This polymerization reaction will reduce the proton transport ability of the electrolyte and thus increase the resistance of the cell. It is also possible that the formed HCl replaces the phosphoric acid in the membrane, the conductivity of HCl-doped PBI being at least 10 times lower than PBI doped with phosphoric acid [41]. However, since the performance increased on reverting to oxygen (Figure 3.7) and the consequential production of water inside the polymer electrolyte, it is more probable that the polymerization of phosphoric acid is the cause of the increased cell resistance.

If an increase of the ohmic resistance in the membrane is the only effect of the dehydration of the membrane, an iR-corrected cell voltage should be constant with time. From Figure 3.7 it can be seen that the iR-corrected cell voltage shows a linear decrease with time, thus a simple increase of the membrane resistance cannot fully explain the reduction in cell performance. A fuel cell

electrode has a porous, three dimensional structure consisting of polymer electrolyte, gas pores and a electronically conductive phase. Considering this, an increase of the resistance of the polymer electrolyte will decrease the effective utilization of the catalyst particles furthest away from the membrane. This is effectively the same as decreasing the active catalytic area of the fuel cell and will have an additional negative effect on the performance of the fuel cell. It is therefore not necessarily any corrosion of the platinum catalyst occuring in this system.

To investigate the possibility of platinum catalyst degradation, an oxide catalyst, expected to be more stable in the relevant environment was tested. An MEA with a cathode containing 2 mg cm^{-2} IrO$_2$ as electrocatalyst was prepared using the same procedure as described in section 3.3.3. However, the fuel cell showed similar behaviour with loss of cell performance and an increase of cell resistance. Thus, a rapid degradation of the cathode platinum electrocatalyst can be considered to be unlikely. The long term catalyst stability however, might be poor. The degree of gas humidification was also increased to see if this could counteract the observed resistance increase. The bubble flasks was immersed in a temperature controlled water bath and the cell was run at a constant potential of 0.6 V. No appreciable change in cell performance was observed on increasing the bath temperature from room temperature up to 80 °C

A possible solution to the problem of water removal and the subsequent conductivity decrease of the PBI membrane might be to include a certain amount of oxygen bleed into the chlorine flow. This addition of oxygen would, at low enough cell voltages, lead to production of water inside the membrane and possibly retard the polymerisation of phosphoric acid.

3.4.5   Comparison of the fuel cell systems

The systems studied possess different properties which are more or less advantageous. All have a rather high open circuit voltage compared to ordinary hydrogen - oxygen fuel cells and the chlorine electrode kinetics is far more beneficial than for the oxygen electrode. Both of these properties lays a good foundation for a fuel cell system with high power density and energy efficiency. However, all of the systems studied suffers from severe stability problems.

The main issue for the two cell designs with a solid polymer electrolyte seems to be the highly hygroscopic nature of HCl. Both systems need a certain amount of

water to maintain an appreciable electrolyte conductivity and with the production of large amounts of HCl the essential part of the water is removed from the system. Even with a high degree of humidification in the Nafion system it was not possible to obtain a proper water management, neither was the low amount of water needed in the PBI system [39, 42] able to remain in the electrolyte.

The composite system was designed to avoid the humidification problem observed in the Nafion system and seemed to fulfill this task. However, the inclusion of the liquid electrolyte dramatically increases the corrosivity of the system since it consists of a highly acidic aqueous solution with large amounts of aggressive chloride anions and dissolved oxidative chlorine. The liquid HCl electrolyte has a low viscosity and the surface tension of HCl solutions is lower than that of water [43]. These physical properties makes it extremely hard to contain the electrolyte and place stringent design conditions on the cell housing, gas diffusion electrodes and auxiliary equipment.

3.5 Conclusions

Three low temperature fuel cell designs were evaluated for use as a hydrogen - chlorine fuel cell for co-production of hydrochloric acid and electric power. It was found that the chlorine reduction kinetics are much faster than the corresponding oxygen reduction reaction, leading to low activation losses at the fuel cell cathode. However, the nature of the reactant, chlorine, and the product, HCl, places strict demands on the corrosion resistance of the construction materials and drastically increases the difficulties related to water management in the cells. Due to these effects, none of the investigated systems were able to demonstrate stable operation under the conditions used in this study. The PBI cell showed best potential and seems to be the system in which the humidification and corrosion difficulties easiest can be remedied. The first design criteria for such a system should be the minimisation of the existence of liquid water, ideally a hydrogen/chlorine fuel cell system should operate in totally water free environment and consist of a high temperature proton conductor.

Chapter 4

Computational Model of a Hydrogen - Chlorine Fuel Cell

M. Thomassen[1], B. Børresen[1], K. Scott[2], R. Tunold[1]

[1]*Department of Materials Technology*

Norwegian University of Science and Technology

NO-7491 Trondheim, Norway

[2]*School of Chemical Engineering and Advanced Materials*

University of Newcastle upon Tyne

Newcastle upon Tyne, NE1 7RU, UK

4.1   Abstract

A two dimensional, isothermal mathematical model of an H_2 - Cl_2 single fuel cell with an aqueous HCl electrolyte is presented. The model focuses on the electrode reactions in the chlorine cathode and also includes the mass and momentum balances for the electrolyte and cathode gas diffusion layer. There is good agreement between the model predictions and experimental results. Distributions of physical parameters such as reactant and product concentrations, solution and solid phase potentials and local current densities and overpotentials as a function of cell voltage are presented. Effects of varying the initial electrolyte concentration and operating pressure are analysed. It was found that an electrolyte inlet concentration of 6 mol dm^{-3} gave the best cell performance and that an increase of operating pressure gave a steady increase of the fuel cell performance.

4.2   Introduction

Fuel cells are in general used as generators of electric energy, either for mobile or stationary applications. In a H_2 - Cl_2 fuel cell, oxygen is replaced by chlorine as the oxidizing agent, hence, the product from this cell is not water, but hydrogen chloride. Consequently, the H_2 - Cl_2 fuel cell is as much an electrochemical reactor as a generator of electric power. The use of H_2 - Cl_2 fuel cells for co-production of hydrochloric acid and electric power in industrial applications has been proposed for plants having an excess of hydrogen and chlorine readily available; the chlor-alkali industry has a potential for energy savings with the use of H_2 - Cl_2 fuel cells [23]. The use of H_2 - Cl_2 fuel cells in industrial processes where chlorine is produced as a by-product, for example in magnesium electrolysis, can also be beneficial. H_2 - Cl_2 fuel cells have also been proposed for space applications [19] and for distributed energy storage systems [16,18,24].

A mathematical model of a fuel cell provides a better understanding of the complex, coupled phenomena that occurs in such systems, as well as useful information for scale-up and design. It also enables prediction of the cell performance as a function of operating conditions. To our knowledge, no mathematical models of H_2 - Cl_2 fuel cells have previously been presented in the literature. However, the system has strong resemblances to the alkaline fuel cell, of which several models have been presented [44,45]. In addition, the system also has similarities with the PEM fuel cell which has been extensively modeled [46–55].

In this paper, a two dimensional, isothermal model for a single cell of a hydrogen chlorine fuel cell is presented. The model considers four of the six layers of the H_2 - Cl_2 single cell; membrane, separator, cathode catalyst layer and the cathode gas diffusion layer. The mathematical model is solved using the Femlab 3.0a$^{\circledR}$ program package and the chemical engineering toolbox from Comsol AB. Profiles of local overpotential, current density and electrolyte concentration are obtained as a function of cell voltage and electrolyte concentration.

4.3   Description of system

The H_2 - Cl_2 - FC single cell considered in this study consists of six layers; an anode gas diffusion layer, an anode catalyst layer, a Nafion$^{\circledR}$-117 membrane, a separator layer, a cathode catalyst layer and a cathode gas diffusion layer. A schematic diagram of the cell is shown in Figure 4.1. The anode is a conventional PEMFC-electrode, based either on a carbon cloth or carbon paper, with a thin layer of Pt/C electrocatalyst bonded to a Nafion$^{\circledR}$-117 membrane. The separator layer consists of a porous PPS (polyphenylene sulphide)-cloth and a circulating hydrochloric acid electrolyte. The cathode is constructed of a highly Teflon -impregnated carbon paper acting as the gas diffusion layer and a thin, porous catalytic layer consisting of RuO_2 particles.

The most distinct feature of the H_2 - Cl_2 fuel cell is the cathode catalyst layer and the separator (electrolyte) layer. To simplify the model, the anode gas diffusion and catalyst layers are considered to play a negligible role in the overall performance of the cell, due to the rapid hydrogen oxidation kinetics and high diffusivity, and are thus omitted from the mathematical model. In addition, the Nafion$^{\circledR}$ 117 membrane is considered to be both an ideal proton conductor with a constant conductivity and an impermeable barrier for the electrolyte, its dissolved species and gaseous hydrogen. The gaseous chlorine supplied to the cathode gas chamber diffuses across the cathode gas-diffusion layer and the catalyst layer through macropores in the electrode. The chlorine then dissolves in the electrolyte in the catalyst layer, diffuses through the electrolyte film covering the catalyst particles and reacts electrochemically on the catalyst surface according to the following reaction:

$$Cl_{2,(aq)} + 2e^- \rightleftharpoons 2Cl^- \tag{4.1}$$

The electrons needed by the above reaction move from the current collector,

across the gas-diffusion and catalyst layers where they are consumed by the chlorine reduction reaction. The product, hydrochloric acid, either diffuses into the bulk electrolyte (separator layer) or evaporates and diffuses through the gas diffusion layer and into the gas channels. Each layer of the cell is assumed to be a superposition of two or more continua. This assumption is based on the porous electrode model presented by Newman [56]. It is also assumed that in the gas diffusion electrode, the micropores are occupied only by the liquid phase and the macropores only by the gas phase.
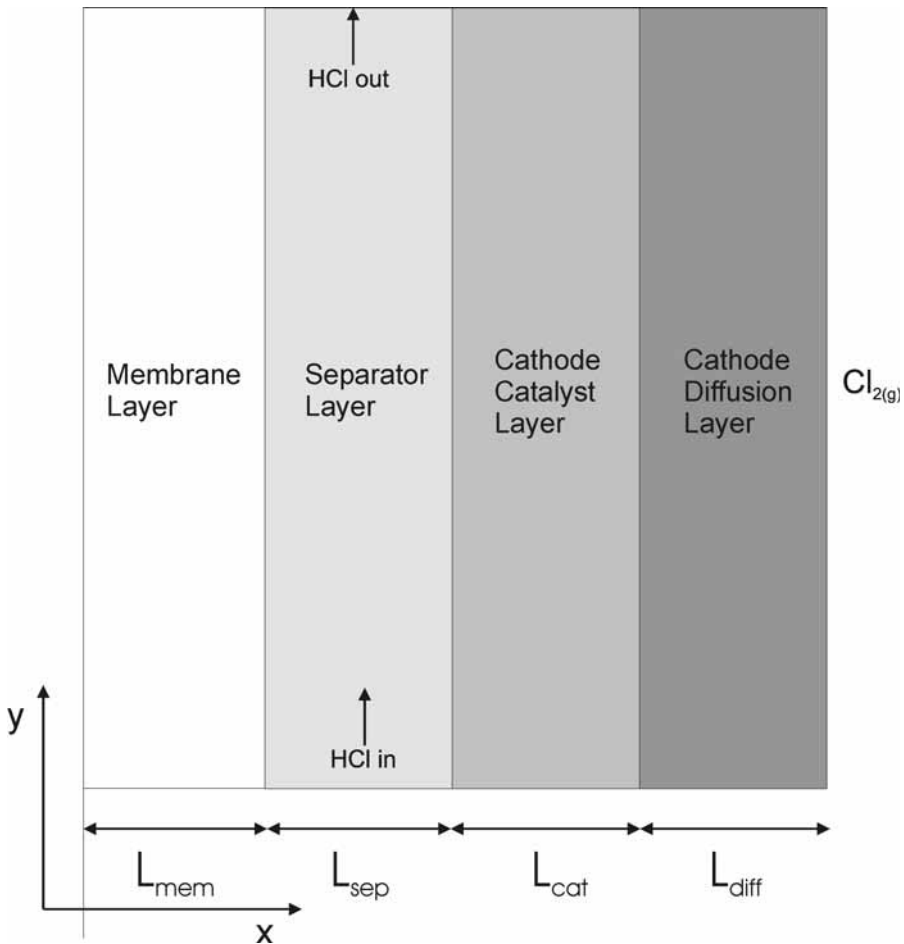
Figure 4.1: Schematic diagram of the H_2 - Cl_2 - FC single cell

4.4 Mathematical modeling

4.4.1 Governing equations

The equation of continuity for species i in a porous medium can be written in the general form:

$$\frac{\partial \epsilon c_i}{\partial t} = -\nabla N_i + R_i^e + R_i^p \tag{4.2}$$

Where

$$
\begin{aligned}
\epsilon &= \quad \text{porosity} \\
t &= \quad \text{time} \\
c_i &= \quad \text{concentration of species } i \\
N_i &= \quad \text{molar flux of species } i \\
R_i^e &= \quad \text{electrochemical reaction rate of species } i \text{ per unit volume} \\
R_i^p &= \quad \text{mass transfer rate of species } i \text{ over a phase boundary}
\end{aligned}
$$

4.4.2 The flux expression

The flux expression, N_i, depends on whether the species exists in the gas or liquid phase. It is assumed that only chlorine and hydrogen chloride exists in the gas phase, thus Fick's law for binary diffusion can be used

$$N_i^g = -D_i^{'g}\nabla p_i \tag{4.3}$$

Where

$$
\begin{aligned}
D_i^{'g} &= \quad \text{effective gas diffusivity of species } i \\
p^i &= \quad \text{partial pressure of species } i
\end{aligned}
$$

For the liquid phase it is assumed that the flux equation for dilute solutions can be employed:

$$N_i^l = -D_i^{'l}\nabla c_i - z_i u_i' F c_i \nabla \Phi + c_i v \tag{4.4}$$

Where

$$
\begin{aligned}
F &= \quad \text{Faraday's constant} \\
\Phi &= \quad \text{solution phase potential} \\
D_i^{'l} &= \quad \text{effective liquid phase diffusivity of species } i
\end{aligned}
$$

$$
\begin{array}{rcl}
z_i & = & \text{charge number, species } i \\
u_i^{'} & = & \text{effective mobility, species } i \\
v & = & \text{volume average velocity}
\end{array}
$$

The effective diffusivity and mobility is corrected for porosity and tortuosity by applying the Bruggemann correction [56]:

$$
\begin{array}{rcl}
D_i^{'} & = & D_i \epsilon^{1.5} \\
u_i^{'} & = & u_i \epsilon^{1.5}
\end{array}
\tag{4.5}
$$
$$
\tag{4.6}
$$

Where D_i and u_i are the free stream diffusivity and mobility of species i respectively.

Interfacial mass transfer

With the assumption of equilibrium at the gas-electrolyte interface the mass transport rate, R_i^p, for species i across a phase boundary can be approximated to:

$$
R_i^p = -a^g D_i^l \left(\frac{H_i p_i - c_i}{\delta} \right)
\tag{4.7}
$$

Where

$$
\begin{array}{rcl}
a^g & = & \text{specific area of the gas-electrolyte interface} \\
H_i & = & \text{Henry's law constant of species } i \\
\delta & = & \text{thickness of electrolyte film}
\end{array}
$$

Electrochemical reaction rate

The electrochemical reaction rate of species i per unit volume, R_i^e, can be represented by:

$$
R_i^e = -\frac{s_i a^l i}{nF}
\tag{4.8}
$$

Where

$$
\begin{array}{rcl}
a^l & = & \text{specific area of the catalyst-electrolyte interface} \\
n & = & \text{number of electrons transferred}
\end{array}
$$

$$i \quad = \quad \text{local current density}$$
$$s_i \quad = \quad \text{stoichiometric coefficient of species } i$$

The stoichiometric coefficient is given by expressing an electrochemical reaction in the form:

$$\sum_i s_i M_i^{z_i} \rightarrow ne^- \tag{4.9}$$

Where M_i is a symbol for the chemical formula of species i.

The local current density, i, can be described by the Butler-Volmer equation:

$$i = i_0 \left[\prod_i \left(\frac{c_i}{c_i^0} \right)^{m_i} \exp \left(\frac{\alpha_a n F \eta}{RT} \right) - \prod_j \left(\frac{c_j}{c_j^0} \right)^{m_j} \exp \left(\frac{-\alpha_c n F \eta}{RT} \right) \right] \tag{4.10}$$

Where

$$i_0 \quad = \quad \text{exchange current density}$$
$$c_i^0 \quad = \quad \text{concentration of species } i \text{ at a reference condition}$$
$$m_i \quad = \quad \text{reaction order of species } i$$
$$\alpha_a \quad = \quad \text{apparent anodic transfer coefficient}$$
$$\alpha_c \quad = \quad \text{apparent cathodic transfer coefficient}$$

The local overpotential, η, is given by:

$$\eta = U - \Phi - E^{rev} \tag{4.11}$$

Where

$$U \quad = \quad \text{electrical potential of an electronically conductive solid phase}$$
$$E^{rev} = \quad \text{reversible electrode potential at the given concentrations}$$

E^{rev} is given by:

$$E^{rev} = E^0 - \frac{RT}{nF} \sum_i s_i \ln \left(\frac{c_i}{c_i^0} \right) \tag{4.12}$$

Where E^0 is the theoretical open circuit potential at standard conditions

Electroneutrality

In the liquid phase the distribution of the charged species must obey the electroneutrality condition:

$$\sum_i z_i c_i = 0 \tag{4.13}$$

4.4.3   Membrane layer

There are no electrochemical reactions in this layer and there are no gas, liquid or electronic conductive phases present. It is assumed that the potential drop in this layer can be described by Ohm's law.

$$\nabla E = \frac{I}{\kappa_m} \tag{4.14}$$

Where I is the total current of the single cell and κ_m the conductivity of the membrane. Since there are no electrochemical reactions occurring in this layer, the current density is constant. By differentiating Eq. 4.14, the potential drop in the membrane can be expressed as:

$$\nabla^2 U_{mem} = 0 \tag{4.15}$$

4.4.4   Separator (electrolyte) layer

There are no electrochemical reactions in this layer and there are no gas phase or electrically conductive solid phase present. Four species exists in this layer; liquid water, dissolved chlorine and two ions; $H^+_{(aq)}$ and $Cl^-_{(aq)}$. By employing the continuity equation and the transport equations to all species, except water one obtains:

$$\nabla \left(D'_+ \nabla c_+ \right) + \nabla \left(\frac{z_+ D'_+ F}{RT} c_+ \nabla \Phi \right) - \nabla \left(c_+ v \right) = 0 \tag{4.16}$$

$$\nabla \left(D'_{-} \nabla c_{-} \right) + \nabla \left(\frac{z_{-} D'_{-} F}{RT} c_{-} \nabla \Phi \right) - \nabla \left(c_{-} v \right) = 0 \qquad (4.17)$$

$$\nabla \left(D'_{Cl_2} \nabla c_{Cl_2} \right) - \nabla \left(c_{Cl_2} v \right) = 0 \qquad (4.18)$$

Since there are no reactions or mass transfers over phase boundaries in this layer, there is no change in the volume average velocity (neglecting the influence of the density change due to HCl dissolution) :

$$\nabla v = 0 \qquad (4.19)$$

Due to the porous PPS-cloth, which the electrolyte has to flow through, it is assumed that the electrolyte flow in the y-direction can be described by a plug flow characteristic.

4.4.5 Catalyst layer

Assuming that there are no electrochemical reactions in the gas phase of the catalyst layer; gaseous chlorine dissolves into the electrolyte before reacting. The product, HCl, either diffuses into the bulk electrolyte or evaporates into the gas phase and diffuses to the gas channels. Because of the low vapour pressure of water at 25 °C it is assumed that there is negligible amounts of water vapour in the gas phase, thus the transport equation for chlorine gas becomes:

$$N_{Cl_2} = -D'_{Cl_2} \nabla p_{Cl_2} \qquad (4.20)$$

and the following equation can be obtained from the continuity equation:

$$\nabla \left(D'^{g}_{Cl_2} \nabla p_{Cl_2} \right) - a^{g}_{c} D'^{g}_{Cl_2} \left(\frac{H_{Cl_2} p_{Cl_2} - c_{Cl_2}}{\delta_c} \right) = 0 \qquad (4.21)$$

In the liquid phase, the mass transport of the dissolved reactant gases can be written by using the Nernst-Planck equation (Eq. 4.4). Since the dissolved chlorine gas is an electrically neutral specie, the second term on the right hand side is zero. The dissolved gas reacts electrochemically at the catalyst-electrolyte interface, thus the following equation is obtained at steady state:

$$\nabla \left(D_{Cl_2}^{'l} \nabla c_{Cl_2} \right) - \nabla \left(c_{Cl_2} v \right) + a_c^g D_{Cl_2}^{'g} \left(\frac{H_{Cl_2} p_{Cl_2} - c_{Cl_2}}{\delta_c} \right) - \frac{s_{Cl_2} a_c^l i_c}{n_c F} = 0 \quad (4.22)$$

The local current density at the cathode, i_c, is described by applying the Butler-Volmer equation to the chlorine reduction reaction:

$$i_c = i_{0,c} \left[\left(\frac{c_-}{c_-^0} \right)^{m_-} \exp \left(\frac{\alpha_a F \eta_c}{RT} \right) - \left(\frac{c_{Cl_2}}{c_{Cl_2}^0} \right)^{m_{Cl_2}} \exp \left(\frac{-\alpha_c F \eta_c}{RT} \right) \right] \quad (4.23)$$

The transport equation for gaseous hydrochloric acid becomes:

$$N_{HCl} = -D_{HCl}^{'} \nabla p_{HCl} \quad (4.24)$$

Thus, the following equation can be obtained from the continuity equation:

$$\nabla \left(D_{HCl}^{'g} \nabla p_{HCl} \right) - a_c^g D_{HCl}^{'g} \left(\frac{p_{HCl} - p_{HCl}^v}{\delta_c} \right) = 0 \quad (4.25)$$

Where p_{HCl}^v is the concentration dependent vapour pressure of HCl.

Protons do not react electrochemically at the cathode, while the electrochemical reaction rate for chloride ions follows Eq. 4.8. Thus, using the continuity, flux and Butler-Volmer equations, we get:

$$\nabla \left(D_+^{'l} \nabla c_+ \right) + z_+ F \nabla \left(u_+ c_+ \nabla \Phi \right) - \nabla \left(c_+ v \right) \quad (4.26)$$
$$+ a_c^g D_{HCl}^{'g} \left(\frac{p_{HCl} - p_{HCl}^v}{\delta_c} \right) = 0$$

$$\nabla \left(D_-^{'l} \nabla c_- \right) + z_- F \nabla \left(u_- c_- \nabla \Phi \right) - \nabla \left(c_- v \right) - \frac{s_- a_c^l i_c}{n_c F} \quad (4.27)$$
$$+ a_c^g D_{HCl}^{'g} \left(\frac{p_{HCl} - p_{HCl}^v}{\delta_c} \right) = 0$$

The total current density, I, obtained from the single cell must be equal to the integrated value of the local current density, i, with respect to the thickness (x) of the cathode catalyst layer:

$$I = - \int\limits_{0}^{L_{cat}} a^l i \, dz \tag{4.28}$$

As for the membrane layer, Ohm's law can describe the potential drop in the solid catalyst particles. Differentiating Eq. 4.28 and combining it with Ohm's law gives the following expression for the potential drop in the cathode catalyst layer:

$$\nabla^2 E = \frac{a_c^l i_c}{\kappa_c} \tag{4.29}$$

Where κ_c is the effective electrical conductivity of the cathode.

4.4.6 Gas diffusion layer

There are no electrochemical reactions in this layer; gaseous chlorine diffuses from the gas channels towards the catalyst layer while the product, HCl, diffuses from the catalyst layer towards the gas channels. As for the catalyst layer, it is assumed that no water vapour exists in the gas phase. The transport equation for chlorine gas and gaseous hydrochloric acid becomes:

$$N_i = -D_i^{'} \nabla p_i \tag{4.30}$$

As for the catalyst layer, the potential drop can be described by Ohm's law:

$$\nabla E = \frac{I}{\kappa_m} \tag{4.31}$$

Where κ_d is the effective conductivity of the diffusion layer. Since no electrochemical reactions occur in the gas diffusion layer, I is constant. By differentiating Eq. 4.31, the potential drop in the layer can be expressed as:

$$\nabla^2 U_{diff} = 0 \tag{4.32}$$

4.4.7   Boundary conditions

Anode / Membrane interface

At this interface only protons are transferred and the flux of protons must be equal to the total current density:

$$N_+|_{SEP} = \frac{I}{nF} \tag{4.33}$$

Since the anode has been omitted from this model, the electrical potential at the anode/membrane interface can be arbitrarily fixed. Hence, the membrane potential at this boundary is set to zero:

$$\Phi_{mem}|_{AN} = 0 \tag{4.34}$$

Membrane / Separator interface

The membrane acts as an impermeable barrier for the electrolyte and its dissolved species. Thus, the fluxes of anions and chlorine are zero, while the flux of protons is continuous at this interface

$$N_{Cl_{2,(aq)}}\Big|_{SEP} = 0 \tag{4.35}$$
$$N_-|_{SEP} = 0 \tag{4.36}$$
$$N_+|_{MEM} = N_+|_{SEP} \tag{4.37}$$

The solution potential is equal to the membrane potential.

$$\Phi_{mem}|_{MEM} = \Phi_{sep}|_{SEP} \tag{4.38}$$

Separator / Cathode catalyst interface

It is assumed that the PPS-separator prevents gaseous reactants from flowing towards the opposite electrode. Thus the fluxes of gaseous chlorine and hydrochloric acid are zero at this interface:

$$N_{i(g)}\big|_{CCL} = 0 \Rightarrow \nabla p_i\big|_{CCL} = 0 \tag{4.39}$$

Since the separator is an electronic insulator, the electronic current density in this layer is zero:

$$\nabla E_C\big|_{CCL} = 0 \tag{4.40}$$

The fluxes of dissolved chlorine and ions are continuous at this interface:

$$N_+\big|_{CCL} = N_+\big|_{SEP} \tag{4.41}$$
$$N_-\big|_{CCL} = N_-\big|_{SEP} \tag{4.42}$$
$$N_{Cl_{2(aq)}}\big|_{CCL} = N_{Cl_{2(aq)}}\big|_{SEP} \tag{4.43}$$

Cathode catalyst / Gas diffusion layer interface

Since the gas-diffusion layer prevents leakage of electrolyte, it is assumed that the fluxes of the electrolyte and its dissolved species are zero at this boundary. The fluxes of chlorine gas and gaseous hydrochloric acid are continuous at this boundary.

$$N_{i(g)}\big|_{DIFF} = N_{i(g)}\big|_{CCL} \tag{4.44}$$
$$N_+\big|_{DIFF} = 0 \tag{4.45}$$
$$N_-\big|_{DIFF} = 0 \tag{4.46}$$
$$N_{Cl_{2,(aq)}}\big|_{DIFF} = 0 \tag{4.47}$$

Gas diffusion layer / Gas channel interface

The electrical potential can be arbitrarily fixed either at the anode or cathode current collector. Setting the value of the anode to zero, U_c at this interface will be:

$$U_c = U_{cell} \tag{4.48}$$

Where U_{cell} is the total cell voltage.

Assuming a uniform distribution of gases in the gas channels, the partial pressure of chlorine and hydrochloric acid can be set to:

$$
\begin{aligned}
p_{Cl_2} &= p_{Cl_2}^0 & \text{(4.49)}\\
p_{HCl} &= 0 & \text{(4.50)}
\end{aligned}
$$

Electrolyte inlet

At $y = 0$, the electrolyte concentration and volume average velocity is known. It is also assumed that the chlorine concentration in the supplied electrolyte is equal to 1% of the saturation amount since the electrolyte is recycled and removal of all chlorine gas from this electrolyte is difficult.

$$
\begin{aligned}
c_e|_{y=0} &= c_e^0 & \text{(4.51)}\\
v_x|_{y=0} &= v_x^0 & \text{(4.52)}\\
c_{Cl_2}|_{y=0} &= 0.01 \cdot c_{Cl_2,sat} & \text{(4.53)}
\end{aligned}
$$

Electrolyte outlet

At $y = 1$, the change in electrolyte and chlorine concentration is zero. It is assumed that the mass transport due to diffusion and migration is negligible compared to the convective flux.

$$
\begin{aligned}
\nabla \left(c_e|_{y=1} \right) &= 0 & \text{(4.54)}\\
\nabla \left(c_{Cl_2,(aq)}\big|_{y=1} \right) &= 0 & \text{(4.55)}\\
\nabla \left(v_y|_{y=1} \right) &= 0 & \text{(4.56)}
\end{aligned}
$$

4.5 Model parameters and correlation

Using realistic values for the modeling parameters are essential for the viability
of the mathematical model. A reasonable choice of the parameter values is thus
as important as the mathematical modeling itself. Hence, an effort has been
made to supply as realistic values as possible for these parameters.

4.5.1 Thermodynamic properties

Solubility of chlorine

It is assumed that the solubility of chlorine gas obeys Henry's law:

$$c_i = H_i p_i \tag{4.57}$$

The solubility of chlorine changes linearly with the hydrochloric acid concen-
tration in the range applicable for this model. Using the data from [57], the
following correlation was obtained for the solubility of chlorine in hydrochloric
acid at 25 °C

$$H_{Cl_2}\left(c_{H^+}\right) = 0.0077 \cdot c_{H^+} + 6.0 \times 10^{-5} \tag{4.58}$$

Vapour pressure of HCl

The vapour pressure of HCl over hydrochloric acid increases exponentially with
increasing hydrochloric acid concentration. At 25 °C, the following correlation
was obtained using the data from Perry's Chemical Engineers' Handbook [58]:

$$p_{HCl}^v\left(c_{H^+}\right) = 1.0 \times 10^{-10} \exp\left(961.46 c_{H^+}\right) \tag{4.59}$$

Transport properties

The mobility of the electrolyte species changes with electrolyte concentration.
Using the data in [59] the following correlations were obtained:

$$u_{Cl^-} = 7 \cdot 10^{-9} \cdot \exp\left(-171.51 \cdot c_e\right) \tag{4.60}$$

$$u_{H^+} = 4 \cdot 10^{-8} \cdot \exp\left(-171.51 \cdot c_e\right) \tag{4.61}$$

The diffusivities of the charged species were found using the Nernst-Einstein equation:

$$D_i = RTu_i \tag{4.62}$$

The diffusion coefficient for chlorine is assumed not to be influenced by the acid concentration. The diffusion coefficient in 0.1 N HCl at 25 °C has been found to be 1.38×10^{-5} cm^2 s^{-1} [60]. The electrical conductivities of the catalyst and gas diffusion layers are reported to be 7.14 [61] and 12.5 S cm^{-1} respectively. Earlier work from our group [62] investigated the conductivity of Nafion$^{®}$ 117 and found a value of 0.1 S cm^{-1} at 25 °C in a 0.3 mol dm^{-3} HCl solution.

Kinetic parameters

The exchange current density, i_0, for chlorine reduction on RuO$_2$ has been measured to be $\sim 1.0 \times 10^{-5}$ in 1 mol dm^{-3} HCl saturated with Cl$_2$ using the rotating disc electrode technique [29]. The anodic and cathodic Tafel slopes for the chlorine evolution/reduction reaction on RuO$_2$ have been reported by several authors to be 40 and 120 mV dec^{-1} respectively [63, 64]. Thus, the anodic and cathodic transfer coefficients, α_a and α_c, are 0.75 and 0.25 respectively. Since the electrochemical reactions within the cathode catalyst layer are considered to be elementary reactions, the same absolute values as the stoichiometric coefficients are used as reaction orders of the reactants and products. The electrochemical kinetic parameters are listed in Table 4.1.

Structural parameters

The thickness of the cathode catalyst layer was found to be 10 μm by analysing a cross section of an electrode in a scanning electron microscope. The gas diffusion electrode, Toray carbon paper had a thickness of 0.4 mm. The specific surface area of the RuO$_2$ catalyst was 45 - 65 m^2 g^{-1} (Alpha Aesar) and the catalyst

Table 4.1: Electrochemical kinetic parameters

Parameter	Value
Number of electrons transferred, n	2
stoichiometric coefficient of chlorine, s_{Cl_2}	1
stoichiometric coefficient of chloride, s_{Cl^-}	-1
reaction order of chlorine, m_{Cl_2}	1
reaction order of chloride, m_{Cl^-}	2
anodic transfer coefficient, α_a	0.75
cathodic transfer coefficient, α_c	0.25
Exchange current density, i_0 (A cm^{-2})	1.0×10^{-5}

loading was 2 mg cm^{-2}. By assuming perfect wetting of the whole catalyst surface, the specific catalyst-electrode interface area, a^l, can be calculated from:

$$a^l = \frac{d_{cat}}{V_{cat}} \cdot A_{cat} \qquad (4.63)$$

Where

$$
\begin{array}{lll}
d_{cat} & = & \text{catalyst loading (g cm}^{-2}) \\
V_{cat} & = & \text{specific catalyst volume (cm)} \\
A_{cat} & = & \text{catalyst surface area (cm}^2 \text{ g}^{-1})
\end{array}
$$

Hence, the value of a^l in the cathode catalyst layer has a value of 9×10^5 cm^2 cm^{-3}. Several researchers have reported specific gas - electrolyte interface areas of the order of 10^3cm^{2}cm^{-3} and an electrolyte film thickness of $\sim 0.5\mu$m [59,65]. Thus, the values for a^g and δ has been set to 1.0×10^3 and 0.5 μm respectively. The structural parameters are listed in Table 4.2.

Table 4.2: Base case structural parameters

Parameter (unit)	Membrane layer	Separator layer	Catalyst layer	Gas diffusion layer
Layer thickness, L_i (cm)	0.0175	0.08	1.0×10^{-3}	0.04
Gas phase porosity, ϵ^g			0.1	0.7
Liquid phase porosity, ϵ^l		0.5	0.3	
Solid phase porosity, ϵ^s			0.6	0.3
Specific area of gas-electrolyte interface, a^g (cm^{-1})			1.0×10^3	
Specific area of catalyst-electrolyte interface, a^l (cm^{-1})			1.0×10^5	
Thickness of electrolyte film, δ (cm)			5.0×10^{-4}	
Electrical conductivity, (S cm^{-1})	0.10		7.14	12.5

Operating conditions

The operating conditions for the laboratory test cell are ambient temperature and pressure. The base case operating conditions for the model are listed in Table 4.3.

Table 4.3: Base case operating conditions

Parameter (unit)	Value
Electrolyte inlet concentration, C_e (mol cm^{-3})	0.003
Operating temperature, T ($^\circ C$)	25
Operating pressure, p^0 (bar)	1
Electrolyte flow rate, v (cm s^{-1})	0.02

4.5.2 Method of solution

The model equations are highly coupled and non-linear and a numerical solution is required. The finite element method program Femlab$^{®}$ 3.0a with the chemical engineering toolbox from Comsol AB was employed to solve the equations. A multiphysics model incorporating three application modes and six dependent variables was created and a weak, non-linear parametric solver was used to solve the constructed model.

4.6   Results and discussion

The model developed is a two-dimensional model and the fuel cell performance and the distribution of the physical parameters will vary along the cell length (y-axis). It was found that, for the base case electrolyte velocity, this variation was negligible from a distance of 0.05 cm from the electrolyte inlet for all current densities. The results presented in this section are taken from a point 0.5 cm from the electrolyte inlet and is considered to give a good representation of the distribution of the physical parameters inside the whole cell.

4.6.1   Comparison of model with experimental results

A comparison of the model prediction for the base case with experimental data obtained with a 6 cm^2 laboratory test cell operated at 25 °C with an electrolyte inlet concentration of 3 mol dm^{-3} HCl is presented in Figure 4.2. The open squares represent the experimental values while the full line is the model prediction.

4.6.2   Polarisation curve for base case

The polarization curve for the base case presented in Figure 4.2 displays a typical shape for low temperature fuel cells. It includes two of the three distinguishable zones; activation controlled, ohmic controlled and mass transport controlled polarization. The activation-controlled zone is much less pronounced than in similar polarization curves for H$_2$ - O$_2$ fuel cells. This is most probably because the kinetics of chlorine reduction is faster than the kinetics for oxygen reduction; the exchange current density for chlorine reduction on ruthenium oxide is ∼1.0 10^{-5} A cm^{-2}, compared to the exchange current density of oxygen reduction on platinum, which has a value of ∼1.0 10^{-9} A cm^{-2} [66]. The slope of the linear region corresponds to a cell resistance of approximately 0.56 Ω cm^2. The fuel cell has an open circuit voltage of 1.26 V and at a cell voltage of 0.2 V, no limiting current can be observed. Although a slight increase of the slope of the polarization curve can be seen. The maximum power density of the cell is about 0.58 W cm^{-2} at a cell voltage of 0.55 V. The iR drop in the membrane and electrolyte and the cathodic overpotential predicted by the mathematical model are also shown in Figure 4.2. The overpotential dominates the losses at low current densities, while at current densities above 0.6 A cm^{-2} the iR drop
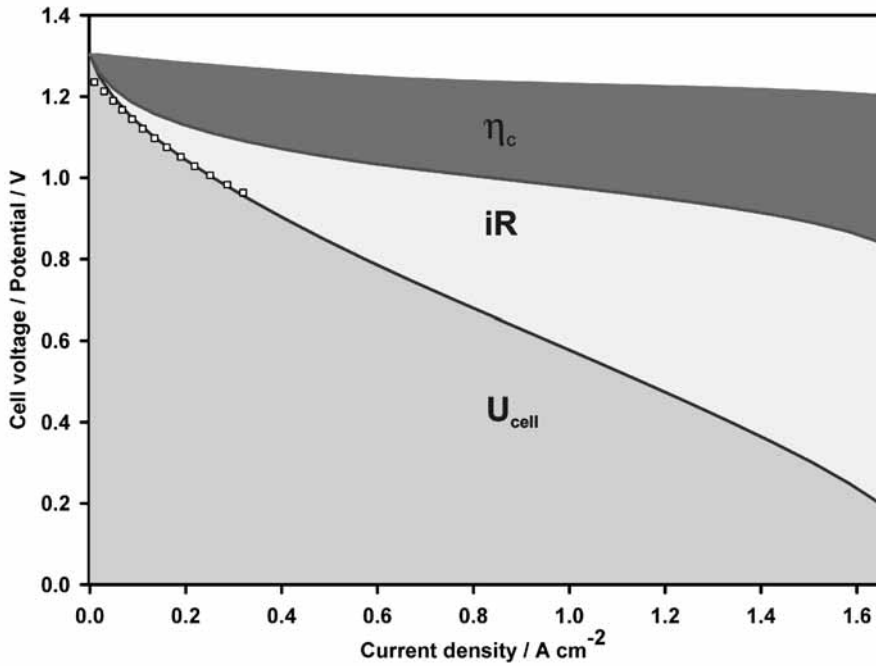
Figure 4.2: Polarisaton curve for base case. The open squares are experimental results from a 6 cm^2 laboratory cell. The cathodic overpotential (η_c) and iR drop of the cell are also shown.

is responsible for more than 50% of the polarization losses. At very high current densities (>1.6 A cm^{-2}), the cathode overvoltage starts to increase more rapidly, indicating an impending mass transport controlled limiting current.

4.6.3   Distribution of physical variables

The distribution of the partial pressure of gaseous chlorine as a function of cell voltage and dimensionless distance (ξ) is given in Figure 4.3. It can be seen that with decreasing cell voltage, the distribution of the partial pressure of chlorine becomes less uniform. At a cell voltage of 0.2 V, the partial pressure of chlorine inside the catalyst layer is approximately 0.85 atm with a small gradient towards the diffusion layer. This indicates that even though there exist a certain mass transfer resistance for the chlorine gas, it is not the factor limiting the total cell performance.
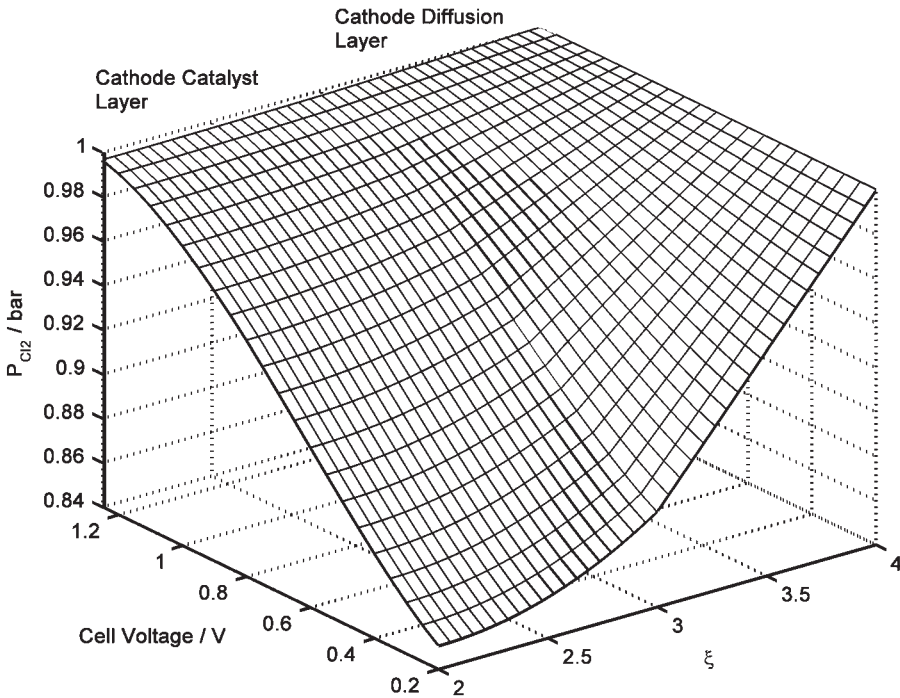
Figure 4.3: Chlorine partial pressure distribution in the cathode catalyst and diffusion layer as a function of cell voltage.

The distribution of dissolved chlorine is shown in Figure 4.4. At cell voltages between 1.2 and 0.9 V there is only a very slight decrease of the chlorine concentration. With a further lowering of the cell voltage an interesting phe-

nomenon occurs; the concentration of dissolved chlorine increases and reaches a peak value at $U_{cell} \approx 0.75V$. Below 0.75 V, the chlorine concentration rapidly decreases. This unexpected behaviour is due to the increasing solubility of chlorine with increasing electrolyte concentration (see Figure 4.5 and Eq. 4.58). At 0.75 V, the electrolyte concentration reaches a plateau value and lowering the cell voltage further increases the electrochemical reduction rate of the chlorine reduction reaction and the concentration of dissolved chlorine drops. The low concentration of dissolved chlorine at low cell voltages indicates that this parameter is the cause of the tendency of a limiting current behaviour observed in Figure 4.2.
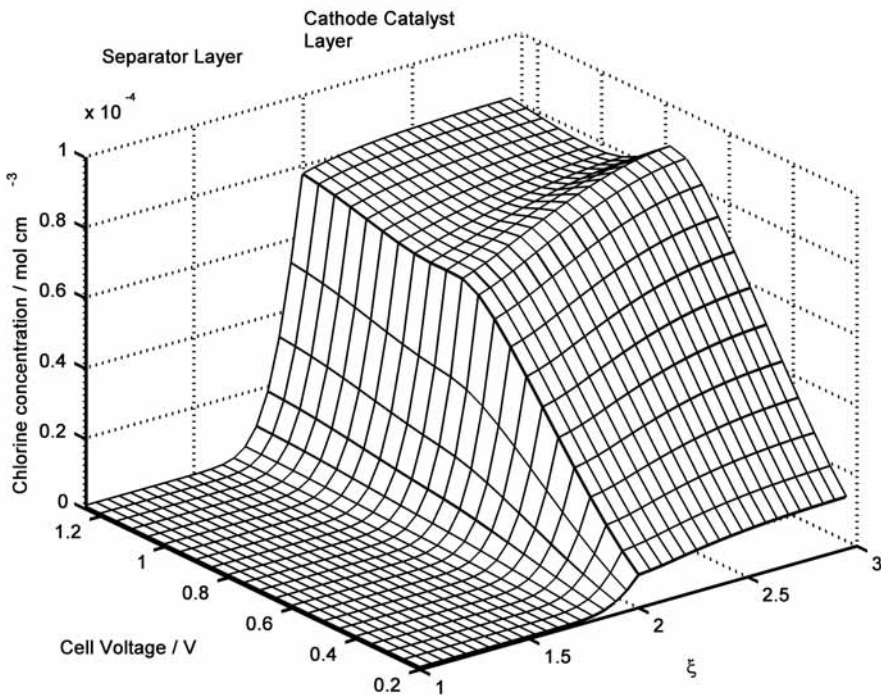
Figure 4.4: Dissolved chlorine concentration distribution in electrolyte and cathode catalyst layers as a function of cell voltage

Figure 4.5 displays the concentration distribution of HCl in the electrolyte as a function of cell voltage. It can be seen that there is a drastic increase in acid concentration with decreasing cell voltage down to 0.6 V where it reaches a

plateau value. This increase is caused by the production of chloride ions from the reduction of chlorine and the diffusional and migrational fluxes of chloride ions are too low to maintain a concentration close to the inlet concentration. This high electrolyte concentration inside the catalyst layer has several effects; it causes a drop in the reversible voltage of the cathodic reaction and exposes the cathode catalyst to a more corrosive environment. Another effect, not taken into consideration in this work, is the possibility of increased adsorption of Cl^- with increasing HCl concentration which may reduce the chlorine reduction rate. The electrolyte has a maximum conductivity at concentrations close to 5 mol dm^{-3}, thus the concentration build-up inside the catalyst layer has a negative effect on the conductivity in this layer, causing a higher ohmic drop. On the other hand, a positive effect of the concentration increase is a higher solubility of chlorine in the catalyst layer.
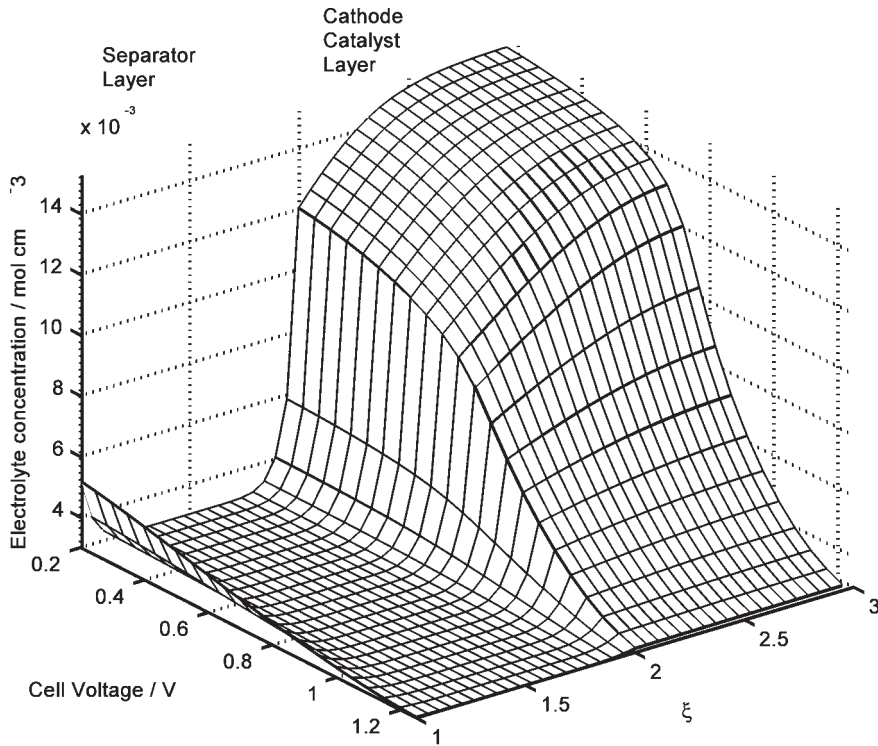
Figure 4.5: Electrolyte concentration distribution in the electrolyte and cathode layer as a function of cell voltage

Figure 4.6 shows the distribution of the partial pressure of gaseous HCl in the catalyst and diffusion layers as a function of cell voltage. The evaporation of HCl has a strong correlation with the concentration of hydrochloric acid in the catalyst layer shown in Figure 4.5. This phenomenon manifests itself only at low cell voltages, where the partial pressure of hydrochloric acid reaches values of approximately 0.15 atm. It does not seem that the mass transport resistance of gaseous hydrochloric acid out of the catalyst layer has any major effect on the cell performance.
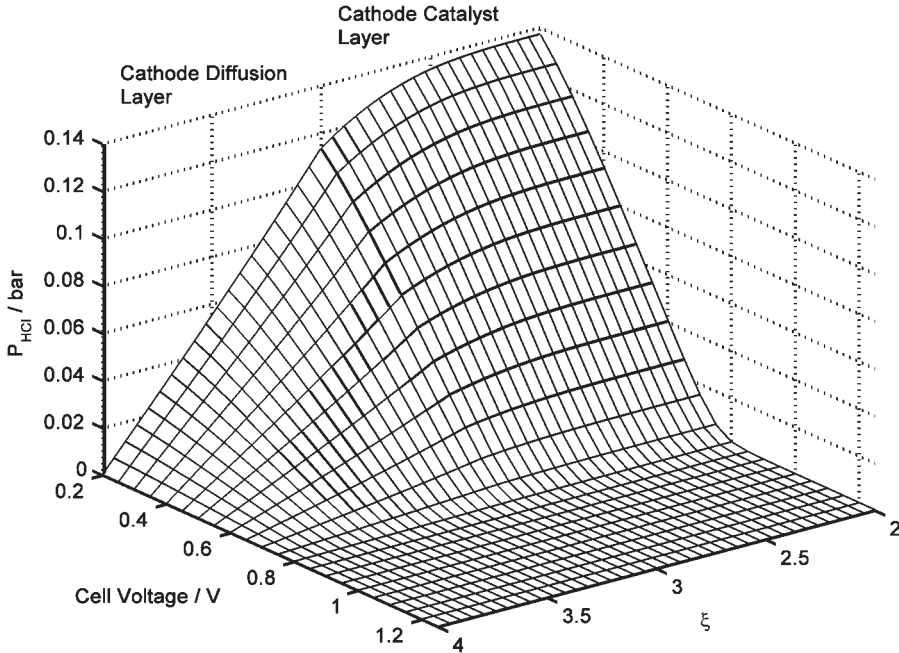
Figure 4.6: HCl partial pressure distribution in the cathode catalyst and diffusion layer as a function of cell voltage.

Figs. 4.7 and 4.8 show the profiles of the local apparent current density and local overvoltage respectively. The distribution of these parameters are very uniform through the catalytic layer at all cell voltages, it is only at low cell voltages that a small curvature close to the separator layer can be seen on the local current density distribution. The local overvoltage of the cathode reaches a value of -0.36 V at a cell voltage of 0.2 V and does not have the typical Tafelian behaviour. This is probably due to the increasing electrolyte concentration and the depletion of dissolved chlorine in the catalyst layer at low cell voltages, which effectively increases the overvoltage value additionally.
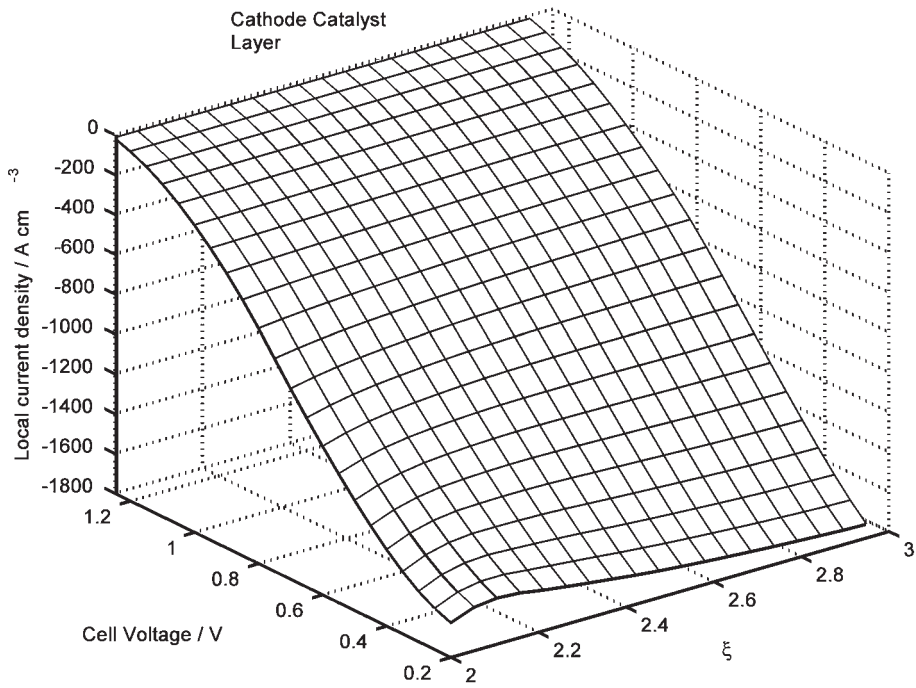
Figure 4.7: Profile of the local current density in the cathode layer as a function of cell voltage.
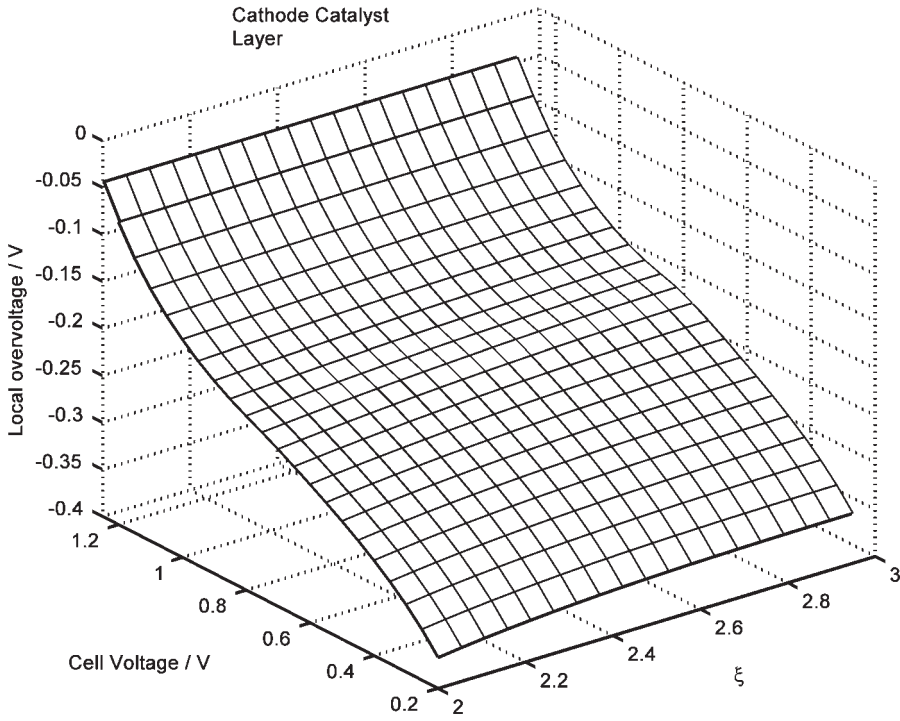
Figure 4.8: Profile of the local overvoltage in the cathode layer as a function of cell voltage.

Figure 4.9 shows the profile of the membrane and solution potentials as a function of cell voltage. The variation across the membrane and separator layers corresponds to the ohmic drop between the electrodes. The potential drop in the cathode catalyst layer is negligible compared to the quite large drops in the separator and membrane layers. The figure also shows that although the separator layer is almost 5 times thicker than the membrane layer, the potential drop across the two layers are nearly equal.
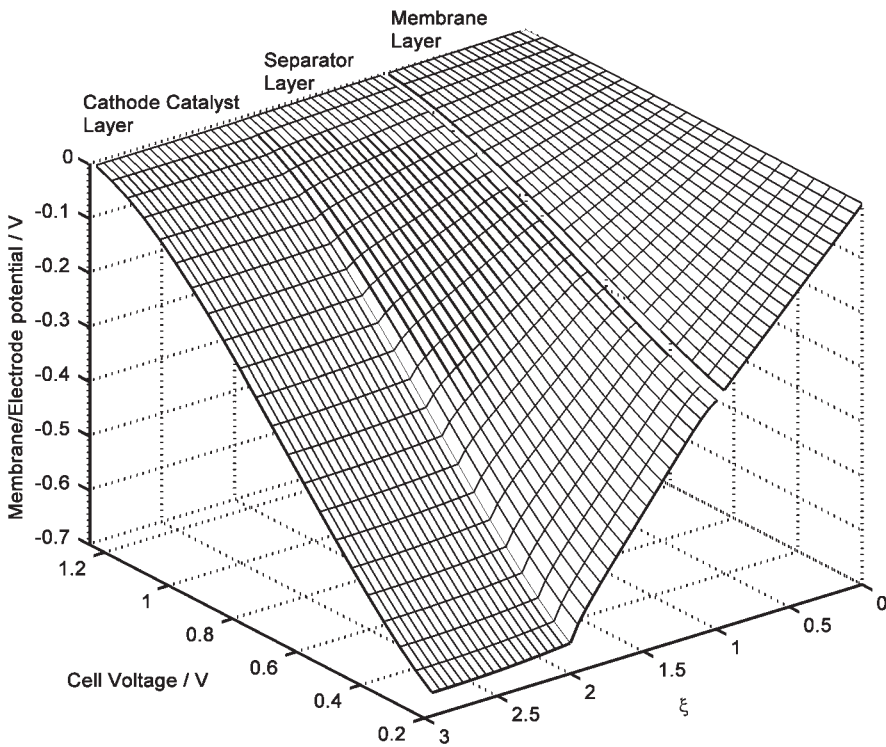
Figure 4.9: Profile of the membrane and solution potentials as a function of cell voltage.

4.6.4   Influence of operating conditions

Initial electrolyte concentration

Since most thermodynamic, transport and kinetic parameters are influenced by the electrolyte concentration, a variation of the initial electrolyte concentration can have a strong effect on the cell performance. For instance, increasing the electrolyte concentration will increase the solubility of chlorine, but above 5 mol dm^{-3}, the conductivity will decrease. In addition, an increase of the chloride concentration will affect the cathode kinetics by increasing the anodic reaction rate and reducing the theoretical open circuit voltage, E_{rev}.

Polarization curves for a single cell with different electrolyte inlet concentrations are given in Figure 4.10. A considerable increase in the cell performance can be seen when increasing the electrolyte concentration from 1 to 3 mol dm^{-3} and as expected, the open circuit voltage drops somewhat. A further increase from 3 to 5 mol dm^{-3} has an negligible effect. This behaviour is also observed experimentally.
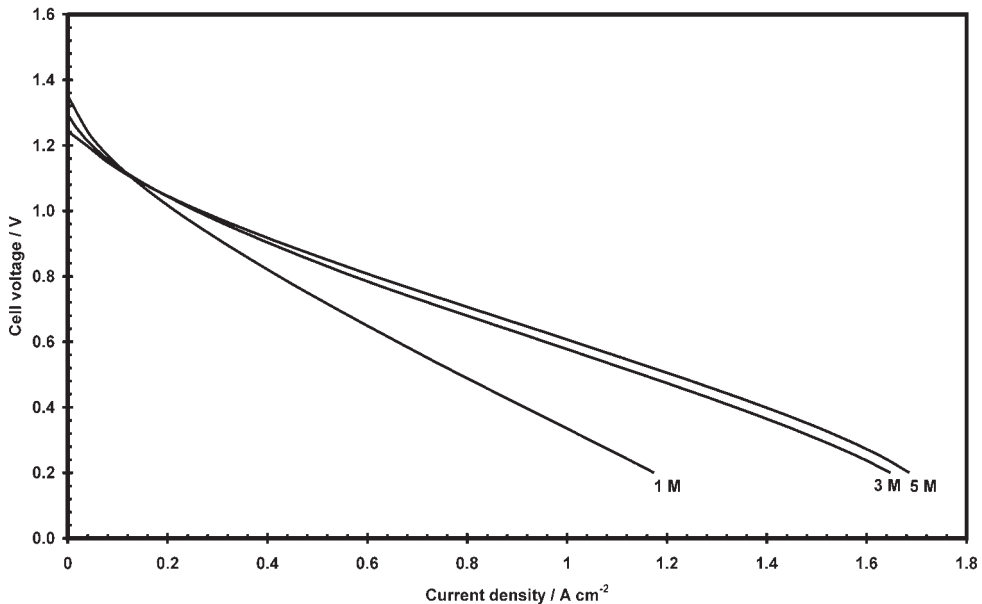
Figure 4.10: Single cell polarization curves at different electrolyte inlet concentrations.

In Figure 4.11, the effect of initial electrolyte concentration on current density as a function of cell voltage is presented. At high cell voltage the variation of electrolyte inlet concentration has a very low effect on the total current density of the cell. At lower cell voltages, the current density increases significantly with increasing concentration from 1 to 3 mol dm^{-3} and moves through a broad maximum at concentrations around 6 mol dm^{-3}. The dashed line in Figure 4.11 shows the conductivity of hydrochloric acid as a function of concentration. It is clear that although the current density concentration dependence have the same trend as the electrolyte conductivity, the effect is not as pronounced. This indicates that other mechanisms, such as electrode kinetics and mass transport, influence the electrolyte concentration dependence of the current density.
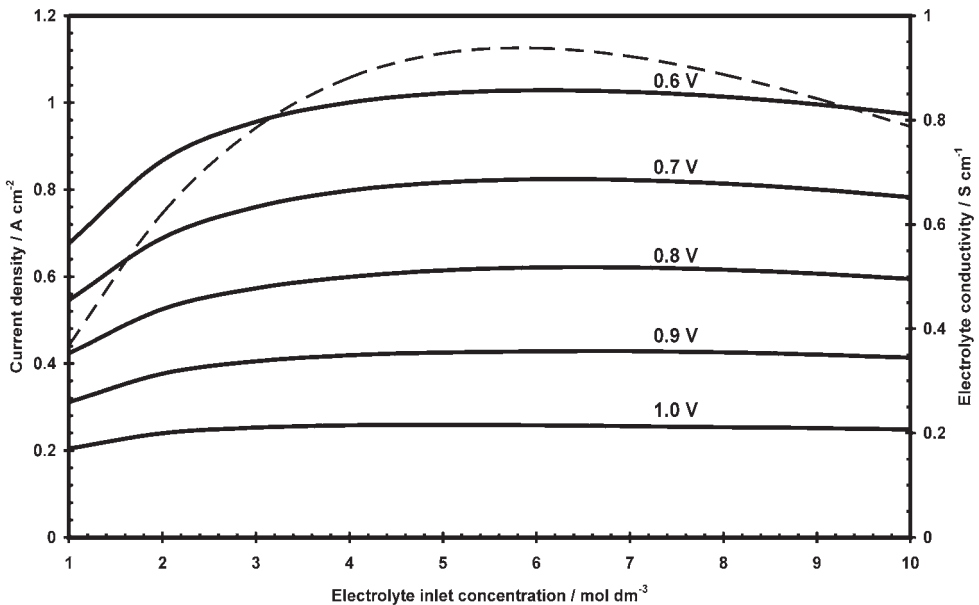
Figure 4.11: Cell current density as a function of electrolyte inlet concentration and cell voltage.

Operating pressure

Polarization curves for the single cell at different operating pressures are presented in Figure 4.12. An increase in the cell current density at all voltages can be observed, while the polarization curves maintains essentially the same slope in the ohmic polarization region. The small tendency towards limiting current behaviour observed at an operating pressure of 1 bar is completely eliminated at higher pressures. The reason for the increased cell performance is a higher interfacial mass transport of chlorine from the gas phase to the liquid phase and a higher solubility of chlorine in the electrolyte. There is no indication that the conductivity of the electrolyte varies with the operating pressure.
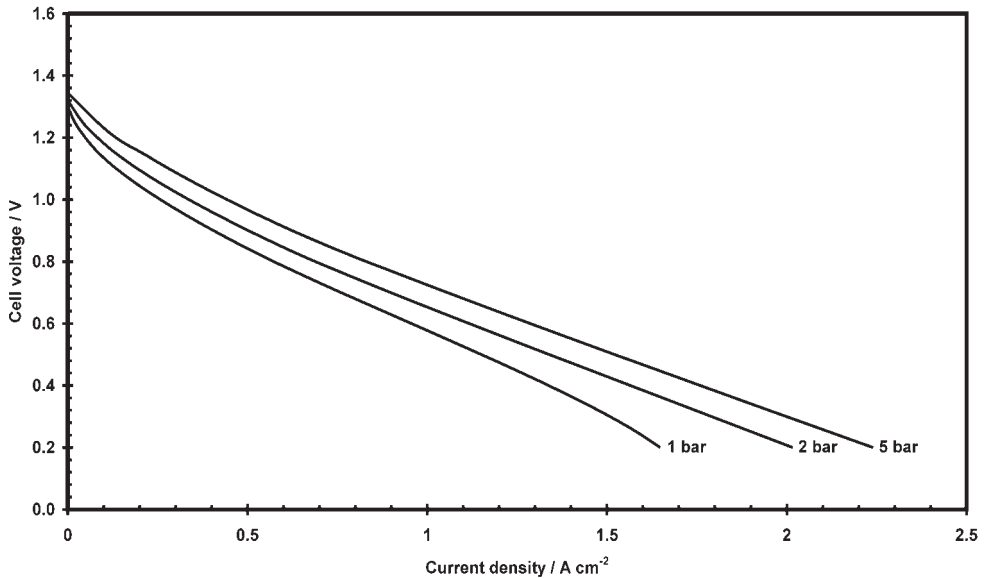
Figure 4.12: Single cell polarization curves at different operating pressures.

4.7 Conclusions

A mathematical model for a H_2 - Cl_2 single fuel cell has been developed. The model describes mass transport and electrochemical reactions occurring in the cathode gas diffusion layer, the cathode catalyst layer and the separator/membrane layers. From the profiles of dissolved chlorine as a function of cell voltage, it is determined that the interfacial mass transport of chlorine between the gas and liquid phase in the cathode probably is the rate-determining step at high current densities. It is found that concentration of the HCl electrolyte inside the cathode catalyst layer approaches values close to that of concentrated hydrochloric acid (12 mol dm^{-3}), especially at high current density.

Influences of the operating condition of the fuel cell are investigated. It is shown that the cell performance increases substantially by increasing the inlet concentration of the hydrochloric acid electrolyte from 1 to 3 mol dm^{-3}. Increasing the electrolyte concentration further only leads to small changes in the overall cell performance. By increasing the operating pressure a steady increase of the cell performance due to faster electrode kinetics can be observed.

4.8 Acknowledgements

Chapter 5

Background theory

This chapter includes brief introductions to the theories of electron transfer kinetics, the development of mechanisms for electrode reactions and the rotating disk electrode and is meant as an introduction to the next two chapters which deals with the kinetics of the chlorine reduction reaction. The background given here are taken from [67–69]

5.1   Kinetics of electron transfer at the metal-liquid interface

Electron transfer at metal electrodes has been studied since the beginning of the last century and kinetic models based on empirical data was developed [70–72]. Later, in the early 1960s various scientists, including Marcus, Gerischer and Levich, started to develop modern theories of electron transfer between molecules in homogeneous solutions and at electrodes [73–75]. Here, the classical model based on the assumption that the electrode reaction progress through an activated complex (transition state) will be used since it is straightforward and sufficiently detailed for analysis of experimental data.

Considering the most simple electrode reaction; the single electron transfer of a redox couple at a metal electrode neither preceded nor followed by any other reactions:

$$O + e^- \rightleftharpoons R \tag{5.1}$$

Figure 5.1 shows a graphical representation of the transition state model in terms of a free energy - reaction coordinate diagram. The energy curves for the reduced and oxidised species and the barrier height for the anodic, $\Delta G_a^\ddagger$, and cathodic, $\Delta G_c^\ddagger$, reaction at equilibrium (a) and at a cathodic polarisation (b) are depicted. During polarisation, the relative energy of the electron resident on the electrode changes with $-F\Delta\varphi$, hence the curve for the oxidized species moves up or down by that amount. It is assumed that the electric potential only affects the energetics of the oxidised state (the reduced species is uncharged), and thus only the energy curve of the oxidised state is shifted under polarisation. On applying the potential difference $\Delta\varphi$, the activation energy for the cathodic reaction is increased by $(1 - \alpha)zF(\Delta\varphi)$ while the activation energy for the anodic reaction is decreased by $\alpha(zF\Delta\varphi)$. Using this, the dependence of the activation energies on the potential can approximately be described by

$$\Delta G_c^\ddagger = \Delta G_{0c}^\ddagger + (1 - \alpha)zF\Delta\varphi \tag{5.2}$$
$$\Delta G_a^\ddagger = \Delta G_{0a}^\ddagger - \alpha zF\Delta\varphi \tag{5.3}$$

The electron transfer coefficient α can be seen as a representation of the fraction of the input electrical energy by which the electrical part of the activation energy decreases and thus the net rate of the reaction increases. The value of

a

b
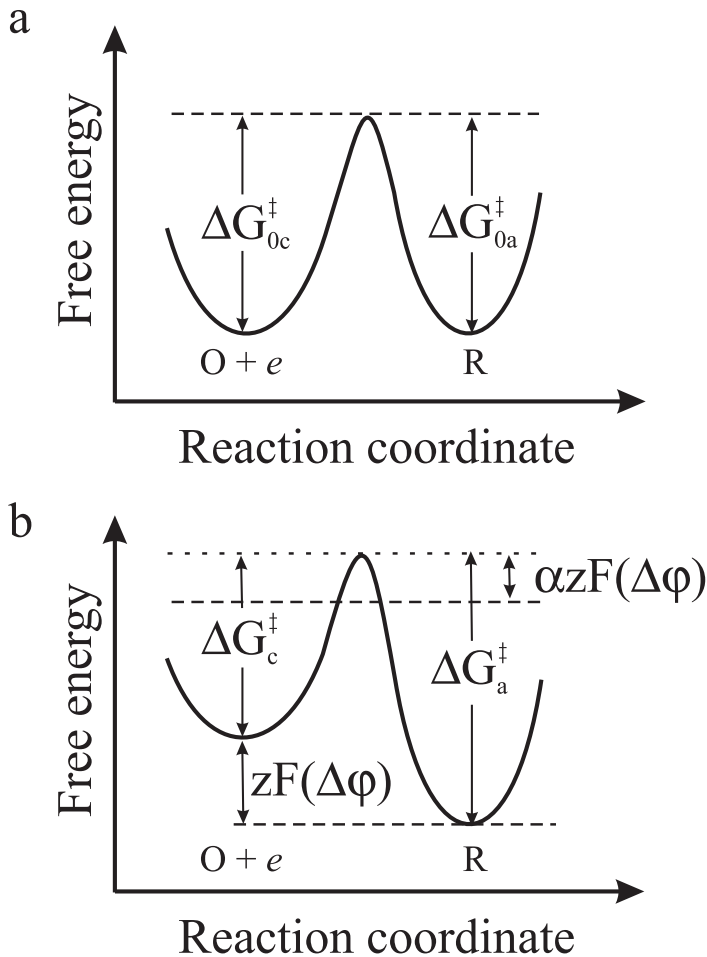
Figure 5.1: Free energy vs. reaction coordinate. a) Equilibrium, b) Under polarisation

α is related to the molecular quantities such as bonding and solvation energies which determine the shape and slopes of the potential energy curves shown in Figure 5.1 [68].

Assuming that the general principles of chemical reaction kinetics remain valid in the case of electrode processes, the rate of reaction will be proportional to the concentration of the activated state, which is determined by the activation energy. The rates of the electrochemical reactions can then be described by an Arrhenius type relation:

$$r_a \;=\; k_a c_R \exp\left(\frac{-\Delta G_a^{\ddagger}}{RT}\right) \tag{5.4}$$

$$r_c \;=\; k_c c_O \exp\left(\frac{-\Delta G_c^{\ddagger}}{RT}\right) \tag{5.5}$$

Inserting the expression for the activation energies, Eqs. 5.2 and 5.3, we get the following expressions for the anodic and cathodic rate

$$r_a \;=\; k_a c_R \exp\left(\frac{-\Delta G_{0a}^{\ddagger} + \alpha z F \Delta\varphi}{RT}\right) \tag{5.6}$$

$$r_c \;=\; k_c c_O \exp\left(\frac{-\Delta G_{0c}^{\ddagger} - (1-\alpha) z F \Delta\varphi}{RT}\right) \tag{5.7}$$

The magnitude of the Galvani potential difference $\Delta\varphi$ is an unmeasurable quantity. It is only possible to measure potentials with respect to a given reference electrode (E). The Galvani potential difference and the potential of the reference electrode will only differ with a constant (B), assuming no potential difference in the diffusive double layer. As a result, the following relationship can be given:

$$\Delta\varphi = E + B - (E^0 + B) = E - E^0 \tag{5.8}$$

The partial anodic and cathodic current densities can thereby be expressed in terms of the directly measured electrode potentials. Using this relationship, Eqs. 5.6 and 5.7 can be rewritten

$$i_a \;=\; zF k_a' c_R \exp\left(\frac{\alpha z F (E - E^0)}{RT}\right) \tag{5.9}$$

$$i_c \;=\; -zF k_c' c_O \exp\left(\frac{-(1-\alpha) z F (E - E^0)}{RT}\right) \tag{5.10}$$

Where

$$k_a' \;=\; k_a \exp\left(\frac{-\Delta G_{0a}^{\ddagger}}{RT}\right) \tag{5.11}$$

$$k_c' \;=\; k_c \exp\left(\frac{-\Delta G_{0c}^{\ddagger}}{RT}\right) \tag{5.12}$$

If the interface is at equilibrium with a solution in which $c_R = c_O$, $E = E^0$ and $k_a' c_R = k_c' c_O$ so that $k_a = k_c$. Thus, E^0 is the potential where the anodic and cathodic rate constants have the same value, also referred to as the standard rate constant k^0. The rate constants at other potentials can then be expressed in terms of k^0. Inserting this into the sum of Eqs. 5.9 and 5.10 we get the complete current-potential characteristic, also known as the *Butler-Volmer equation* :

$$i = zFk^0\left(c_R \exp\left(\frac{\alpha zF(E - E^0)}{RT}\right) - c_O \exp\left(\frac{-(1-\alpha)zF(E - E^0)}{RT}\right)\right) \tag{5.13}$$

At equilibrium, the potential of the electrode will be E^{rev} and the net current zero, but there will still be an exchange of charge between the electrode and the species in the solution. This balanced faradaic exchange of charge is designated the exchange current density i_0 which is equal in magnitude to either i_c or i_a:

$$i_0 \;=\; zFAk^0 c_R \exp\left(\frac{\alpha zF(E^{rev} - E^0)}{RT}\right) \tag{5.14}$$

$$\;=\; -zFk^0 c_O \exp\left(\frac{-(1-\alpha)zF(E^{rev} - E^0)}{RT}\right)$$

Writing the Nernst equation in exponential form and raising it to the α power we obtain:

$$\exp\left(\frac{\alpha zF(E^{rev} - E^0)}{RT}\right) = \left(\frac{c_O}{c_R}\right)^{\alpha} \tag{5.15}$$

Inserting into Eq. 5.14 gives:

$$i_0 = zFAk^0 c_O^\alpha c_R^{(1-\alpha)} \tag{5.16}$$

Using the equations above, the current can be described in terms of the deviation from the equilibrium potential, also called the overpotential; $\eta = E - E^{rev}$

$$i = i_0 \left(\frac{\alpha z F \eta}{RT} - \frac{-(1-\alpha)zF\eta}{RT} \right) \tag{5.17}$$

5.2   Derivation of mechanistic rate equations

In the preceding section, the expression for the rate of a single electron transfer reaction was established. This forms the basis for the development of rate equations for multi-step reaction mechanisms. Using the IUPAC guidelines given in [76, 77] and considering the following electrode reaction:

$$\mathrm{A + e^- \rightleftharpoons 1/2\,D} \tag{5.18}$$

which consists of the following elementary steps:

$$
\begin{array}{rcl}
\mathrm{A + e^-} & \rightleftharpoons & \mathrm{B} \qquad\qquad\qquad\qquad (\mathrm{I}) \\
\mathrm{B + e^-} & \rightleftharpoons & \mathrm{C} \qquad\qquad\qquad\qquad (\mathrm{II}) \\
\mathrm{A + C} & \rightleftharpoons & \mathrm{D} \qquad\qquad\qquad\qquad (\mathrm{III})
\end{array}
$$

where species B and C are reaction intermediates adsorbed on the electrode surface and species A and D are stable, soluble species. The mass action rate law gives the following relation for the rates of the elementary steps:

$$
\begin{aligned}
v_I &= k_{(1,red)}c_A \exp(-(1-\alpha)f\eta) - k_{(1,ox)}c_B \exp(\alpha f\eta) & (5.19) \\
v_{II} &= k_{(2,red)}c_B \exp(-(1-\alpha)f\eta) - k_{(2,ox)}c_C \exp(\alpha f\eta) & (5.20) \\
v_{III} &= k_3 c_A c_C - k_{-3} c_D & (5.21)
\end{aligned}
$$

where $f = \frac{F}{RT}$. Under steady state measurements, the amount of the reaction intermediates is constant and we get for B and C:

$$\frac{\partial c_B}{\partial t} \;=\; v_I - v_{II} = 0 \tag{5.22}$$

$$\frac{\partial c_C}{\partial t} \;=\; v_{II} - v_{III} = 0 \tag{5.23}$$

The current flowing is a direct measure of the total reaction rate, which also can be seen as the rate of production of electrons. Thus we get the following expression for the current:

$$i/nF \;=\; -(v_I + v_{II}) \tag{5.24}$$

The amounts of the adsorbed reaction intermediates are not directly measurable and has to be related to the activity of the species in solution which it is in equilibrium with and the electrical state of the system at a given temperature. This relationship is given by the adsorption isotherm. The general equation for an adsorption isotherm is [78]:

$$a_i^A = a_i^b \exp\left(\frac{\Delta G_i^0}{RT}\right) = \beta_i' c_i^b \tag{5.25}$$

where a_i^A and a_i^b is the activity of species i adsorbed on the electrode surface and in the bulk solution respectively.

Several isotherms exists and are results of different assumptions and models of the adsorption process and the interaction between the adsorbed species. In electrochemistry, three of the most commonly used are the Langmuir, Temkin and Frumkin isotherms. Table 5.1 gives the expressions for the surface activity (a_i^A) for these three isotherms.

Having developed an expression for the activity of the adsorbed species, the rates of the individual elementary steps and thus the total reaction rate can be described by known or measurable quantities by solving a set of linear equations. In this case, the set of equations would be Eqs. 5.22, 5.23 and 5.24.

Table 5.1: Adsorption isotherm activities

Isotherm	Expression of adsorbed species activity (a_i^A)
Langmuir	$\frac{\theta_i}{1-\theta_i}$
Temkin	$\exp\left(\frac{2g\theta_i}{RT}\right)$
Frumkin	$\frac{\theta_i}{1-\theta_i}\exp\left(\frac{-2g\theta_i}{RT}\right)$

$g = \frac{\partial \Delta G_i^0}{\partial \theta_i}$

5.3 The rotating disk electrode

The rotating disk electrode (RDE) is one of the few convective electrode systems for which the hydrodynamic equations and the convective-diffusion equation have been solved rigorously for the steady state. The electrode is quite simple to construct and consists of a disk electrode embedded in a rod of insulating material, for example Teflon or epoxy resin. It is critical that there are no leakage of the solution between the insulating material and the electrode, causing a uncontrolled increase of the electrode area and that the area of the electrode is small compared to the area of the insulating material. The electrode is attached to a motor and rotated at a certain frequency, f (s^{-1}).

5.3.1 Velocity and concentration profiles at the RDE

The velocity profile of a fluid near a RDE was obtained by von Karman and Cochran by solving the hydrodynamic equations under steady state conditions. The spinning disk drags the fluid at its surface along with it and due to the centrifugal force flings it outwards in a radial direction. The solution at the disk surface is replaced by a flow normal to the disk. The hydrodynamic equations can be written in cylindrical coordinates due to the symmetry of the system. The equations of continuity, motion and the convective-diffusion equation and the method of solution are given in [56,78]. A numerical solution of the velocity profile, using the finite element program FEMLAB® is shown in Figure 5.2. From the solution of these equations, the following relationship known as the *Levich equation* is obtained for an anodic reaction:

$$i_{d,a} = 0.620nFAD_R^{2/3}\omega^{1/2}\nu^{-1/6}c_R^b \tag{5.26}$$

and for a cathodic reaction:

$$i_{d,c} = -0.620nFAD_O^{2/3}\omega^{1/2}\nu^{-1/6}c_O^b \qquad (5.27)$$
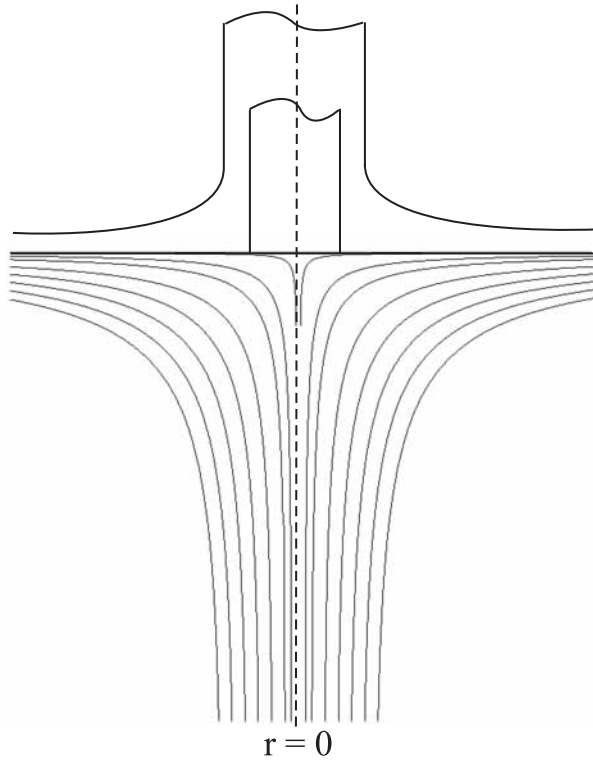
Figure 5.2: The velocity profile at a disk electrode embedded in a larger insulating plane, both rotating at an angular velocity ω

5.3.2   Current/potential curves at the RDE

For currents below the mass transport limited current i_d, the Levich equation is modified to:

$$
\begin{aligned}
i &= 0.620nFAD_R^{2/3}\omega^{1/2}\nu^{-1/6}(c_R^b - c_R^s) \qquad (5.28)\\
&= -0.620nFAD_O^{2/3}\omega^{1/2}\nu^{-1/6}(c_O^b - c_O^s)
\end{aligned}
$$

By combining Eqs. 5.26, 5.27 and 5.28, the concentration at the electrode surface, c_i^s, can be described as:

$$c_i^s = c_i^b \left(1 - \frac{i}{i_{d,i}} \right)$$

(5.29)

Where i denotes the oxidized or reduced species (O or R). From section 5.1 it is known that the current also can be described by the kinetic rate equation:

$$i = nF \left[k_a c_R^s \exp \left(\frac{\alpha nF\eta}{RT} \right) - k_c c_O^s \exp \left(\frac{-(1-\alpha)nF\eta}{RT} \right) \right]$$

(5.30)

Using Eqs. 5.29 and 5.30, rearranging and defining

$$i_k = nF \left[k_a c_R^b \exp \left(\frac{\alpha nF\eta}{RT} \right) - k_c c_O^b \exp \left(\frac{-(1-\alpha)nF\eta}{RT} \right) \right]$$

(5.31)

one obtains the following relation:

$$\frac{1}{i} = \frac{1}{i_k} \left[1 + \frac{D_R^{2/3} k_a \exp \left(\frac{\alpha nF\eta}{RT} \right) + D_O^{2/3} k_c \exp \left(\frac{-(1-\alpha)nF\eta}{RT} \right)}{0.62\nu^{1/6}\omega^{1/2}} \right]$$

(5.32)

Here, i_k represents the obtained current in the absence of any mass transfer effects, i.e., the kinetically controlled current in the case of the mass transfer being efficient enough to keep the concentration at the electrode surface equal to the bulk value. Thus, a plot of i^{-1} vs. $\omega^{-1/2}$ at a constant value of η should be linear, and an extrapolation of $\omega^{-1/2}$ to 0 will yield the value of i_k^{-1} which can be used to determine the kinetic parameters k_0 and α (Figure 5.3).

The method described above have one significant drawback. The current used at different rotation rates must be evaluated at exactly the same value of η, otherwise the linear extrapolation of $\omega^{-1/2}$ to 0 will give incorrect values for i_k^{-1}. In some systems this can be difficult to achieve due to uncompensated resistances in the cell. To avoid this problem, one can combine Eqs. 5.30 and 5.29:

$$\frac{i}{nF} = \left[k_a c_R^b \frac{i_{d,a} - i}{i_{d,a}} \exp \left(\frac{\alpha nF\eta}{RT} \right) - k_c c_O^b \frac{i_{d,c} - i}{i_{d,c}} \exp \left(\frac{-(1-\alpha)nF\eta}{RT} \right) \right]$$

(5.33)
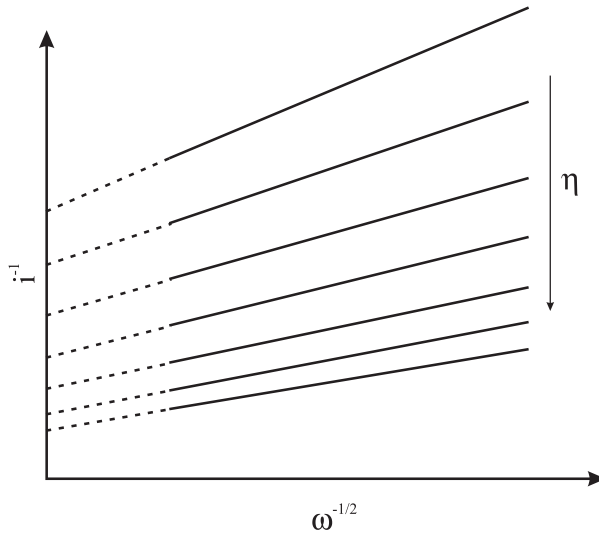
Figure 5.3: Plot of i^{-1} vs. $\omega^{-1/2}$ at different overpotentials for a quasi reversible electrode reaction

Sufficiently far away from equilibrium ($\eta > \frac{2.303RT}{nF}$), the cathodic reaction can be ignored, then Eq. 5.33 and Eq. 5.31 yields

$$i_k(\eta) = \frac{i(\eta)i_{d,a}}{i_{d,a} - i(\eta)} \qquad (5.34)$$

and correspondingly for the cathodic reaction:

$$i_k(\eta) = \frac{i(\eta)i_{d,k}}{i_{d,k} - i(\eta)} \qquad (5.35)$$

A plot of theoretical values of i_k vs. $ii_d(i_d - i)^{-1}$ should coincide for all rotation rates and give the current/potential relation of the reaction without any influence of mass transport, Fig 5.4 shows a schematic plot of i_k vs. η for an anodic reaction studied at three different rotation rates.

The i_k values can be directly utilized for kinetic analysis, trough a classic Tafel analysis or more sophisticated numerical methods.
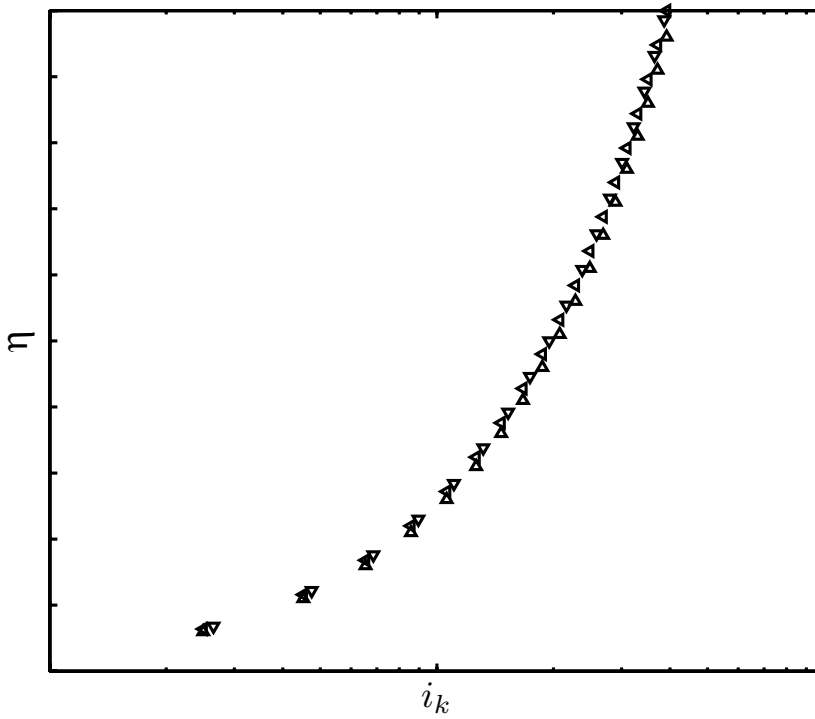
Figure 5.4: Schematic plot of i_k vs. η with values from three different rotation rates

Chapter 6

Chlorine Reduction on Platinum and Ruthenium: The Effect of Oxide Coverage

M. Thomassen, B. Børresen, G. Hagen, R. Tunold

Department of Materials Technology
Norwegian University of Science and Technology
NO-7491 Trondheim, Norway

6.1   Abstract

The rate and mechanism of the electroreduction of chlorine on electrochemically oxidised Pt and Ru electrodes has been investigated relative to the state of oxide formation. Current/potential curves for the reduction process in 1 M HCl solution saturated with Cl$_2$ have been obtained for electrode surfaces in various states of preoxidation with the use of the rotating disc electrode technique (RDE). In the case of chlorine reduction on platinum, the results indicate that adsorption of chlorine molecules with a subsequent rate determining electrochemical adsorption step is the dominant mechanism. The exchange current density seems to decrease linearly with the logarithm of the amount of surface oxide.

Chlorine reduction on ruthenium is best described by a Heyrovsky-Volmer mechanism with the first charge transfer reaction as the rate determining step. The Krishtalik mechanism incorporating adsorbed O$^{\bullet}$Cl^{+} intermediates is also able to describe the reaction successfully. The reaction order is constant for all oxide coverages while the exchange current density apparently moves through a maximum at intermediate oxide coverages ($\sim$100 mC cm^{-2}). The results show that the electrocatalysis of the cathodic reduction of chlorine is very sensitive to the state of the oxide film on the surface.

6.2   Introduction

The chlorine electrode has a potential for use in fuel cells due to its fast kinetics and relatively high standard potential (1.36 V vs. SHE). Compared to a H$_2$ - O$_2$ fuel cell, a H$_2$ - Cl$_2$ fuel cell has the possibility of a higher power density and energy efficiency [28]. Due to the product being HCl instead of H$_2$O, the environment of this fuel cell is very corrosive and ordinary carbon supported Pt electrocatalysts are not stable, as reported earlier [28]. A substitute must therefore be found. It is therefore necessary to study the chlorine reduction reaction on platinum and other metals and metal oxides in order to understand the reaction mechanism and consequently be able to tailor new, active and stable electrocatalysts.

6.2.1 The chlorine electrode reaction on platinum

The chlorine electrode reaction (ClER) in aqueous solutions is conveniently studied only in the potential range where surface oxide, hydroxides or chemisorbed oxygen form on platinum. These oxide species can inhibit both the evolution and reduction of chlorine, and since their equilibrium amount varies with potential it is difficult to interpret results from conventional, steady state, kinetic measurements. Previously reported current/overpotential curves [79,80] for the chlorine reduction reaction show some hysteresis attributed to variation in the extent of oxidation of the electrode surface, but the results from these studies are not in agreement. Chang and Wick [79] found that the relation between the overpotential and the logarithm of the current was curved, the currents at higher overpotentials being smaller than expected from a linear relation. Frumkin and Tedoradze [80] reported that the reaction was first order with respect to chlorine but independent of chloride with a stoichiometric number of two. They suggested that the mechanism was

$$Cl_{2(aq)} + e^- \quad \rightarrow \quad Cl_{ad} + Cl^-_{(aq)} \tag{6.1}$$

$$Cl_{ad} + e^- \quad \rightarrow \quad Cl^-_{(aq)} \tag{6.2}$$
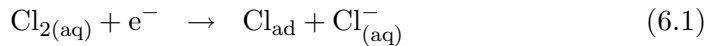
i.e. the two steps are comparable in rate and both reverse reactions are negligibly slow at moderate overpotentials. Dickinson, Greef and Lord Wynne-Jones [81] studied the chlorine electrode reaction at a platinum surface with constant oxide coverage and evaluated the quantitative effect of the oxide layer on the rates of the processes involved. They concluded that increasing the quantity of oxide on the platinum surface causes a decrease in the rate of chlorine reduction at constant potential and a decrease of the transfer coefficient for at least one of the steps in the process. They determined that the reaction was first order with respect to chlorine at low chlorine concentration, but decreased to 0.8 - 0.6 at higher concentrations. They proposed that the most probable mechanism, which was in agreement with their obtained results, is;

$$Cl_{2(aq)} + e^- \quad \rightleftharpoons \quad Cl_{ad} + Cl^-_{(aq)} \tag{6.3}$$

$$Cl_{ad} + e^- \quad \rightarrow \quad Cl^-_{(aq)} \tag{6.4}$$
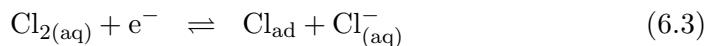
which differs from the proposed mechanism of Frumkin and Tedoradze [80] only in that the reverse process in step 1 is considered to be comparable in rate to the forward process in step 2. Burrows, Entwisle and Harrison [82] found a cathodic Tafel slope of 81 mV on a virtually oxide free platinum surface, which they found consistent with the reaction scheme presented by Frumkin and Tedoradze; Müller and Kaiser [83] determined that for ($p_{Cl_2} > 0.1$ atm) the reaction order for chlorine is 0.5 with a stoichiometric number of 2 and suggested that the reaction takes place according to the following mechanism:

$$Cl_{2(aq)} \; \rightleftharpoons \; 2Cl_{ad} \tag{6.5}$$

$$Cl_{ad} + e^- \; \rightarrow \; Cl^-_{(aq)} \tag{6.6}$$

For lower partial pressures of chlorine ($p_{Cl_2} < 0.1$ atm), they found that the mechanism changes and that fast chemisorption of chlorine is replaced by slow electrochemical adsorption as the rate determining step. Feng-Bin, Hillman, Lubetkin & Roberts [84] investigated the ClER under potentiodynamic conditions using a platinum-coated quartz crystal for electrochemical quartz crystal microbalance (EQCM) studies. They showed that the surface coverage of chlorides is essentially 100% between -0.5 and 0.6 V vs SCE. In the range 0.6-1.1 V an anodic adsorption of approx. 25% of a monolayer of atomic chlorine is observed. This increases with the concentration of dissolved chlorine in the solution reaching up to 50% with their experimental conditions.

6.2.2   The ClER on RuO$_2$

The fundamental steps in the chlorine evolution reaction on RuO$_2$ and mixed ruthenium titanium oxides (RTO) have been discussed in many papers through the Volmer-Krishtalik mechanism [63, 85–87]

$$Cl^-_{(aq)} \; \rightleftharpoons \; Cl_{ad} + e^- \tag{6.7}$$

$$Cl_{ad} + e^- \; \rightarrow \; (Cl_{ad})^+ + e^- \tag{6.8}$$

$$(Cl_{ad})^+ Cl^-_{(aq)} \; \rightleftharpoons \; Cl_2 \tag{6.9}$$
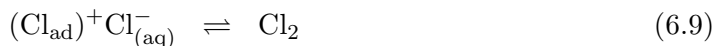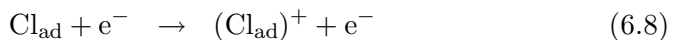
Hepel, Pollak & O'Grady [88] suggested from single crystal experiments that the natural oxygen sites available only on the ideal (110) surface of RuO_2 provide active centres for the formation of surface $O^{\bullet}Cl^+$ groups that are intermediates in the Krishtalik mechanism. Fernández, Gennero de Chialvo and Chialvo [89] performed a mathematical kinetic analysis of the current/potential relation and surface coverage of the adsorbed intermediates for the chlorine evolution reaction under the Volmer-Krishtalik mechanism and obtained Tafel regions which slopes cannot be derived from the use of the rate determining step criteria. They also demonstrated the existence of kinetically limiting current densities. In a series of three papers, the same authors performed a detailed kinetic study of the chlorine evolution on Ti/RuO_2 through the polarisation resistance in which they concluded with proposing a Volmer-Kristalik-Tafel mechanism for the ClER. [90–92]

$$S^Z + H^+ \ \rightleftharpoons \ SH^{Z+1} \tag{6.10}$$

$$S^Z \ \rightleftharpoons \ S^{Z+1} + e^- \tag{6.11}$$

$$e^- + SCl^{Z+1} \ \rightleftharpoons \ S^{Z+1} + Cl^-_{aq} \tag{6.12}$$

$$S^Z + Cl_2 \ \rightleftharpoons \ SCl^{Z+1} + Cl^-_{aq} \tag{6.13}$$

$$2S^{Z+1} + Cl_2 \ \rightleftharpoons \ 2SCl^{Z+1} \tag{6.14}$$
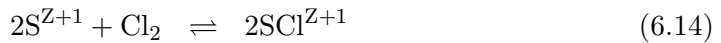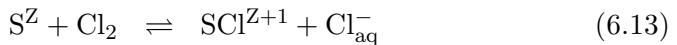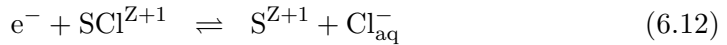
Where SZ and S^{+1} are non-oxidised and oxidised surface sites respectively.

6.2.3   Purpose of present work

With the exception of the work of Dickinson, Greef and Lord Wynne-Jones [81], none of the studies on platinum mentioned above take into account the changes in oxidation state of the electrode surface. Roscoe and Conway [93] showed that the state of the oxide film on Cl_2 evolving platinum anodes can have a substantial effect on the chlorine evolution kinetics, but did not examine the effect of oxide on the chlorine reduction reaction. Although the industrially important chlorine evolution reaction on RuO_2 and mixed ruthenium titanium

oxides (RTO) has been extensively examined, the corresponding reduction reaction is explored to a much less extent. In the present work, we have examined the influence of the oxidation state of Pt and Ru surfaces on the Cl$_2$ reduction with special reference to well defined states of the surface oxide films. These are prepared in situ before the kinetic measurements are performed, removing the role of potential and time dependent changes of state of the oxide film that can complicate the interpretation of the kinetics of the reaction. This opens the possibility to determine if there exists any catalytic or inhibitive effect of electrode surface oxides towards electroreduction of chlorine.

6.3   Experimental

A rotating ring-disc electrode (PINE instruments MTI34) with an interchangeable disk was used to establish a well-defined mass transfer regime and hence the effect of mass transport could be isolated. The ring was not used in the following experiments. The disk electrode had a diameter of 6.0 mm and consisted of either platinum (99.99%, PINE instruments) or ruthenium (99.9%, Goodfellow). The electrodes had been polished to a mirror finish using alumina powder down to 0.5 μm in size. The cell was a cylindrical glass vessel of 300 ml capacity, with a double bottom in which temperature controlled water could circulate. All experiments were performed at 25° C. The cell also consisted of an inlet and outlet for chlorine gas, a glass capillary connected to the reference electrode compartment and an opening for the rotating disk electrode. The glass cell was made gas tight with the use of a PTFE-plug with a ball bearing fitted around the electrode shaft. The electrolyte was 1.0 M HCl, made from conc. Suprapur$^{®}$ HCl (Merck) and distilled water (18.2 MW). An external Ag/AgCl (Metrohm) reference electrode immersed in 1.0 M HCl was employed and all the reported potentials are referred to this electrode. The potential of the working electrode was controlled with a Solartron SI 1287 potentiostat. The current and potential was recorded using an ADC-212 digital oscilloscope (Pico Technologies). Before every new set of experiments, the cell was washed with distilled water and fresh electrolyte was added.

6.3.1   Determination of oxide coverage

Platinum

The amount of oxide on the electrode surface as a function of potential and polarisation time was determined by cathodic stripping. The working electrode was immersed in a clean 1 M HCl electrolyte and continuously purged with N_2 to remove any dissolved oxygen. The electrode was then brought to a reproducible state of activity by polarizing for a few seconds alternately at 1.7 V and 0 V vs. Ag/AgCl five times. This treatment appeared to remove all oxide from the electrode surface. The cleaning process was followed by a treatment designed to establish a reproducible quantity of oxide on the electrode. The electrode was held at one of the four potentials listed in Table 6.1 for the time indicated. To determine the oxide coverage after the different pre-treatments a cathodic stripping current of 5 mA cm^{-2} was applied until the potential of the electrode was below the potential of the CV oxide reduction peak (~ 0.1 V vs. Ag/AgCl). The total charge passed, Q_{ox}, was used as a measure of the amount of oxide formed during the anodic potential hold.

Ruthenium

The oxide formation on ruthenium is much faster and occurs at more cathodic potentials than on platinum [94]. Thus, the potential steps and the duration of the pre-treatment had to be modified. The electrode was brought to a reproducible state of activity by polarizing it for 180 s at -0.15 V vs. the Ag/AgCl electrode. This treatment appeared to remove all the oxide from the surface. The electrode was then held at one of the three potentials listed in Table 6.2 for the period shown. After the specified oxidation period, a cathodic stripping current of 50 mA cm^{-2} was applied until the potential of the electrode reached -0.15 V vs Ag/AgCl. As with the platinum electrode, the total charge passed, Q_{ox}, was used as a measure of the amount of oxide formed during the anodic potential hold.

6.3.2   Chlorine reduction

The HCl electrolyte was continuously purged with chlorine gas 30 minutes in advance of and during all experiments in order to ensure a saturated solution.

Platinum

The chlorine reduction measurements were performed in the potential range between 0.9 V and 1.125 V vs. the Ag/AgCl electrode with 25 mV intervals. Before every measurement of the chlorine reduction reaction, the platinum electrode went through the cleaning and pre-treatment procedures described previously and visualized in Figure 6.1. This procedure was repeated for several electrode rotation speeds between 500 and 9000 rpm.
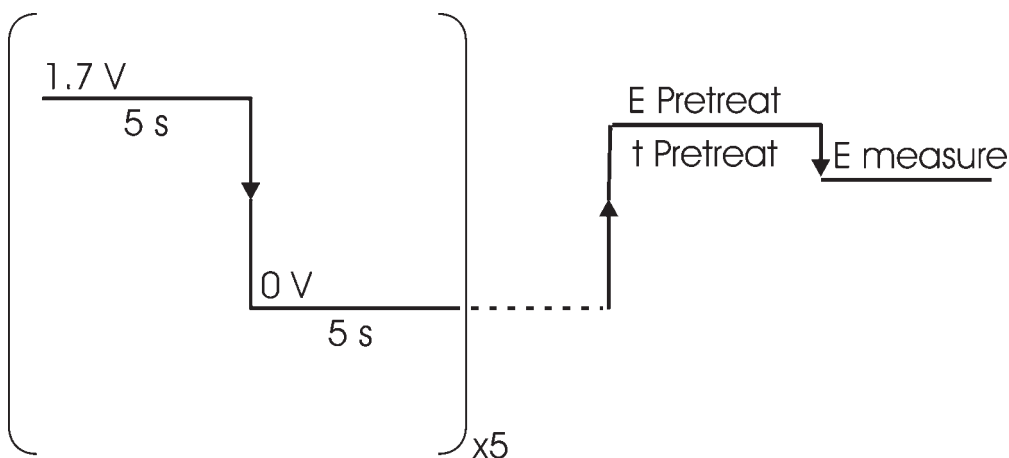
Figure 6.1: Pre-treatment potential profile, platinum electrode

Ruthenium

Before each measurement, the ruthenium electrode was polished with 0.5 μm alumina powder, washed with distilled water and inserted in the cell. It was then brought to a reproducible state of activity by polarizing it for 180 s at -0.15 V vs. Ag/AgCl. Measurements were performed in the potential range between 0.65 V and 1.1 V with 50 mV intervals. This procedure was repeated for several electrode rotation speeds between 500 and 9000 rpm.

6.4   Results

The current for chlorine reduction was studied as a function of potential and rotation speed of the electrode at different, but constant Q_{ox} values. The values

of Q_{ox} resulting from the four standard pre-treatment periods for platinum and the three standard pre-treatment periods for ruthenium are shown in Tables 6.1 and 6.2 respectively. The values for platinum are approx. 10% higher than those found by Dickinson et al. [81] and Roscoe and Conway [93], indicating that the method used is capable of determining the amount of oxide on the electrode surface in a reproducible manner.

Table 6.1: Oxide coverage on platinum after pre-treatment

Potential (V)	Time (s)	Q_{ox} (μC cm^{-2})
0.9	60	115 $\pm$ 2
1.6	10	440 $\pm$ 15
1.7	10	580 $\pm$ 7
1.8	60	690 $\pm$ 55

Table 6.2: Oxide coverage on ruthenium after pre-treatment

Potential (V)	Time (s)	Q_{ox} (mC cm^{-2})
0.7	60	70 $\pm$ 2
0.8	60	95 $\pm$ 1
0.9	60	115 $\pm$ 2

6.4.1 Reaction order with respect to chlorine

When a rotating disk electrode is used, the reaction order may be determined from the relation between the current at constant potential and the rotation speed of the electrode. At potentials sufficiently far from the reversible open circuit potential, where the reverse reaction may be ignored, we have

$$i = k[Cl_2]_S^p \tag{6.15}$$

where i is the observed current, k is the potential dependent rate constant, $[Cl_2]_S$ the concentration of chlorine at the electrode surface and p the reaction order. The concentration of chlorine is here used instead of the activity since the activity coefficient is probably very close to unity [95]. The Levich theory of the rotating disc electrode gives [96]:

$$i = B([Cl_2] - [Cl_2]_s)\omega^{1/2} \tag{6.16}$$

where B is constant at constant temperature, $[Cl_2]$ the bulk concentration of chlorine and ω the angular velocity of the rotating electrode.

When the current is mass transfer limited, $[Cl_2]_S = 0$ and

$$i_d = B[Cl_2]\omega^{1/2} \tag{6.17}$$

where i_d is the diffusion limiting current at the applied electrode rotation rate. Combining (6.16) and (6.17) gives

$$[Cl_2]_s = \frac{i_d - i}{i_d}[Cl_2] \tag{6.18}$$

Substituting into (6.15) and taking logarithms we get;

$$\log i = \log k + p \log \left(\frac{i_d - i}{i_d}\right)[Cl_2] \tag{6.19}$$

Thus, at constant Q_{ox} and potential, a plot of $\log i$ against $\log[Cl_2](i_d-i)(i_d)^{-1}$ will have a slope equal to the reaction order. The values for the reaction order with respect to chlorine on platinum and ruthenium for the different pretreatments are given in Table 6.3.

Table 6.3: Reaction order, p, with respect to chlorine

Potential (V)	Time (s)	p
Platinum		
0.9	60	1.1 ± 0.5
1.6	10	0.6 ± 0.1
1.7	10	0.7 ± 0.1
1.8	60	0.7 ± 0.1
Ruthenium		
0.7	60	1.0 ± 0.1
0.8	60	1.1 ± 0.1
0.9	60	1.1 ± 0.1

It has been shown [97] that for reactions with complex mechanisms with formation of stable soluble intermediates, e.g. the oxygen reduction mechanism, the number of electrons exchanged per reactant is a function of the potential of the

electrode and cannot be evaluated theoretically in a simple manner. The use of the rotating disk technique in elucidating the overall kinetic parameters for such processes is limited and should be performed with caution. Earlier observations [28] confirming that the chlorine reduction reaction is more reversible than the oxygen reduction reaction supports the assumption of a less complex mechanism and a complete two-electron transfer per reactant.

6.4.2   Current/Potential relation

The kinetically controlled part of the total current can be isolated from the experimental data using the relation [81]:

$$i_k = i \left(\frac{i_d}{i_d - i} \right)^p = k[Cl_2]^p \tag{6.20}$$

A plot of ik against E will show the current/potential relation without any effect of mass transport. The results for all the standard pre-treatments and rotation rates are given in Figure 6.2 (platinum) and Figure 6.6 (ruthenium). These graphs are in no case linear over any appreciable potential range.
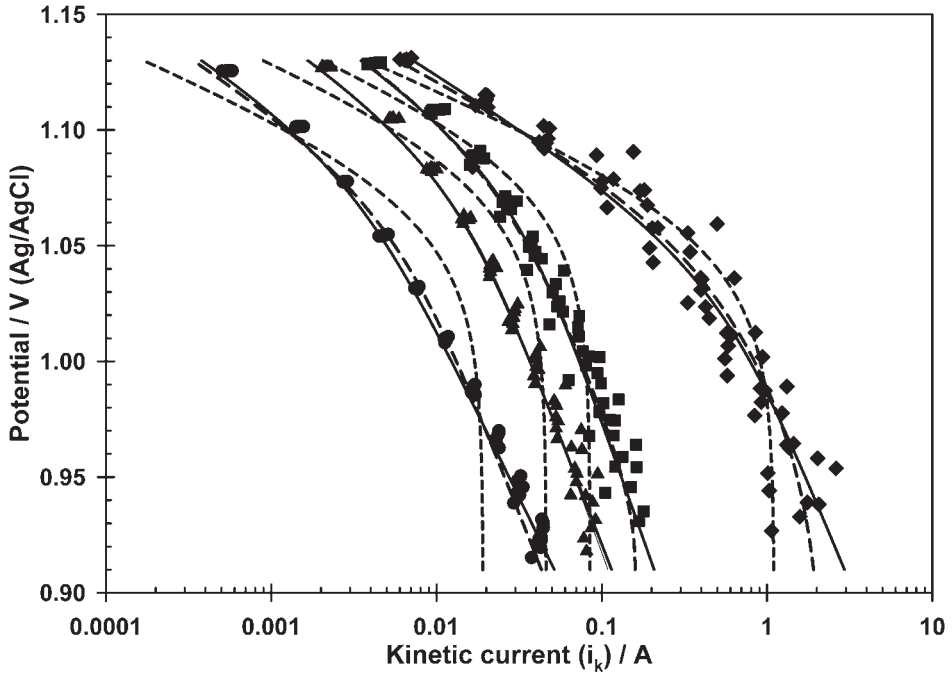
Figure 6.2: Current/potential relation with different pre-treatments, platinum electrode. Pre-treatment: ($\blacklozenge$) 0.9 V for 60 s, ($\blacksquare$) 1.6 V for 10 s, ($\blacktriangle$) 1.7 V for 10 s, ($\bullet$) 1.8 V for 60 s. The full lines are the relation predicted by mechanisms C, D and BI. The long, dashed lines are the relationship predicted by mechanism BII while the short lines represent mechanism AI.

6.5 Chlorine reduction mechanisms

Four reaction schemes have been considered in attempting to explain the experimental results. Two basic schemes incorporating one adsorbed species (A, B) and two schemes involving two adsorbed species (C, D).

$$Cl_{2(aq)} \rightleftharpoons 2Cl_{ad} \qquad \text{(Tafel)} \qquad \text{(AI)}$$

$$Cl_{ad} + e^- \rightleftharpoons Cl^-_{(aq)} \qquad \text{(Volmer)} \qquad \text{(AII)}$$

$$Cl_{2(aq)} + e^- \rightleftharpoons Cl_{ad} + Cl^-_{(aq)} \quad \text{(Heyrovsky)} \qquad \text{(BI)}$$

$$Cl_{ad} + e^- \rightleftharpoons Cl^-_{(aq)} \qquad \text{(Volmer)} \qquad \text{(BII)}$$

$$Cl_{2(aq)} \rightleftharpoons Cl_{2,ad} \qquad \text{(CI)}$$

$$Cl_{2(ad)} + e^- \rightleftharpoons Cl_{ad} + Cl^-_{(aq)} \quad \text{(Heyrovsky)} \qquad \text{(CII)}$$

$$Cl_{ad} + e^- \rightleftharpoons Cl^-_{(aq)} \qquad \text{(Volmer)} \qquad \text{(CIII)}$$

$$Cl_{2(aq)} + e^- \rightleftharpoons Cl^-_{(aq)} + Cl^+_{ad} \quad \text{(Krishtalik)} \qquad \text{(DI)}$$

$$Cl^+_{ad} + e^- \rightleftharpoons Cl_{ad} \qquad \text{(Heyrovsky)} \qquad \text{(DII)}$$

$$Cl_{ad} + e^- \rightleftharpoons Cl^-_{(aq)} \qquad \text{(Volmer)} \qquad \text{(DIII)}$$
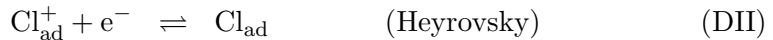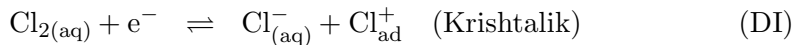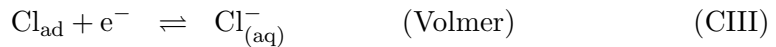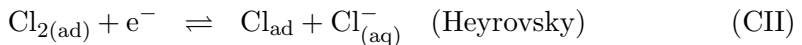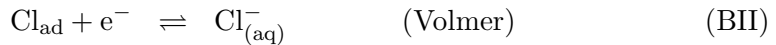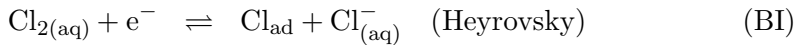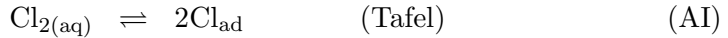
Mechanism A and B are the basic Tafel - Volmer and Tafel - Heyrovsky mechanisms known from the hydrogen evolution reaction (HER). Mechanism C involves the adsorption of molecular chlorine and a subsequent electrochemical reaction to an adsorbed chlorine atom and a chloride ion. The last step, CIII, is a normal Volmer reaction. Mechanism D is the well-known Krishtalik [63]

mechanism for chlorine evolution on DSA electrodes, which assumes that the surface oxide has the ability to rapidly and easily change oxidation states. It involves a reaction between a chlorine molecule and the surface, forming a chloride ion and a Cl$^+_{ad}$ species, which in two sequential steps is reduced to a chloride ion. The assumption of a surface able to rapidly change valency renders this mechanism improbable for chlorine reduction on platinum. The adsorption of molecular chlorine (mechanism C) or the formation of an adsorbed Cl$^+_{ad}$ complex (mechanism D) have to be considered to be less probable than the adsorption of atomic chlorine and the surface coverage of these species should therefore be relatively low, compared to the amount of Cl$_{ad}$ on the surface. The rate equations developed from the above reaction schemes have been derived for the following conditions:

1. Adsorption obeys the Langmuir isotherm

2. The transfer coefficients for the two electron-transfer steps may differ, but are independent of potential.

3. The reaction steps other than the rate determining step has been considered to be in rapid equilibrium

4. The concentration of chloride ions at the electrode is considered to be essentially equal to the bulk concentration.

The rate equations for the four reaction schemes are listed in Table 6.4. The derivation of the rate equation for D2 (mechanism D with step DII as rate determining) is given in chapter 6.9.

Table 6.4: Rate equations for possible mechanisms

Mech	Rate determining step	i_T Current	Designation
A	I	$k_1 C_{Cl_2}^S \left(1 - \dfrac{k_{-2} C_{Cl^-}^S}{k_2 \exp(-fE) + k_{-2} C_{Cl^-}^S}\right)^2$	AI
	II	$nF k_2 (1-\theta)^2 \exp(-(1-\gamma)fE)$	AII
B	I	$2FA k_1 C_{Cl_2}^S \left(1 - \dfrac{k_1 C_{Cl_2}^S \exp(-(1-\alpha)fE) + k_{-2} C_{Cl^-} \exp(\gamma fE)}{k_1 C_{Cl_2}^S \exp(-(1-\alpha)fE) + k_{-2} C_{Cl^-} \exp(\gamma fE) + k_2 \exp(-(1-\gamma)fE)}\right) \exp(-(1-\alpha)fE)$	BI
	II	$2FA \dfrac{k_1 C_{Cl_2}^S \exp((1-\gamma)fE) + k_{-1} C_{Cl^-} \exp((2-\gamma)fE) + k_2 \exp(-(1-\alpha)fE)}{k_1 k_2 C_{Cl_2}^S}$	BII
C	II	$2FA \dfrac{k_{-1} k_3 \exp((1-\alpha)fE) + k_{-1} k_{-3} C_{Cl^-} \exp((2-\alpha)fE) + k_1 k_3 C_{Cl_2}^S \exp((1-\alpha)fE)}{k_1 k_2 k_3 C_{Cl_2}^S}$	CII
	III	$2FA \dfrac{k_{-2} C_{Cl^-} - C_{Cl_2}^S \exp((2-\gamma)fE) + k_1 k_2 C_{Cl_2}^S \exp((1-\gamma)fE) + k_{-1} k_{-2} C_{Cl^-} \exp((2-\gamma)fE)}{k_1 k_2 k_3 C_{Cl_2}^S}$	CIII
D	II	$2FA \dfrac{k_{-1} k_3 C_{Cl^-} \exp((1-\alpha)fE) + k_{-1} k_{-3} C_{Cl^-}^2 \exp((2-\alpha)fE) + k_1 k_3 C_{Cl_2}^S \exp((1-\alpha)fE)}{k_1 k_2 k_3 C_{Cl_2}^S}$	DII
	III	$2FA \dfrac{k_1 k_{-2} C_{Cl_2}^S \exp((2-\gamma)fE) + k_1 k_2 C_{Cl_2}^S \exp((1-\gamma)fE) + k_{-1} k_{-2} C_{Cl^-} \exp((2-\gamma)fE)}{k_1 k_2 k_3 C_{Cl_2}^S}$	DIII

It is not possible to distinguish between mechanism C and D from the performed experiments, since the only difference between the rate equations for these mechanisms is the dependence of the chloride concentration, which was not altered during the experimental runs. A study of the effect of chloride concentration as well as the pH of the solution on the chlorine reduction reaction will be performed in the near future. However, as previously discussed, it is very unlikely that mechanism D is valid for a platinum electrode while it has been proposed several times for chlorine evolution on ruthenium oxides. It is therefore assumed that mechanism C is possible on platinum while mechanism D could be favoured on ruthenium.

6.6   Discussion

6.6.1   Tests of the theoretical rate equations

The theoretical rate equations for all the reaction schemes were tested against the experimental results by the following procedure:

Current-potential relation

The values for the rate constants and the electron transfer coefficients in the theoretical rate equations were determined from the experimental results using the *lsqcurvefit* - function in Matlab, which solves nonlinear curve-fitting (data-fitting) problems by the method of least-squares. An analysis of the attained values can indicate if some, all or none of the proposed mechanisms are able to describe the chlorine reduction reaction.

Dependence of reaction order on chlorine concentration

The theoretical rate equations with the parameters from the curve fitting procedure can be used to calculate the chlorine reaction order by varying the chlorine concentration $C_{Cl_2}^S$. These calculated reaction orders can then be compared to the experimental values found by using the relation in Eq. 6.19.

Surface coverage of adsorbed species

From the derivation of the theoretical rate equations it is possible to develop expressions for the relationship between surface coverage of the adsorbed intermediates and potential, as shown for mechanisms B1 and C2 below:

With mechanism B1, since the first step is rate determining,

$$\begin{aligned}
\frac{\partial \theta}{\partial t} &= k_1 C^s_{Cl_2}(1-\theta)\exp(-(1-\alpha)fE) + k_{-2}C_{Cl^-}(1-\theta) \\
&\times \exp(\gamma fE) - k_2\theta\exp(-(1-\gamma)fE) = 0
\end{aligned} \tag{6.21}$$

so that

$$\theta = \frac{k_1 C^s_{Cl_2}\exp(-(1-\alpha)fE) + k_{-2}C_{Cl^-}\exp(\gamma fE)}{k_1 C^s_{Cl_2}\exp(-(1-\alpha)fE) + k_{-2}C_{Cl^-}\exp(\gamma fE) + k_2\exp(-(1-\gamma)fE)} \tag{6.22}$$

With mechanism C2 there exists two adsorbed surface species, adsorbed chlorine molecules and chlorine atoms, with surface coverages of θ_I and θ_{II} respectively. The relation between surface coverage and potential of these species are given in Eqs. 6.23 and 6.24.

$$\theta_I = \frac{k_1 k_3 C^s_{Cl_2}\exp(-fE)}{k_{-1}k_3\exp(-fE) + k_{-1}k_{-3}C_{Cl^-} + k_1 k_3 C_{Cl_2}\exp(-fE)} \tag{6.23}$$

$$\theta_{II} = \frac{k_{-3}C_{Cl^-} - k_{-3}C_{Cl^-}\theta_I}{k_3\exp(-fE) + k_{-3}C_{Cl^-}} \tag{6.24}$$

The two mechanisms assume that adsorption follows the Langmuir isotherm. It is likely that the adsorption may follow another isotherm, like the Temkin or Frumkin isotherms. If this is so, the coverages calculated in this work is erroneous since they are derived from the concentration dependence predicted by Langmuir conditions. It might be possible that another mechanism will give better results if more general equations for the adsorption of reactants could be applied.

6.6.2   Chlorine reduction on platinum

Figure 6.2 shows the experimental values of the kinetic current i_k, found by Eq. 6.20, for chlorine reduction on platinum at different states of oxide formation.

The full lines are those attained when curve fitting mechanisms B1, C2&3 and D2&3 to the experimental values while the long dashed lines are those attained from the curve fitting of mechanism B2. The short dashed lines are related to mechanism A1. From Figure 6.2 it can be concluded that mechanism A1 does not describe the experimental results satisfactorily, especially at high surface oxide coverage, while the curves obtained for mechanism B and C all have acceptable fits to the experimental current potential relations. The values of the fitting parameters are physically reasonable, the value of the rate constant for the rate determining step is at least two orders of magnitude lower than the other rate constants and the electron transfer coefficients have values between 0.3 and 0.7. Mechanism AII was not at all able to describe the experimental results.

Figure 6.3 and Figure 6.4 show plots of $\log i$ vs. $\log([Cl_2](i_d - i)(i_d)^{-1})$ for chlorine reduction on platinum with the four standard pretreatments. The lines represent the predictions of mechanism B1/B2 (Figure 6.3) and C2/C3 (Figure 6.4) respectively. Mechanism B1 has the same slope as the experimental value for the platinum electrode pre-treated at 0.9 V for 60 s, but there is a significant offset between the experimental and theoretical $\log i$ values. For the other electrode pre-treatments, mechanism B1 gives an incorrect value for the chlorine reaction order. Mechanism B2 also describes a correct reaction order for the 0.9 V / 60 s pre-treatment, but for the other pre-treatments it predicts a reaction order close to zero. Mechanism C3 is unable to describe any of the experimentally found reaction orders, predicting values close to or equal to zero for all pre-treatments. C2 is the only mechanism able to give correct reaction orders for all pre-treatments in addition to having a good fit to the experimental results, except for a small offset for the 1.7 V / 10 s pre-treatment.
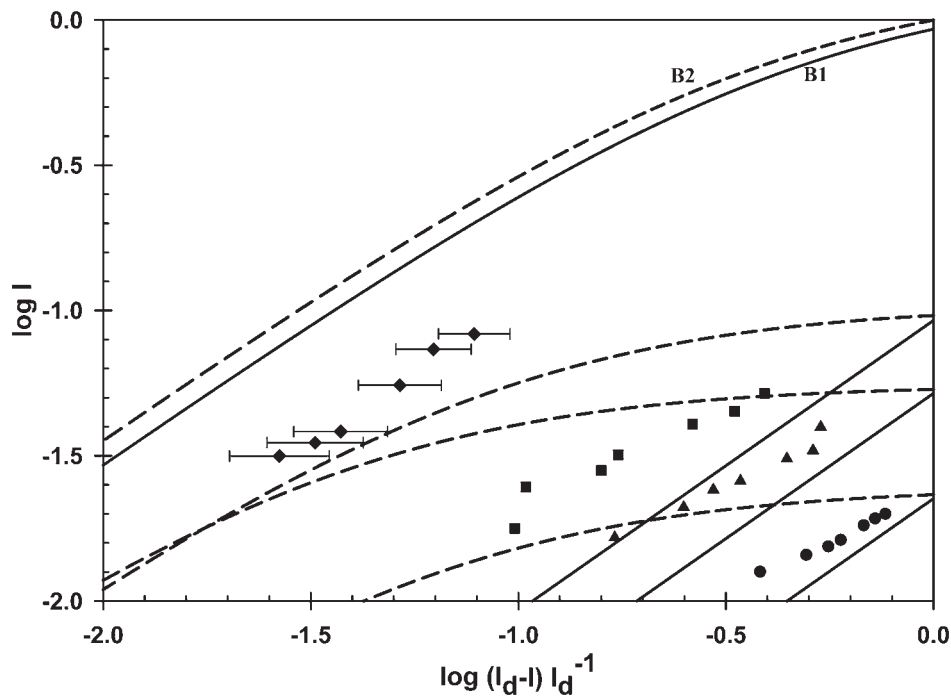
Figure 6.3: Determination of reaction order by variation of rotation speed. Platinum electrode, potential = 0.9 V. Pre-treatment: (♦) 0.9 V for 60 s, (■) 1.6V for 10 s, (▲) 1.7 V for 10 s, (●) 1.8 V for 60 s. The full lines are the ones predicted by mechanism BI while the dashed lines are the ones predicted by mechanism BII.
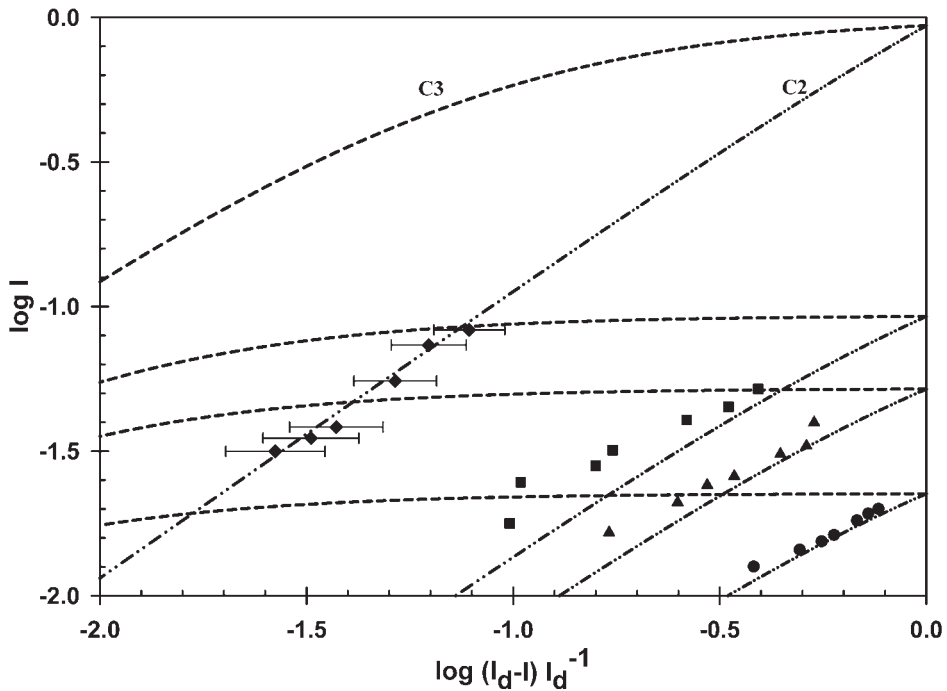
Figure 6.4: Determination of reaction order by variation of rotation speed. Platinum electrode, potential = 0.9 V Pre-treatment: (♦) 0.9 V for 60 s, (■) 1.6V for 10 s, (▲) 1.7 V for 10 s, (●) 1.8 V for 60 s. The dashed lines are the ones predicted by mechanism CIII/DIII while the dashed-dotted lines are the ones predicted by mechanism CII/DII.

Fig 6.5 shows the calculated surface coverages of Cl$_{2,ad}$ and Cl$_{ad}$ according to mechanism C2. The amount of adsorbed molecular chlorine is relatively low at moderate overpotentials, increasing slowly as the electrode becomes more cathodically polarised, while the amount of adsorbed atomic chlorine decreases with increasing cathodic overpotential. This behaviour is as expected from the mechanism proposed, where the reduction of molecular chlorine is assumed to be the rate-determining step.
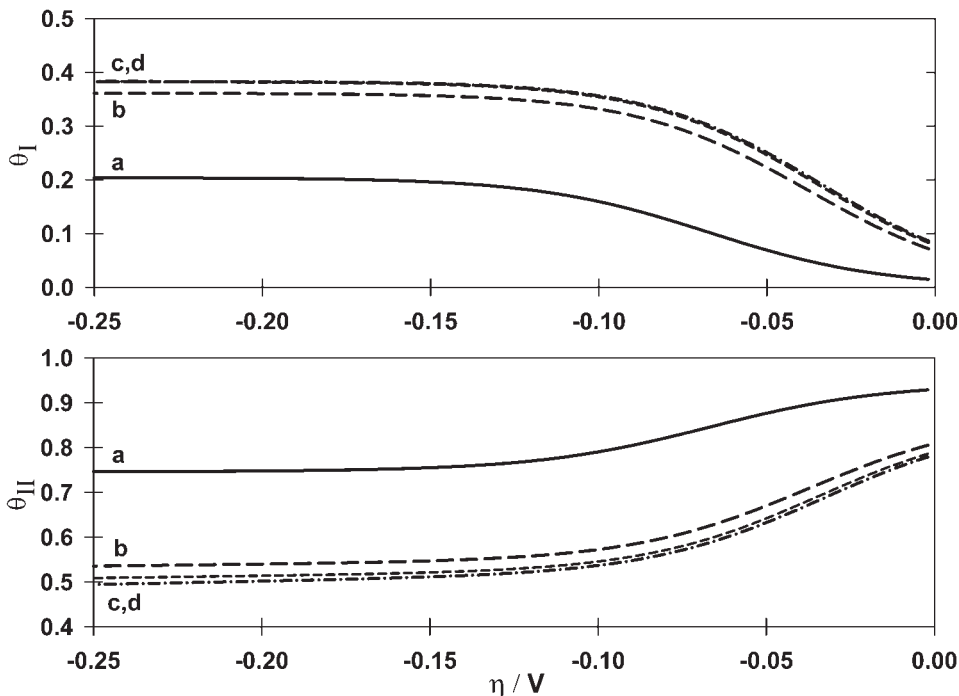
Figure 6.5: Calculated surface coverage of adsorbed intermediates on platinum according to mechanisms CII and DII. $\theta_I = Cl_{2,ad}$, $\theta_{II} = Cl_{ad}$. Pre-treatments: (a) 0.9V for 60 s, (b) 1.6 V for 10 s, (c) 1.7 V for 10 s (d) 1.8 V for 60 s.

6.6.3 Chlorine reduction on ruthenium

Figure 6.6 shows a plot of i_k vs. electrode potential for chlorine reduction on ruthenium. The full lines are those predicted by mechanisms C2/D2, C3/D3 and B1. The dashed lines corresponds to mechanism B2. The full lines have a good fit to the experimental values for all the standard pre-treatments, while the broken lines (mechanism B2) erroneously predict a decrease in the kinetic current at high overvoltages. The fitting parameters all have physically reasonable values, the rate constant for the rate determining step is at least three orders of magnitude lower than the other rate constants and the electron transfer coefficients have values between 0.5 and 0.75. The only exception is mechanism B1 describing the reaction on the ruthenium electrode with the highest amount of oxide, where the second electron transfer coefficient has a value of 1.
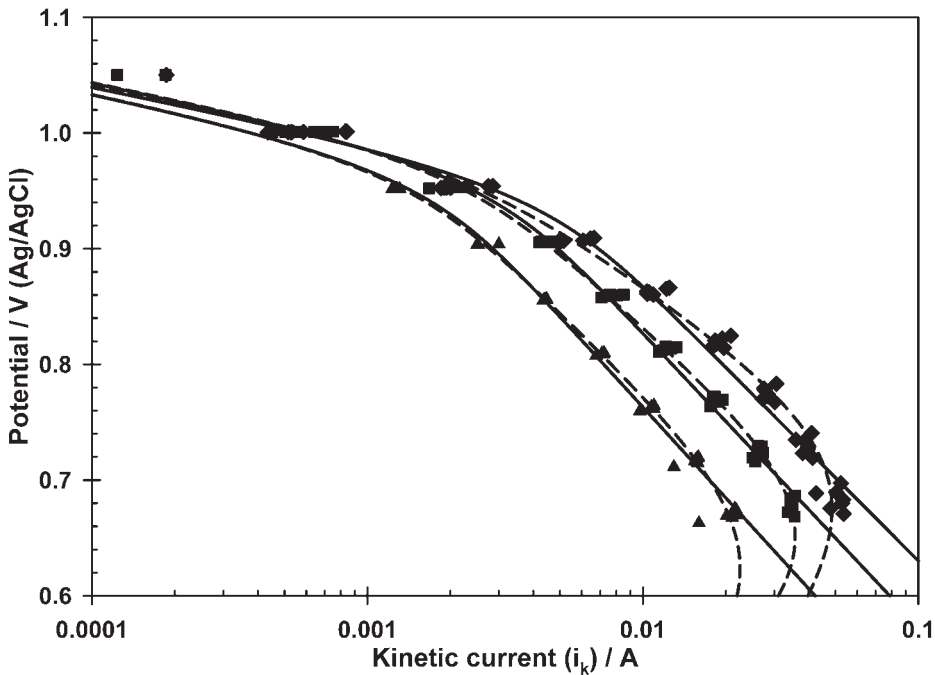
Figure 6.6: Current/potential relation with different pre-treatments, ruthenium electrode. Pre-treatment: ($\blacklozenge$) 0.7 V for 60 s, ($\blacksquare$) 0.8 V for 60 s, ($\blacktriangle$) 0.9 V for 60 s. The full lines are the relation predicted by mechanisms CII/DII, CIII/DIII and BI. The dashed lines are the relationship predicted by mechanism BII.

Figure 6.7 and Figure 6.8 show plots of $\log i$ vs. $\log([Cl_2](i_d - i)(i_d)^{-1})$ for chlorine reduction on ruthenium for the three standard pretreatments. The lines represent mechanisms C2/D2 - B1 and C3/D3 - B2 respectively. Mechanisms B1 and C2/D2 both have excellent fits to the experimental data. The only difference is that mechanisms C2/D2 predicts a slightly lower chlorine reaction order. Mechanisms B2 and C3/D3 are not able to describe the experimental results, predicting reaction orders close to or equal to zero.
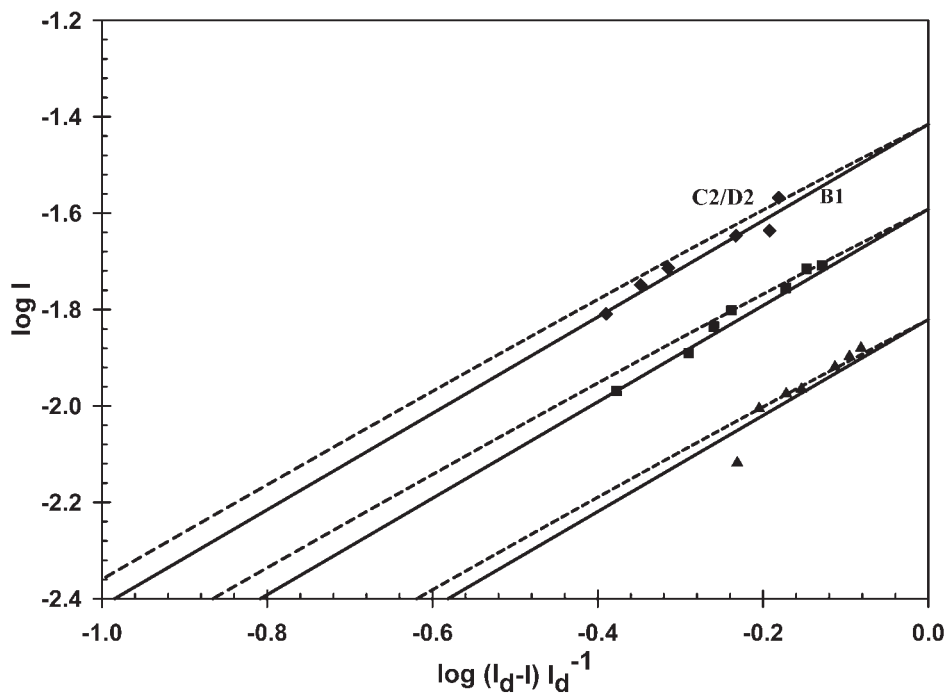
Figure 6.7: Determination of reaction order by variation of rotation speed. Ruthenium electrode, potential = 0.7 V Pre-treatment: (♦) 0.7 V for 60 s, (■) 0.8 V for 60 s, (▲) 0.9 V for 60 s. The dashed lines are the ones predicted by mechanism CII/DII while the full lines are the ones predicted by mechanism BI.
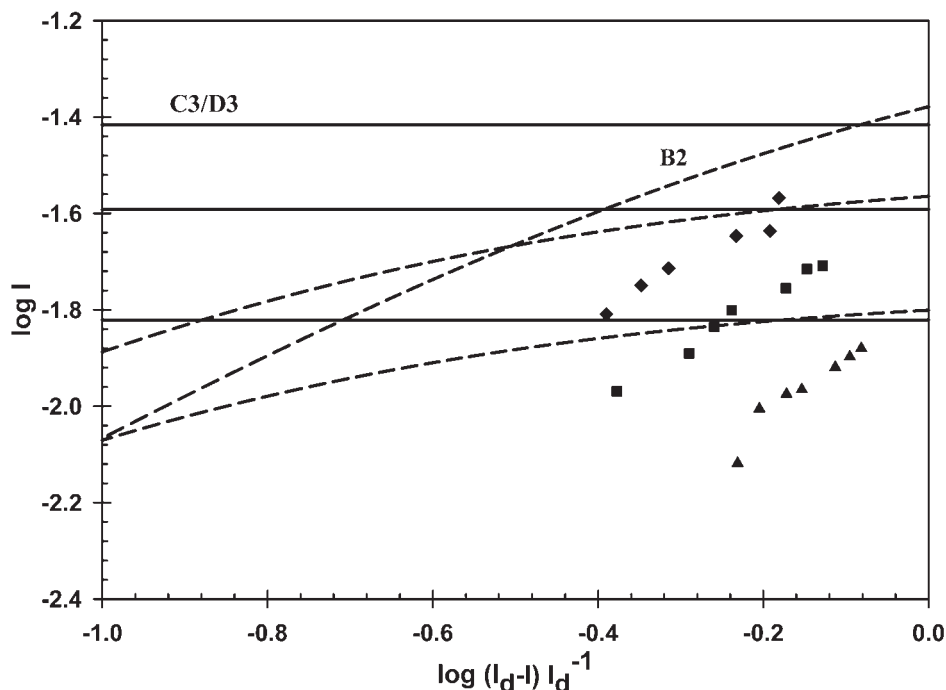
Figure 6.8: Determination of reaction order by variation of rotation speed. Ruthenium electrode, potential = 0.7 V Pre-treatment: ($\blacklozenge$) 0.7 V for 60 s, ($\blacksquare$) 0.8 V for 60 s, ($\blacktriangle$) 0.9 V for 60 s. The dashed lines are the ones predicted by mechanism BII while the full lines are the ones predicted by mechanism CIII/DIII.

Figure 6.9 shows the calculated surface coverage of the two adsorbed species present in mechanisms C2 and D2. The amount of Cl$_{2,ad}$ or Cl$_{ad}^+$ is very close to zero at open circuit, increasing slowly to 0.1-0.15 when the electrode is ca- thodically polarised while the surface coverage of adsorbed atomic chlorine is reduced correspondingly. According to mechanism B1, the surface coverage of adsorbed atomic chlorine should decrease from 1 to approximately zero at a ca- thodic overpotential of 250 mV as shown in Figure 6.10. Both these behaviours are consistent with the expected results from the proposed mechanisms.
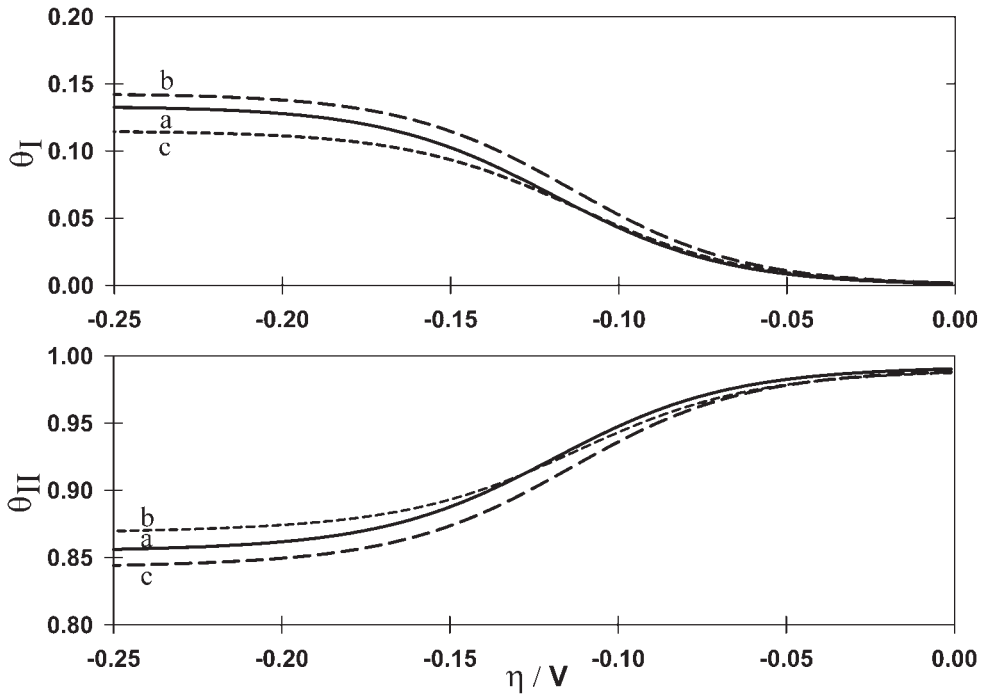
Figure 6.9: Calculated surface coverage of adsorbed intermediates on ruthenium according to mechanisms CII and DII. $\theta_I = \mathrm{Cl}^+_{\mathrm{ad}}$ or $\mathrm{Cl}_{2,\mathrm{ad}}$, $\theta_{II} = \mathrm{Cl}_{\mathrm{ad}}$. Pretreatments: (a) 0.7V for 60 s, (b) 0.8 V for 60 s, (c) 0.9 V for 60 s.
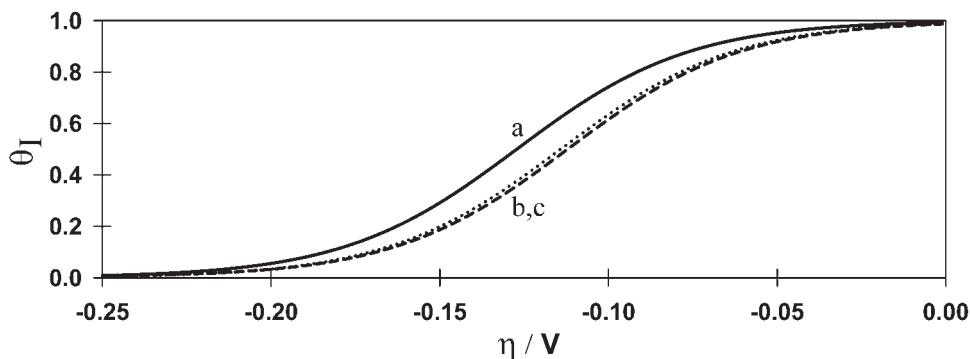
Figure 6.10: Calculated surface coverage of the adsorbed intermediate (Cl_{ad}) on ruthenium, according to mechanism BI. Pre-treatments: (a) 0.7V for 60 s, (b) 0.8 V for 60 s, (c) 0.9 V for 60 s.

6.6.4   Most probable mechanism

From the presented mechanistic analysis it appears that mechanism C2 is the only mechanism capable of describing the experimental results for chlorine reduction on platinum. (As previously discussed, the formation of Cl_{ad}^+ on platinum is very unlikely). This differs from the analysis performed by Dickinson, Greef and Lord Wynne Jones [81] who concluded that mechanism B2 is the most probable mechanism. An explanation for this discrepancy may be that Dickinson, Greef and Lord Wynne Jones applied a maximum chlorine concentration of approximately 15% of the concentration used in this study. At these relatively low concentrations, the amount of adsorbed molecular chlorine might have been too low or the speed of adsorption too high compared to the overall reaction rate to see any effect on the current - potential relation. However, using the rate equation for mechanism B2 with the kinetic parameters found in this study with the chlorine concentrations used by Dickinson et. al, the prediction of the chlorine reaction order coincides with the experimental results of Dickinson et. al. This suggest that there is a change in mechanism from B2 to C2 as the chlorine concentration approaches the point of saturation.

From the mechanistic analysis performed on the chlorine reduction on ruthenium, it can be concluded that mechanisms B1 and C2/D2 are able to describe the experimental results. Since the Krishtalik mechanism is frequently reported as a probable mechanism for chlorine evolution on ruthenium oxide, it seems

most probable that mechanism D2 rather than C2 is valid. Both mechanism B1 and D2 has the first charge transfer reaction, a Heyrovsky type, as the rate determining step, the only difference being that D2 has two adsorbed species rather than one with one adsorption/reaction step preceding the rate determining step. Thus it seems that this preceding step does not have a critical importance under the conditions this study was performed.

6.6.5 Effect of surface oxide

It is very difficult to draw unambiguous conclusions on the effect of surface oxide since the different pre-treatments probably alters both the amount of oxide and adsorbed chloride and chlorine. If the total amount of active surface area is considered to be independent of the pre-treatment, the results in Figures 6.2 and 6.6 indicate that increasing quantities of oxide on the surface causes a decrease in the rate of chlorine reduction at constant potential. Figure 6.11 shows the exchange current density and transfer coefficients as a function of the extent of surface oxidation on platinum (left) and ruthenium.
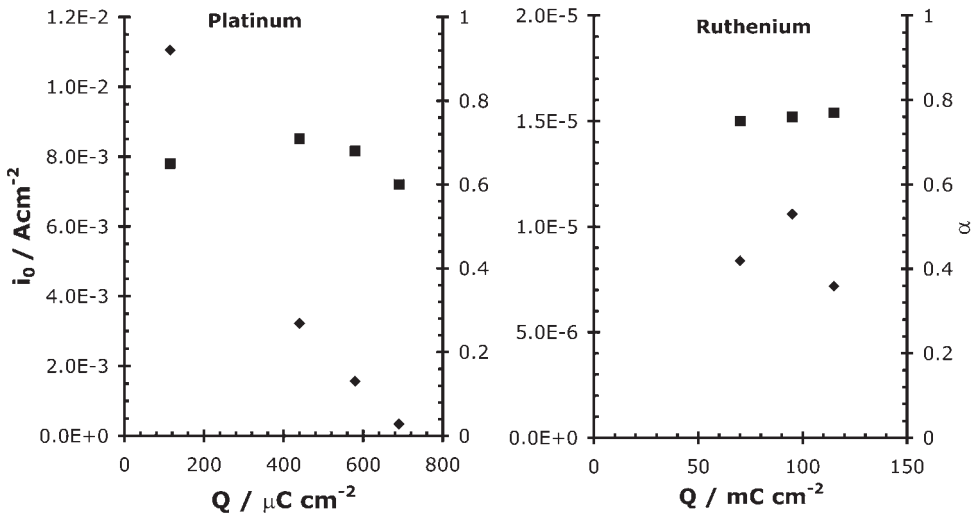

Figure 6.11: Exchange current density and transfer coefficient as a function of oxide coverage on platinum and ruthenium. The two dotted, vertical lines mark one monolayer of adsorbed OH and O respectively. (■) Electron transfer coefficient, (♦) exchange current density.

There is a significant decrease in the exchange current density on platinum with increasing degree of surface oxidation, the value of the exchange current density being inversely proportional to the logarithm of Q_{ox}. The transfer coefficient for chlorine reduction on platinum moves through a maximum at an amount of oxide corresponding to a full monolayer of O. This behaviour was also seen by Dickinson, Greef and Lord Wynne-Jones [81] which they attributed to the discharge process moving from a metal surface to a surface almost completely covered with oxide. The exchange current density on ruthenium seems to move through a maximum at intermediate oxidation states, resembling a "volcano" behaviour. This might suggest that there is one or more ruthenium oxide species being more active towards chlorine reduction, but the amount of experimental results in this study is not adequate to ascertain this hypothesis. The transfer coefficient is close to constant for all oxidation states.

As different ruthenium oxide species, Ru possesses the ability of changing its valence between 2+ and 6+ [98]. The amount of ruthenium oxide on the electrode during the experiments (~ 100mC cm^{-2}) is close to a bulk oxide. This, together with the presented analysis indicates that the chlorine reduction reaction on the ruthenium electrode takes place on the ruthenium oxide surface which actively participates in the reaction. For the platinum electrode however, the thickness of the oxide layer varies from less than one monolayer of OH to approximately two monolayers of O (Figure 11). At these degrees of oxidation it is unlikely that definite stoichiometric phases exist since the oxidation of the Pt surface is a progressive process [99–101]. Due to the lack of well defined oxide structures on the electrode surfaces it is not suitable to use these experimental results as a background for a thorough discussion of the effects of the material properties of these oxide species on the chlorine reduction reaction. However, one major difference between platinum oxide and ruthenium oxide films is that PtO$_2$ is an insulator (106 Ω^{-1} cm^{-1}), whereas RuO$_2$ is conductive (3-5$\times$10^{-5} Ω^{-1} cm^{-1}) [98]. It is therefore likely that the platinum oxide species forms an inactive, insulating barrier on the electrode surface which prevents the transfer of electrons between the platinum electrode and the reactants.

6.7   Conclusions

Experiments have been performed on Pt and Ru electrodes with controlled degree of oxidation in order to quantitatively evaluate the relation between the electrocatalytic behaviour of the materials for chlorine reduction and the degree

of surface oxidation. In the case of chlorine reduction on platinum, the results indicate that adsorption of chlorine molecules with a subsequent rate determining Heyrovsky discharge step is the dominant mechanism. The exchange current density decreases linearly with the logarithm of the amount of surface oxide Chlorine reduction on ruthenium is best described by a Heyrovsky-Volmer mechanism with the first charge transfer reaction as the rate determining step. The Krishtalik mechanism incorporating adsorbed $O^\bullet Cl^+$ intermediates is also able to describe the reaction successfully. The reaction order is constant for all oxidation states while the exchange current density apparently moves through a maximum at intermediate oxidation states ($\sim 100 \text{mC cm}^{-2}$).

6.8   Acknowledgements

6.9   Appendix A: Derivation of the theoretical rate equation for mechanism DII

Mechanism DII may be written as

$$Cl_{2(aq)} + e^- \; \rightleftharpoons \; Cl^-_{(aq)} + Cl^+_{ad} \quad \text{(Krishtalik)} \tag{A.1}$$

$$Cl^+_{ad} + e^- \; \rightarrow \; Cl_{ad} \qquad \text{(Heyrovsky)} \tag{A.2}$$

$$Cl_{ad} + e^- \; \rightleftharpoons \; Cl^-_{(aq)} \qquad \text{(Volmer)} \tag{A.3}$$
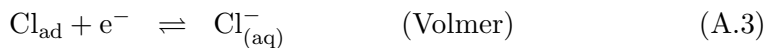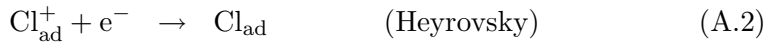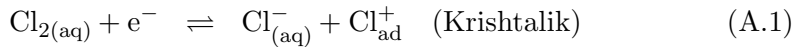
where the second step is rate determining.

The reaction rate of the individual steps can be represented with the equations below by neglecting the reverse reaction in step A.2.

$$v_1 \;=\; k_1 C^s_{Cl_2}(1 - \theta_I - \theta_{II}) - k_{-1} C_{Cl^-} \theta_I \tag{A.4}$$

$$v_2 \;=\; k_2 \theta_I \exp(-(1-\alpha)fE) \tag{A.5}$$

$$v_3 \;\; = \;\; k_3\theta_{II}\exp(-(1-\gamma)fE) - k_{-3}C_{Cl^-}(1-\theta_I-\theta_{II})\exp(\gamma fE) \quad \text{(A.6)}$$

By considering steps I and III to be in rapid equilibrium and using the steady state approximation, expressions for the surface coverages of the reaction intermediates can be found:

$$v_1 \;\; = \;\; 0 \Rightarrow k_1 C_{Cl_2}(1-\theta_I-\theta_{II}) = k_{-1}C_{Cl^-}\theta_I \quad \text{(A.7)}$$

$$\theta_I \;\; = \;\; \frac{k_1 C_{Cl_2}(1-\theta_{II})}{k_{-1}C_{Cl^-} + k_1 C_{Cl_2}} \quad \text{(A.8)}$$

$$v_2 \;\; = \;\; 0 \Rightarrow k_3\theta_{II}\exp(-(1-\gamma)fE)$$
$$= \;\; k_{-3}C_{Cl^-}(1-\theta_I-\theta_{II})\exp(\gamma fE) \quad \text{(A.9)}$$

$$\theta_{II} \;\; = \;\; \frac{k_{-3}C_{Cl^-} - k_{-3}C_{Cl^-}\theta_I}{k_3\exp(-fE) + k_{-3}C_{Cl^-}} \quad \text{(A.10)}$$

Combining Eqs. (A.8) and (A.10):

$$\theta_I = \frac{k_1 C_{Cl_2}\left(1 - \frac{k_{-3}C_{Cl^-} - k_{-3}C_{Cl^-}\theta_I}{k_3\exp(-fE) + k_{-3}C_{Cl^-}}\right)}{k_{-1}C_{Cl^-} + k_1 C_{Cl_2}} \quad \text{(A.11)}$$

$$\theta_I = \frac{k_1 k_3 C_{Cl_2}\exp\left(-fE\right)}{k_{-1}k_3 C_{Cl^-}\exp\left(-fE\right) + k_{-1}k_{-3}C_{Cl^-}^2 + k_1 k_3 C_{Cl_2}\exp\left(-fE\right)} \quad \text{(A.12)}$$

Since step A.2 is rate determining, the total current is assumed to be:

$$i_T = 2FAv_{II} = 2FAk_2\theta_I\exp(-(1-\alpha)fE) \quad \text{(A.13)}$$

Inserting Eq. (A.12) into Eq. (A.13) gives the following expression for the total current for chlorine reduction:

$$\begin{aligned} i_T \;\; = \;\; & 2FA\frac{k_1 k_2 k_3 C_{Cl_2}}{k_{-1}k_3 C_{Cl^-}\exp\left((1-\alpha)fE\right) + k_{-1}k_{-3}C_{Cl^-}^2} \\ & \times \exp\left((2-\alpha)fE\right) + k_1 k_3 C_{Cl_2}\exp\left((1-\alpha)fE\right) \end{aligned} \quad \text{(A.14)}$$

Chapter 7

Chlorine Reduction on Electrooxidised Ruthenium

M. Thomassen, B. Børresen, C. Karlsen, R. Tunold
Department of Materials Technology
Norwegian University of Science and Technology
NO-7491 Trondheim, Norway
Submitted for publication in Electrochimica Acta

7.1   Abstract

The rate and mechanism of the electroreduction of chlorine on electrooxidised ruthenium has been investigated with focus on the effect of solution pH. Steady state current/potential curves for the reduction process in solutions with constant chloride concentration of 1.0 mol dm^{-3} and a varying H$^+$ concentration have been obtained with the use of the rotating disk electrode technique (RDE). It was found that the rate of chlorine reduction is highly inhibited in solutions with high H$^+$ concentrations and that it can be satisfactorily described by the Erenburg mechanism, previously suggested for the chlorine evolution on RuO$_2$ and mixed ruthenium titanium oxides (RTO). The expression of the kinetic current as a function of chlorine and H$^+$ concentration was obtained by solving the elementary rate equations of the kinetic mechanism. The kinetic constants obtained from the numerical fitting of the kinetic current expression to the experimental data were used to simulate the dependence of the surface coverages and elementary reaction rates on overpotential.

7.2   Introduction

The chlorine electrode reaction (ClER) :

$$Cl_{2(g)} + 2e^- \rightleftharpoons 2Cl^-_{aq} \qquad (7.1)$$

has been extensively studied on several electrode materials and significant advances have been achieved on its understanding [102]. Due to their application as the anodic material in the chlor-alkali process, oxide electrodes, especially those based on thermally prepared RuO$_2$ and mixed ruthenium titanium oxides (RTO) have been given special attention. However, performing kinetic studies of the chlorine evolution reaction is not without difficulty. Thermodynamically, oxygen evolution is favoured and if the pH of the solution is too high, it can contribute substantially to the overall current. In addition, the oxygen evolution will affect the pH close to the electrode, making it difficult to evaluate the effect of the H$^+$ concentration. Furthermore, corrosion processes, especially in the case of RuO$_2$, with formation of species with high oxidation states and the chlorine gas evolution itself, constantly changing the active area of the electrode, are factors not easily corrected for. Thus, the experimental conditions

have to ensure the minimisation of the contributions of the above mentioned effects.

Studying the cathodic reduction reaction gives the possibility to overcome most of these difficulties. Due to the more cathodic potentials applied, the corrosion of the electrode is minimised, there are no competing reactions occuring (dissolved oxygen is removed by chlorine purging) and no gas bubbles are produced. Since the solubility of chlorine in hydrochloric acid is relatively high [57], considerable current densities can be achieved, especially when employing a rotating disc electrode [29]. The study of chlorine reduction kinetics can thereby add crucial information concerning the ClER. In addition, the chlorine reduction reaction itself is interesting in the context of fuel cell technologies. The chlorine electrode has a potential for use in fuel cell based electrochemical reactors due to its fast kinetics and relatively high standard potential [18, 19, 25, 28]

In 1987, Trasatti [102] presented a detailed review of the available literature on the mechanism for chlorine evolution. Factors discussed included mixed potentials, porosity, removal of Cl_2, bubble formation, support passivation, morphology, ion specific adsorption and pH effects. A detailed chronological overview of proposed mechanisms were also given. The first mechanistic study of the chlorine evolution reaction at RuO_2 based electrodes was published by Erenburg, Krishtalik and coworkers in 1972 [103]. They found an anodic Tafel slope of 30-33 mV and a cathodic limiting current followed by a Tafel slope of approximately 68 mV. They proposed the classical mechanistic steps frequently used for Cl_2 evolution on platinum:

$$Cl_{aq}^{-} \quad \rightleftharpoons \quad Cl_{ad} + e^{-} \tag{7.2}$$

$$Cl_{ad} + Cl_{aq}^{-} \quad \rightarrow \quad Cl_2 + e^{-} \tag{7.3}$$

$$Cl_{ad} + Cl_{ad} \quad \rightarrow \quad Cl_2 \tag{7.4}$$
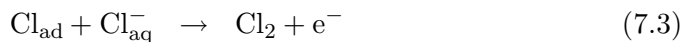
In 1975, the same authors analysed the Cl_2 evolution mechanism again, based on new experimental data [104–106] and proposed the following elementary steps:

$$Cl_{aq}^- \ \rightleftharpoons \ Cl_{ad} + e^- \tag{7.5}$$

$$Cl_{ad} \ \rightleftharpoons \ (Cl_{ad})^+ + e^- \tag{7.6}$$

$$(Cl_{ad})^+ + Cl_{aq}^- \ \rightleftharpoons \ Cl_2 \tag{7.7}$$
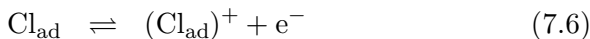
The nature of $(Cl_{ad})^+$ was not specified. This mechanism is known as the Volmer-Krishtalik mechanism and has been extensively discussed in the literature [63, 85–87]. Hepel, Pollak and O'Grady [88] suggested from single crystal experiments that the natural oxygen sites available only on the ideal (110) surface of RuO_2 provide active centres for the formation of surface $O^\bullet Cl^+$ groups that are intermediates in the Krishtalik mechanism. Fernández, Gennero de Chialvo and Chialvo [89] performed a mathematical kinetic analysis of the current/potential relation and surface coverage of the adsorbed intermediates for the chlorine evolution reaction under the Volmer-Krishtalik mechanism and obtained Tafel regions which slopes cannot be derived from the use of the rate determining step criteria. They also demonstrated the existence of kinetically limiting current densities.

The first paper concerning the effect of pH on the Cl_2 evolution was published by Erenburg in 1984 [107]. From experimental results for 30 mol% RuO_2 + TiO_2 electrodes showing the retarding effect of H^+, the following mechanism was proposed:

$$H_2O \ \rightleftharpoons \ OH_{ad} + H^+ + e^- \tag{7.8}$$

$$OH_{ad} + Cl^- \ \rightarrow \ HOCl + e^- \tag{7.9}$$

$$HOCl + HCl \ \rightleftharpoons \ Cl_2 + H_2O \tag{7.10}$$
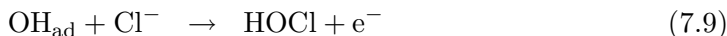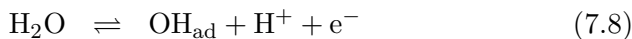
This mechanism laid the basis for a new generation of mechanisms for the Cl_2 evolution on oxide electrodes based on the possibility of acid-base equilibria at the oxide electrode surface [108]:

$$M - OH_2^+ \quad \rightleftharpoons \quad M - OH + H^+ \tag{7.11}$$

$$M - OH \quad \rightleftharpoons \quad M - O^- + H^+ \tag{7.12}$$
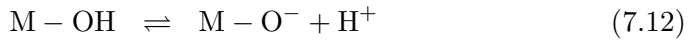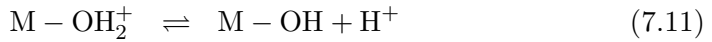
In a series of three papers, Fernández and coworkers performed a detailed kinetic study of the chlorine evolution on Ti/RuO_2 through the polarisation resistance in which they concluded with proposing a Volmer-Krishtalik-Tafel mechanism for the ClER. [90–92]

$$S^Z + H^+ \quad \rightleftharpoons \quad SH^{Z+1} \tag{7.13}$$

$$S^Z \quad \rightleftharpoons \quad S^{Z+1} + e^- \tag{7.14}$$

$$S^{Z+1} + Cl_{aq}^- \quad \rightleftharpoons \quad e^- + SCl^{Z+1} \tag{7.15}$$

$$SCl^{Z+1} + Cl_{aq}^- \quad \rightleftharpoons \quad S^Z + Cl_{2(g)} \tag{7.16}$$

$$2SCl^{Z+1} \quad \rightleftharpoons \quad 2S^{Z+1} + Cl_{2(g)} \tag{7.17}$$
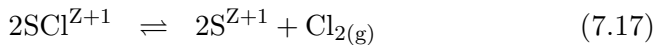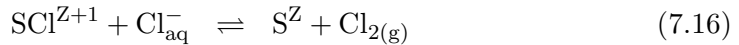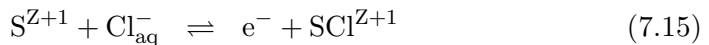
Where SZ and SZ^{+1} are non-oxidised and oxidised surface sites respectively.

7.2.1   Purpose of the present work

As mentioned above, the industrially important chlorine evolution reaction on RuO_2 and mixed ruthenium titanium oxides (RTO) has been extensively examined, there are still several kinetic aspects that continue to be under discussion. The corresponding reduction reaction has been explored to a much less extent and most frequently as a small section in a larger investigation of the chlorine evolution reaction. In the present work, we have examined the influence of H^+ concentration on the relatively uninvestigated chlorine reduction kinetics, with the purpose of trying to further elucidate the nature of the ClER mechanism and to increase the understanding of the chlorine reduction reaction on oxide electrodes. Mechanisms proposed for the chlorine evolution reaction has been

evaluated against the experimental data and the most promising have been analysed closely by derivation of rate equations and numerical curve-fitting to the experimental data.

7.3   Experimental

A rotating ring-disc electrode (PINE instruments MTI34 , AFMSRX rotator) with an interchangeable disc was used to establish a well-defined mass transfer regime to the working electrode. The ring was not used in the following experiments. The electrode had a diameter of 6.0 mm and consisted of ruthenium (99.9%, Goodfellow). The electrode was polished to a mirror finish using alumina powder down to 0.5 μm in size. The cell was a cylindrical glass vessel of 300 ml capacity, with a double bottom in which temperature controlled water could circulate. All experiments were performed at 25 $\pm$ 1 °C. The cell also consisted of an inlet and outlet for chlorine gas, a glass capillary connected to the reference electrode compartment and an opening for the rotating disk electrode. The glass cell was made gas tight with the use of a PTFE-plug with a ball bearing fitted around the electrode shaft. An Ag/AgCl (Metrohm) reference electrode immersed in the working electrolyte was employed and all the reported potentials (if not specifically stated) are referred to this electrode. The potential of the working electrode was controlled with a Solartron SI 1287 potentiostat. Before every new set of experiments, the cell was rinsed with distilled water and fresh electrolyte was added. The reported experimental results are all iR corrected, both for the electrolyte resistance and the resistance in the rotating disk electrode.

7.3.1   Cyclic voltammetry

Cyclic voltammograms were recorded to characterise the ruthenium electrode both before and after electrooxidation. The electrolyte (1.00 M HCl) was constantly purged with argon to remove any dissolved oxygen and a potential sweep rate of 500mV s^{-1} was used. The current and potential were recorded using an ADC-212 digital oscilloscope (Pico Technologies). After polishing, the electrode was immersed in the solution and a cyclic voltammogram was immediately recorded. This was assumed to be the response of the non oxidised, metallic ruthenium electrode. The electrode was then polarised at 1.3 V for 10 minutes and a new voltammogram recorded. After the polarisation at 1.3 V

and recording of the CV, the electrode was held at 0.5 V for 10 minutes, -0.2 V for 30 minutes and -0.2 V for 12 hours consecutively. Between each potential hold, a voltammogram was recorded.

7.3.2   Rotating disk electrode measurements

Before each measurement, the ruthenium electrode was polished with 0.5 μm alumina powder, washed with distilled water and inserted in the cell. It was then oxidised at 1.3 V for 10 minutes to ensure a reproducible oxidation state of the electrode. Chlorine reduction measurements were then performed in the potential range between open circuit and -0.2 V with intervals of 25 mV at low overpotentials and 50 mV at higher overpotentials. The potential steps lasted 15 s or until a stable current within 1% was achieved. This procedure was repeated for several electrode rotation speeds ranging from 200 to 4000 rpm. The electrolyte consisted of different NaCl - HCl - HClO$_4$ solutions with constant concentration of 1 mol dm^{-3} Cl$^-$ and a concentration of H$^+$ranging between 0.01 mol dm^{-3} and 5 mol dm^{-3}, see Table 7.1. The electrolyte solutions were prepared with NaCl(p.a. Merck), conc Suprapur$^{\textregistered}$ HCl (Merck) and HClO$_4$ (70% Fluka) The electrolyte was saturated with chlorine gas (2.8 Gerling Holtz) by gas bubbling for 30 min before each experiment.

Table 7.1: Electrolyte concentrations mol dm^{-3}

Solution	c_{HCl}	c_{NaCl}	c_{HClO_4}
1	0.010	0.990	0
2	0.024	0.976	0
3	0.059	0.941	0
4	0.143	0.857	0
5	0.349	0.651	0
6	0.847	0.153	0
7	1.000	0	1.057
8	1.000	0	4.000

7.4   Results

7.4.1   Cyclic voltammetry measurements

Cyclic voltammograms recorded at 500 mV s^{-1} of non-oxidised and electroox-
idised ruthenium in 1.0 mol dm^{-3} are shown in Figure 7.1. The currents gen-
erated in the cyclic voltammetry, $I = C\frac{dV}{dt}$, provide a measure of the elec-
trochemical capacitance, C, of the oxide system [109, 110]. For RuO$_2$ this in-
cludes a double-layer capacitance and the pseudo-capacitance associated with
Ru redox-processes in the film [109]. It can be observed that the current on
the non-oxidised ruthenium is lower than those for the oxidised electrodes and
having a somewhat different shape with oxidation peaks at higher anodic poten-
tials. The voltammograms for the electrodes held at 1.3 V for 10 minutes, 0.5
V for 10 minutes and -0.2 V for 30 minutes are comparable, the only discernible
difference being the size of the reduction peak at ~0.1 V in the cathodic sweep.
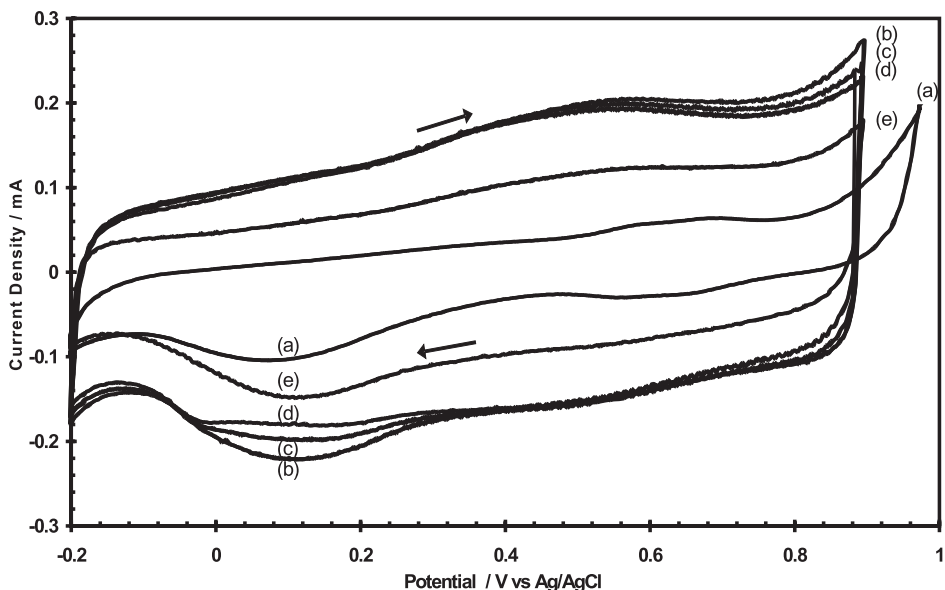
Figure 7.1: Cyclic voltammogram of ruthenium electrode. 1.0 M HCl 500 mV
s^{-1}. (a) polished, non-oxidised ruthenium, and electro-oxidised at (b) 1.3 V for
10 min, (c) 0.5 V for 10 min, (d) -0.2 V for 30 min, (e) -0.2 V for 12 hours

Even when the electrode was held for 12 hours at -0.2 V, the shape of the curve resembles that of ruthenium oxide, although the current is somewhat lower. These results indicate that the oxide formed by electrooxidation at 1.3 V is relatively stable even at potentials down to -0.2 V. Only part of the oxide formed on the ruthenium electrode is possible to reduce electrochemically and then only when held at very cathodic potential for several hours.

7.4.2 Chlorine reduction

The chlorine reduction reaction was studied at different electrode rotation rates. Figure 7.2 shows the current/potential response for various rotation rates in solution 8 (5 mol dm^{-3} H^+).
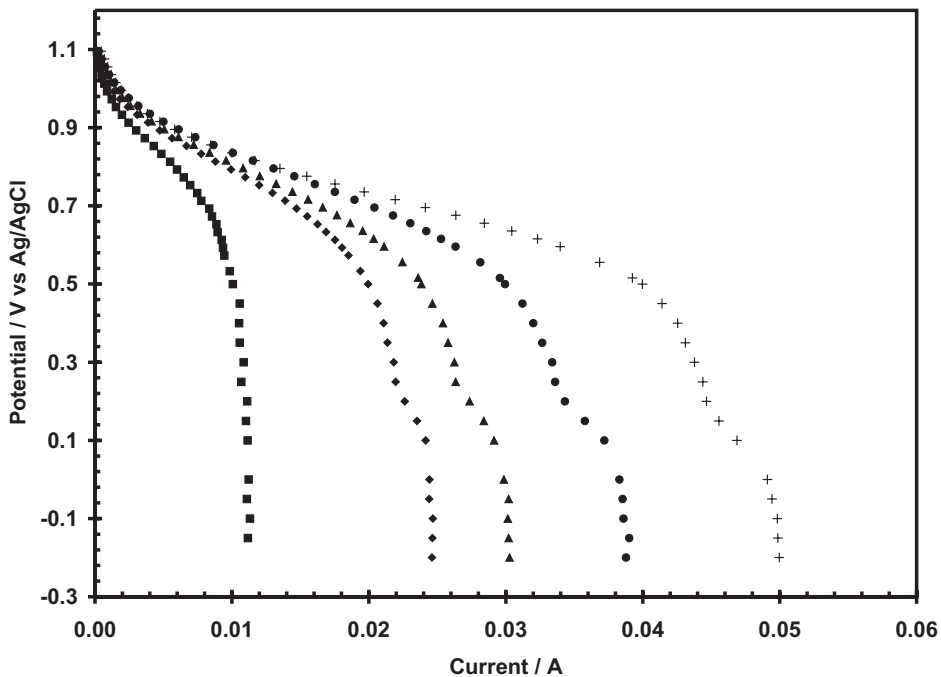
Figure 7.2: Chlorine reduction at different rotation rates, solution 8. ■: 500 rpm, ♦: 1000 rpm, ▲: 1500 rpm, ●: 2500 rpm, +: 4000 rpm

At high rotation rates two different cathodic limiting currents can clearly be

observed. The first appearing at an electrode potential close to 0.5 V, while
the other appears at potentials close to 0 V. This behaviour is also observed
in solution 7, but not in the other solutions with higher pH. A limiting current
can occur either due to mass transport limitations of reactants to the electrode
surface or due to the kinetic mechanism of the reaction. To test if the observed
limiting currents are related to either mass transport or kinetics, plots of i_d
vs. $\sqrt{\omega}$ for the two limiting currents were performed as shown in Figure 7.3.
For a mass transport induced limiting current this plot should be linear and
intersect the current-axis at zero. As can be observed, this is the case for the
limiting current observed at $\sim$0 V (a), while the one appearing close to 0.5 V
(b) neither has a linear relationship between i_d and $\sqrt{\omega}$ nor does it intersect the
y-axis at zero current. This implies that the first limiting current at 0.5 V is
most probably due to the specific chlorine reduction mechanism and not mass
transport control of a reactant to, or products from, the electrode surface. In
all other solutions only one limiting current is observed, which in all cases is
caused by mass transport limitations.
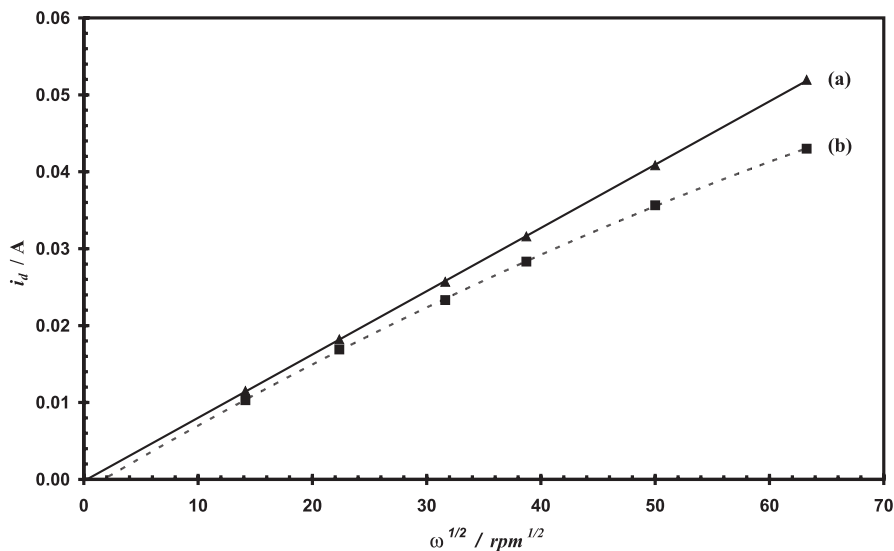
Figure 7.3: Limiting current vs. $\sqrt{\omega}$, obtained at a) 0 V and b) 0.5 V. Solution
8

7.4.3 Rest potential

The rest potential of the electrooxidised (1.3 V, 10 min) ruthenium electrode was measured in solutions 1-8, saturated with chlorine. The variation of the rest potential on H^+ concentration is shown in Figure 7.4. At high concentrations of H^+, the rest potential is shifted to more cathodic values. This effect may be due to a corrosion process of the ruthenium oxide, forming higher valent soluble Ru-species. At intermediate H^+ concentrations the rest potential moves trough a maximum and then decreases with decreasing H^+ concentration. This shift towards more cathodic potentials is probably due to a mixed potential originating from oxygen formation due to water discharge and chlorine reduction [111–114].
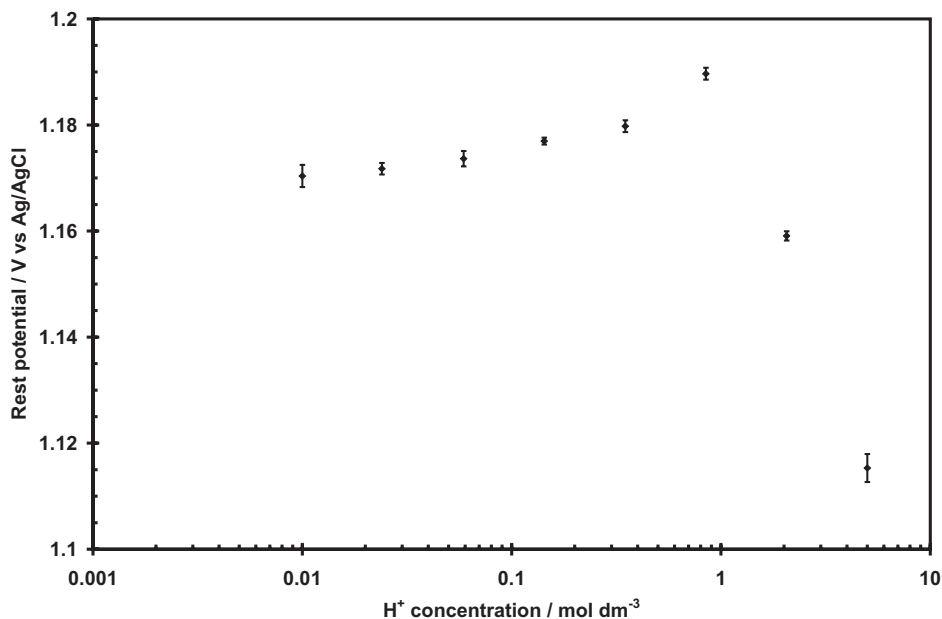
Figure 7.4: Dependence of the rest potential of electrooxidised Ru on H^+ concentration

7.4.4 Charge transfer kinetics

To be able to perform a mechanistic investigation of the chlorine reduction reaction it is imperative to separate the kinetic controlled current from mass

transport effects. By using the rotating disc electrode technique, very good control of the mass transport rate of reactants to the electrode is obtained and it is thus possible to calculate the surface concentration of the reactant and the kinetic controlled current, i_k. Using the following relationship, the kinetically controlled current can be extracted directly from the experimental data [81]:

$$i_k = i \left(\frac{i_d}{i_d - i} \right)^p = k[Cl_2]^p \qquad (7.18)$$

The reaction order with respect to chlorine, p, has in previous work been found to be close to 1 [29]. A plot of i_k against E will show the current/potential relation without any effects of mass transport and should be independent of rotation rate. Figure 7.5 displays this relationship for all solutions and rotation rates.

7.5   Determination of reaction mechanisms and development of rate equations

7.5.1   Reaction mechanisms

To perform a mechanistic analysis of the chlorine reduction reaction on electrooxidised ruthenium it is necessary to derive the theoretical expressions of the dependence of the current density on overpotential. The first step of this derivation is to develop reaction schemes based on elementary reaction steps. These schemes, together with assuming a certain behaviour for the adsorption of the intermediate species, form the basis for the development of the rate equations. In attempting to explain the experimental results, two reaction mechanisms, previously proposed for the chlorine evolution, have been deemed to be the most interesting; The Volmer - Krishtalik (VK) and the Erenburg (E) mechanisms.

The VK - mechanism has been shown by several authors to satisfactorily describe the chlorine evolution on RuO_2 and RTO [63]. Although it does not include any steps that show any pH-dependence directly in the mechanism it has been suggested that a surface equilibrium step independent of the mechanism itself explains the electrode behaviour on pH (Eq. 7.19) [90]. Rewriting this reaction scheme for the reduction of chlorine we get:

$$S^Z + H^+ \;\; \rightleftharpoons \;\; SH^{Z+1} \tag{7.19}$$

$$Cl_2 + S^Z \;\; \rightleftharpoons \;\; SCl^{Z+1} + Cl^- \tag{7.20}$$

$$SCl^{Z+1} + e^- \;\; \rightleftharpoons \;\; S^{Z+1} + Cl^- \tag{7.21}$$

$$S^{Z+1} + e^- \;\; \rightleftharpoons \;\; S^Z \tag{7.22}$$
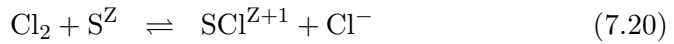
The equilibrium in Eq. (7.19) is based on the assumption that the surface of the oxide electrodes assumes one or more equilibria with the solution [102,108]. It has been established that for the pH regions most commonly used, only one equilibrium is of importance [115]. The above mechanism proposes that the fraction of protonated superficial sites (SH^{Z+1}) is solely dependent on the pH and that these sites are inhibited from participating in any other type of reaction, such as the electrochemical adsorption of chlorine (Eq. 7.20).

Another possibility, is to include the protons directly into the reaction mechanism. Erenburg suggested a reaction scheme for chlorine evolution [102, 107] (Written here for chlorine reduction)

$$S - O + Cl_2 + e^- \;\; \rightleftharpoons \;\; S - OCl + Cl^- \tag{7.23}$$

$$S - OH + Cl_2 \;\; \rightleftharpoons \;\; S - OCl + Cl^- + H^+ \tag{7.24}$$

$$S - OCl + e^- \;\; \rightleftharpoons \;\; S - O + Cl^- \tag{7.25}$$

$$S - O + H^+ + e^- \;\; \rightleftharpoons \;\; S - OH \tag{7.26}$$

$$S - OH + H^+ \;\; \rightleftharpoons \;\; S - OH_2^+ \tag{7.27}$$
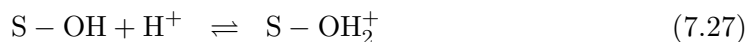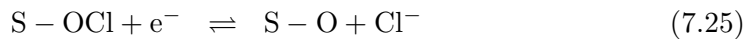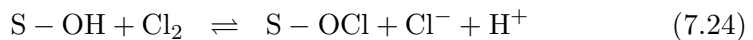
where both an acid-base equilibrium (Eq. 7.27) and an electrochemical step including protons (Eq. 7.26) are included.

7.5.2   Development of rate equations

The rate equations for the proposed mechanisms are developed according to standard electrode kinetics theory [67]. The derivations are based on the following assumptions:

1. The adsorption of the reaction intermediates follow the Langmuir isotherm.

2. The transfer coefficients for the different electron transfer steps are considered to be equal and independent of potential.

3. The concentration of the chloride ions and protons at the electrode surface is considered to be essentially equal to the bulk concentration.

The rate equations for the VK and E mechanisms are listed in Appendix 7.10.

Volmer-Krishtalik mechanism

From the reaction scheme described above (chapter 7.5.1) it can be seen that only one independent reaction route exists. At steady state, the relationship between the global reaction rate and the corresponding rates of the elementary steps can be found by applying a mass balance to all the adsorbed species:

$$\frac{\partial \theta_i}{\partial t} = 0 \tag{7.28}$$

$$\frac{\partial \theta_{S^Z}}{\partial t} = -v_1 - v_2 + v_4 = 0 \tag{7.29}$$

$$\frac{\partial \theta_{SH^{Z+1}}}{\partial t} = v_1 = 0 \tag{7.30}$$

$$\frac{\partial \theta_{SCl^{Z+1}}}{\partial t} = v_2 - v_3 = 0 \tag{7.31}$$

$$\frac{\partial \theta_{S^{Z+1}}}{\partial t} = v_3 - v_4 = 0 \tag{7.32}$$

Where v_1, v_2, v_3 and v_4 corresponds to the rate of Eqs. 7.23 - 7.27 respectively.

Combining equations 7.29-7.32, the following relationship can be extracted:

$$j/F = 2v_2 = 2v_3 = 2v_4 \tag{7.33}$$

The expressions of the rates of the elementary steps are:

$$
\begin{aligned}
v_1 &= k_1 C_{H^+}\theta_I - k_{-1}\theta_{II} & (7.34) \\
v_2 &= k_2 C_{Cl_2}\theta_I - k_{-2}\theta_{III}C_{Cl^-} & (7.35) \\
v_3 &= k_{3_k}\theta_{III}exp(-(1-\alpha)f\eta) - k_{3_a}\theta_{IV}C_{Cl^-}exp(\alpha f\eta) & (7.36) \\
v_4 &= k_{4_k}\theta_{IV}exp(-(1-\alpha)f\eta)) - k_{4_a}\theta_I exp(\alpha f\eta) & (7.37)
\end{aligned}
$$

Using Eqs. (7.33-7.37), the rate equation (the relationship between the kinetic current, i_k, and the known quantities C_{H^+}, C_{Cl^-}, C_{Cl_2} and η) can be found. This equation is listed in chapter 7.10.

Erenburg mechanism

This reaction scheme describes a more complex reaction route for the reduction of chlorine than the Volmer-Krishtalik mechanism above. It can be shown that there exists two parallel reaction routes, either through the oxidised surface site S-O or via the reduced, protonated site S-OH. Performing the same analysis as for the VK-mechanism above, the following relationship between the global reaction rate and the rates of the individual elementary steps are obtained:

$$
\begin{aligned}
\frac{\partial\theta_{S-O}}{\partial t} &= -v_1 + v_3 - v_4 = 0 & (7.38) \\
\frac{\partial\theta_{S-OCl}}{\partial t} &= v_1 + v_2 - v_3 = 0 & (7.39) \\
\frac{\partial\theta_{S-OH}}{\partial t} &= -v_2 + v_4 - v_5 = 0 & (7.40) \\
\frac{\partial\theta_{S-OH_2^+}}{\partial t} &= v_5 = 0 & (7.41)
\end{aligned}
$$

Where v_1, v_2, v_3, v_4 and v_5 corresponds to the rate of Eqs. (7.19 - 7.22) respectively. Combining equations 7.38-7.41 we get:

$$
j/F = v_1 + v_3 + v_4 = v_1 + v_2 + v_3 = 2\,v_1 + 2\,v_2 \qquad (7.42)
$$

The expressions of the rates of the elementary steps are:

$$v_1 \;\; = \;\; k_{1_k} C_{Cl_2} \theta_I exp(-(1-\alpha)f\eta)) - k_{1_a} C_{Cl^-} \theta_{II} exp(\alpha f\eta) \qquad (7.43)$$

$$v_2 \;\; = \;\; k_2 C_{Cl_2} \theta_{III} - k_{-2} C_{Cl^-} C_{H^+} \theta_{II} \qquad\qquad\qquad (7.44)$$

$$v_3 \;\; = \;\; k_{3_k} \theta_{II} exp(-(1-\alpha)f\eta) - k_{3_a} C_{Cl^-} \theta_I exp(\alpha f\eta) \qquad (7.45)$$

$$v_4 \;\; = \;\; k_{4_k} C_{H^+} \theta_I exp(-(1-\alpha)f\eta) - k_{4_a} \theta_{III} exp(\alpha f\eta) \qquad (7.46)$$

$$v_5 \;\; = \;\; k_5 C_{H^+} \theta_{III} - k_{-5} \theta_{IV} \qquad\qquad\qquad\qquad (7.47)$$

The expression for the total current is given in chapter 7.10.

7.6   Test of the theoretical rate equations

7.6.1   Fitting of i_k values

The rate equations for the Volmer-Krishtalik and the Erenburg mechanisms were evaluated against the experimental results by performing a nonlinear curve fitting using the *lsqnonlin* function in MATLAB R14. The fitting procedure takes into account the variation of the kinetic current with both overpotential and pH simultaneously and performs a weighted least square adaptation to the experimental values of i_k. The results of the nonlinear regression analysis of the experimental i_k values and the theoretical rate equations are shown in Figure 7.5.
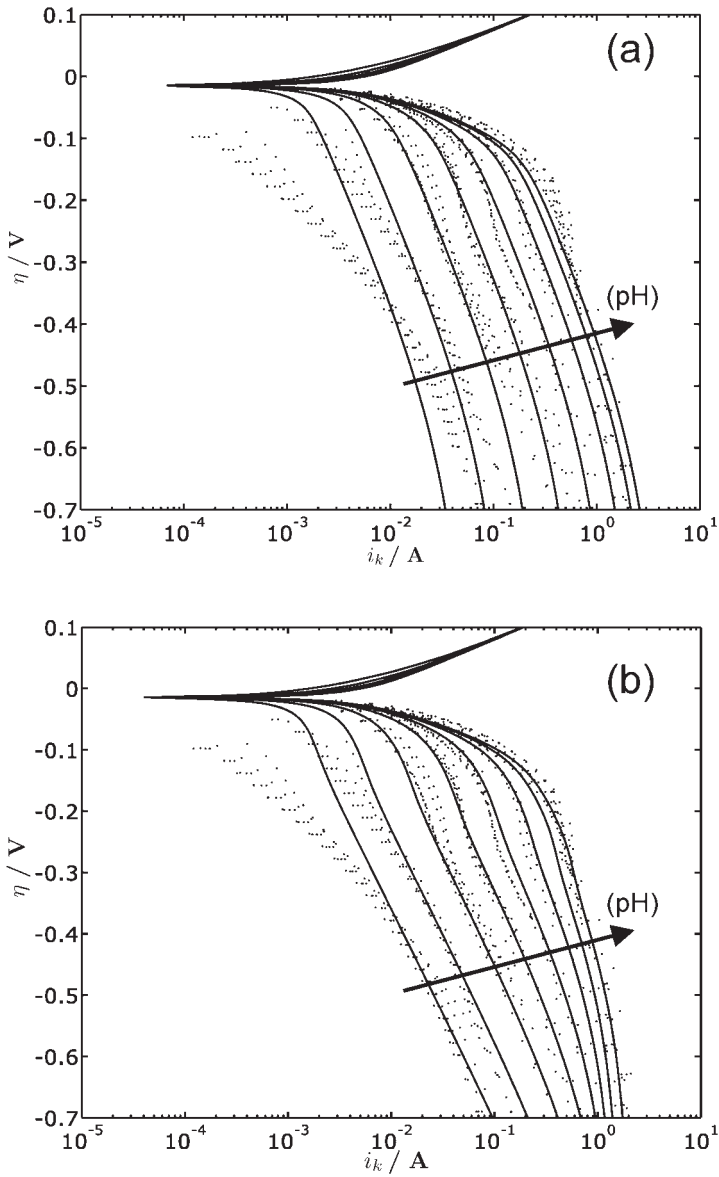
Figure 7.5: Experimental i_k values (dots) as a function of pH and fits by the theoretical rate equations for the Volmer-Krishtalik (a) and Erenburg (b) mechanisms. Experimental conditions are described in chapter 7.4.2

.

As can be seen from Figure 7.5, the resulting fit from the nonlinear regression of the Erenburg mechanism is significantly better than that of the Volmer-Krishtalik mechanism. One of the main differences can be observed at high overpotentials where the Erenburg mechanism describes the variation of i_k with H^+ concentration considerably better than the Volmer-Krishtalik mechanism. The Erenburg mechanism is also able to describe the wave resembling a limiting current behaviour seen at overpotentials close to -0.2 V and intermediate pH values, while the Volmer-Krishtalik mechanism completely ignores this feature. None of the suggested mechanisms describes the chlorine reduction at high H^+ concentrations and low overpotentials satisfactorily. Since this discrepancy only is seen at very low pH (< 0) and at low cathodic overpotentials, it is possible that this might be caused by the occurrence of a competing anodic reaction causing the total current to decrease. This anodic reaction is possibly corrosion of the ruthenium oxide surface which also can explain the low rest potential of the electrode observed at low pH, as described in Chapter 7.4.3.

7.6.2   Prediction of the reaction order

The developed theoretical rate equations with the parameters determined from the curve fitting procedure can be employed to predict the reaction order of both chlorine and chloride. These calculated reaction orders can then be evaluated against experimentally determined values and thus further test the validity of the proposed mechanisms. In Figure 7.6, the predicted reaction orders for chlorine and chloride by both reaction mechanisms are shown.

Figure 7.6: Calculated Cl_2 and Cl^- reaction orders based on kinetic constants in Table 7.2. Volmer-Krishtalik (a) and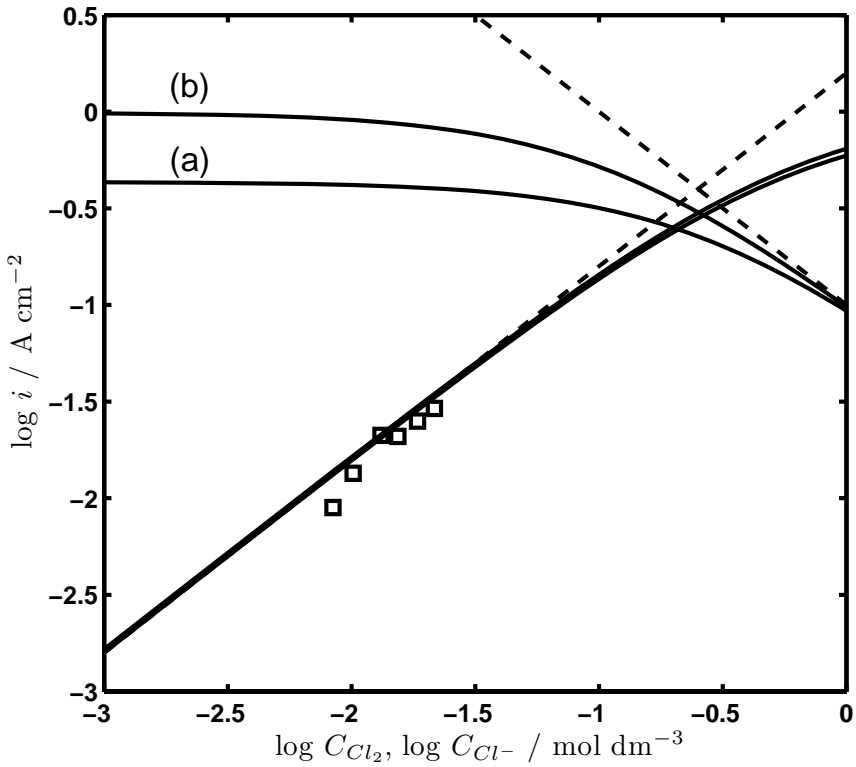 Erenburg (b) mechanisms, dotted lines represents a reaction order of 1 and -1. The open squares are the experimentally obtained variation of i on C_{Cl_2} ($\eta = -0.2$ V, pH $= 0.8$)

It can be seen that both mechanisms predicts a chlorine reaction order of 1 and a chloride reaction order of -1 at high Cl^- concentrations approaching 0 at low concentrations. The only differences seen between the mechanisms are small deviations at high chlorine concentrations and low chloride concentrations respectively.

The surface concentration of chlorine can be varied by altering the rotation rate of the electrode. By monitoring the change in current density one can find the reaction order by applying the following equation [29, 81]:

$$\log i = \log k + p \log \left(\frac{i_d - i}{i_d} \right) [Cl_2] \qquad (7.48)$$

The open squares in Figure 7.6 depict experimentally obtained values for the chlorine reduction current at different chlorine surface concentrations, which correspond well to the predicted reaction order for chlorine. Values found earlier [29, 63] shows comparable results for the reaction order.

The reaction order for chloride in the chlorine evolution reaction has been reported by several authors to be 1 [82, 104–106], and -0.9 for the chlorine reduction reaction [63]. Thus a cathodic Cl^- reaction order of -1, as predicted in Figure 7.6, is a likely value. Figure 7.7 shows experimentally determined and the predicted reaction orders from the developed rate equations for H^+ at three different overpotentials. It can be seen that the Erenburg mechanism coincides better with the experimentally determined values for the H^+ reaction order at low H^+ concentration better than the Krishtalik mechanism and that it is able to describe a reaction order changing with potential.

The predicted reaction orders for Cl_2 and Cl^- described above qualifies both reaction mechanisms as probable descriptions of the experimental results, since both give sensible values for the reaction orders. The analysis of the H^+ reaction order, like the regression analysis, favours the Erenburg mechanism. Thus, the results suggest that the Erenburg mechanism is the mechanism describing the chlorine reduction on electrooxidised ruthenium at these experimental conditions best.
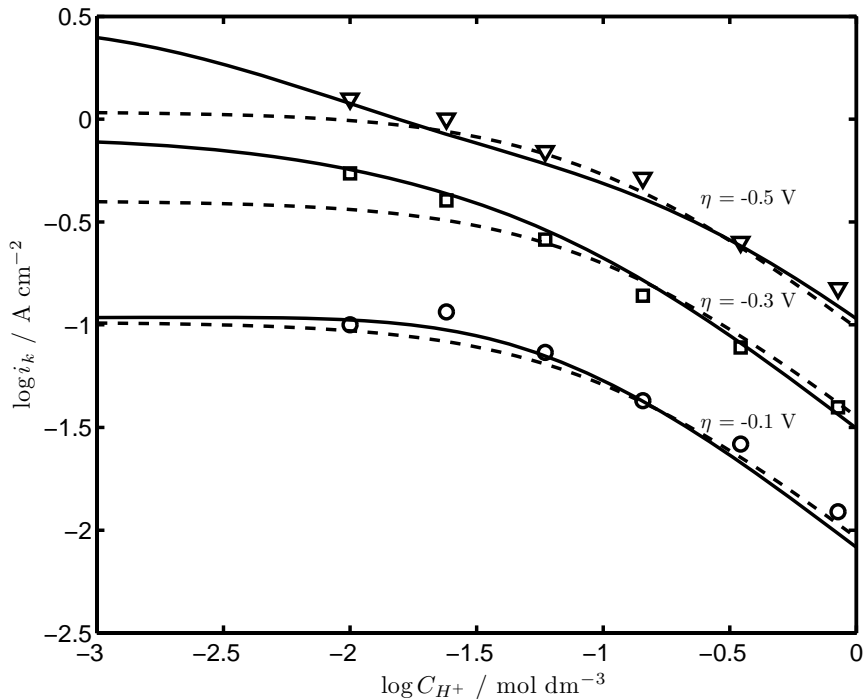
Figure 7.7: Calculated H^+ reaction orders at different overpotentials based on kinetic constants in Table 7.2. The full lines represents the Erenburg mechanism while the dotted lines represents the Volmer-Krishtalik mechanism.

7.7 Discussion

It has been concluded from the nonlinear regression analysis that the Erenburg mechanism describes the chlorine reduction on electrooxidised ruthenium satisfactorily and significantly better than the Volmer Krishtalik mechanism. The main advantage of the Erenburg mechanism over the Volmer-Krishtalik is the addition of an elementary step which is dependent on both the proton concentration and the electrode potential. This property allows the mechanism to describe a H^+-reaction order which changes with potential, as is the case with the measured behaviour of the chlorine reduction reaction. The mechanism also includes two reaction paths, introducing the possibility of the mechanism switching between these paths with potential. This dual reaction pathway prop-

erty provides the Erenburg mechanism with the ability to describe the limiting current wave seen at intermediate potentials and pH values in Figure 7.5.

The evaluation of the two mechanisms is based on the assumption that the Langmuir isotherm is applicable for the adsorbed intermediates. Using other, more complex, isotherms such as the Frumkin or Temkin models would possibly improve the descriptive capability of the mechanisms. On the other hand, introduction of more fitting parameters does not automatically give significantly better fits to the experimental data. The use of these adsorption isotherms has not been evaluated in this work, due to the complexity of the resulting rate equations.

It has been shown [97] that for reactions with complex mechanisms with formation of stable soluble intermediates, e.g. the oxygen reduction mechanism, the number of electrons exchanged per reactant is a function of the potential of the electrode and cannot be evaluated theoretically in a simple matter. The use of the rotating disk technique in elucidating the overall kinetic parameters for such processes is limited and should be performed with caution. In this analysis it has been assumed that all reaction intermediates are adsorbed on the electrode surface and thus are not transported away from the electrode before being completely reduced to chloride. It has been suggested that one of the reaction intermediates could be $HClO$ [106] or ClO_2 [116]. The existence of such soluble reaction intermediates would add an unknown error to the experimental results and render the kinetic analysis incorrect. However, these suggestions have not been substantiated further and the assumption of adsorbed intermediates seems to have more consensus. In addition, the low pH in the solutions used in this study should minimise the amount of the soluble intermediates, if these exist.

7.7.1   Rate of elementary reactions

The values of the kinetic constants in the theoretical rate equations are shown in Table 7.2. Using these values it is possible to calculate the rate of the individual elementary reactions. For the Erenburg mechanism this can illustrate which reaction path is predominant at different pH-values and overpotentials by inserting the parameters in Eqs. (7.43 - 7.46).

Table 7.2: Kinetic constants for the elementary steps of the ClER obtained from the correlation with the experimental data. In $\text{mol s}^{-1}\text{ cm}^{-2}$

Mechanism	k_1	k_2	k_3	k_4	k_5	α
Erenburg	5.70×10^{-5}	0.0023	4.63×10^{-5}	0.0026	4.41×10^{-14}	0.82
Volmer-Krishtalik	2.199×10^{-5}	0.1186	7.15×10^{-5}	0.0153	-	0.86

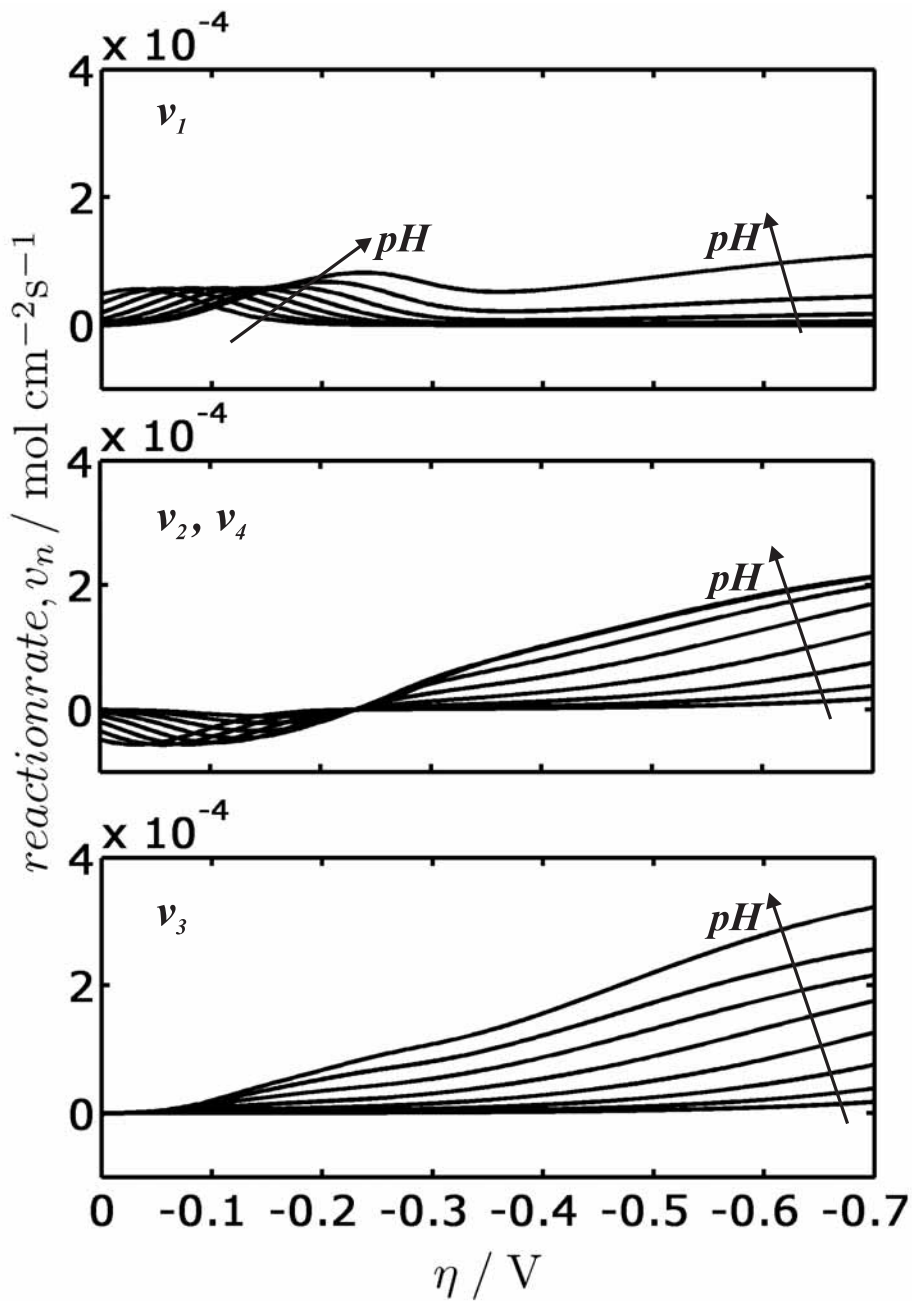| Mechanism	k_{-1}	k_{-2}	k_{-3}	k_{-4}	k_{-5}
Erenburg	1.51×10^{-6}	0.0082	4.11×10^{-3}	1.55×10^{-6}	0.833
Volmer-Krishtalik	1.667×10^{-6}	0.0260	0.3150	3.55×10^{-6}	-

Figure 7.8: Calculated reaction rates for the different elementary steps in the Erenburg mechanism based on kinetic constants in Table 7.2.

Figure 7.8 displays the rates of the elementary steps for the Erenburg mechanism as a function of overpotential and pH. It can be observed that v_1, the reduction of chlorine on the oxidised surface sites (Eq. 7.23), move through a maximum at intermediate overpotentials. The position of this maximum is strongly dependent on the pH of the solution, moving to more cathodic potentials with increasing pH. At high overpotentials a slight increase of the reaction rate can be seen for the solutions with the lowest H^+ concentrations. The rates v_2 and v_4, reduction of chlorine on the reduced surface sites (Eq. 7.24) and the reduction of oxidised surface sites (Eq. 7.26) are identical, as expected from (Eq. 7.42). An interesting result is that the rate of these reactions are negative at low overpotentials, indicating the existence of a back reaction to chlorine from the adsorbed S-OCl surface specie. This back reaction is most pronounced at high pH values, but has a common intersection with the abscissa at an overpotential of -0.25V. This feature might indicate that the electrochemical protonation of the S-O surface sites has an equilibrium potential at this value. At more cathodic potentials however, the rate increases and is heavily dependent on the solution pH. Finally, v_3, the reduction of the S-OCl surface specie (Eq. 7.25) has a low rate of reaction at the more anodic potentials before steadily increasing as the potential of the electrode is shifted to more cathodic values. A small indication of a limiting rate at intermediate overpotentials and high pH can be observed. The rate of this elementary reaction is increasing strongly with pH.

The two different reaction paths are described by the sum of either v_1 and v_3 (path I) or v_3 and v_4 (path II). From Figure 7.8, it can be concluded that path I dominates at low overvoltages due to the S-O surface specie being in majority, while at overpotential more cathodic than -0.3 V path II dominates.

7.7.2 Surface coverages

Figure 7.9 shows the surface coverage of the adsorbed intermediates as a function of overpotential and pH. The analysis showed that $\theta_{S-OH_2^+}$ has a maximum value of 10^{-14} and this surface specie is therefore not depicted in the figure. At high H^+ concentrations the dominating specie at the rest potential is clearly the reduced, protonated surface cite (S − OH), while at higher pH values the oxidised (S − O) sites are in majority. The coverage of the oxidised sites rapidly decrease when polarising the electrode cathodically, as is expected from Eq. (7.26). This rapid decrease is most probably the reason of the low value of v_1 in Figure 7.8. The coverage of the S − OCl surface species moves through a

maximum at intermediate overvoltages before slowly decreasing towards zero at more cathodic potentials. The height of the maximum is strongly dependent on pH and is completely absent in the more acidic solutions. The amount of reduced, protonated surface sites strongly increase with increasing cathodic overvoltage, but at higher pH the increase is retarded and a plateau region at intermediate overvoltages develops. As earlier mentioned, the amount of $\theta_{S-OH_2^+}$ is apparently negligible and it can be concluded that the acid base equilibrium in the proposed Erenburg mechanism (Eq. 7.27) is superfluous and can be removed from future mechanistic analyses.
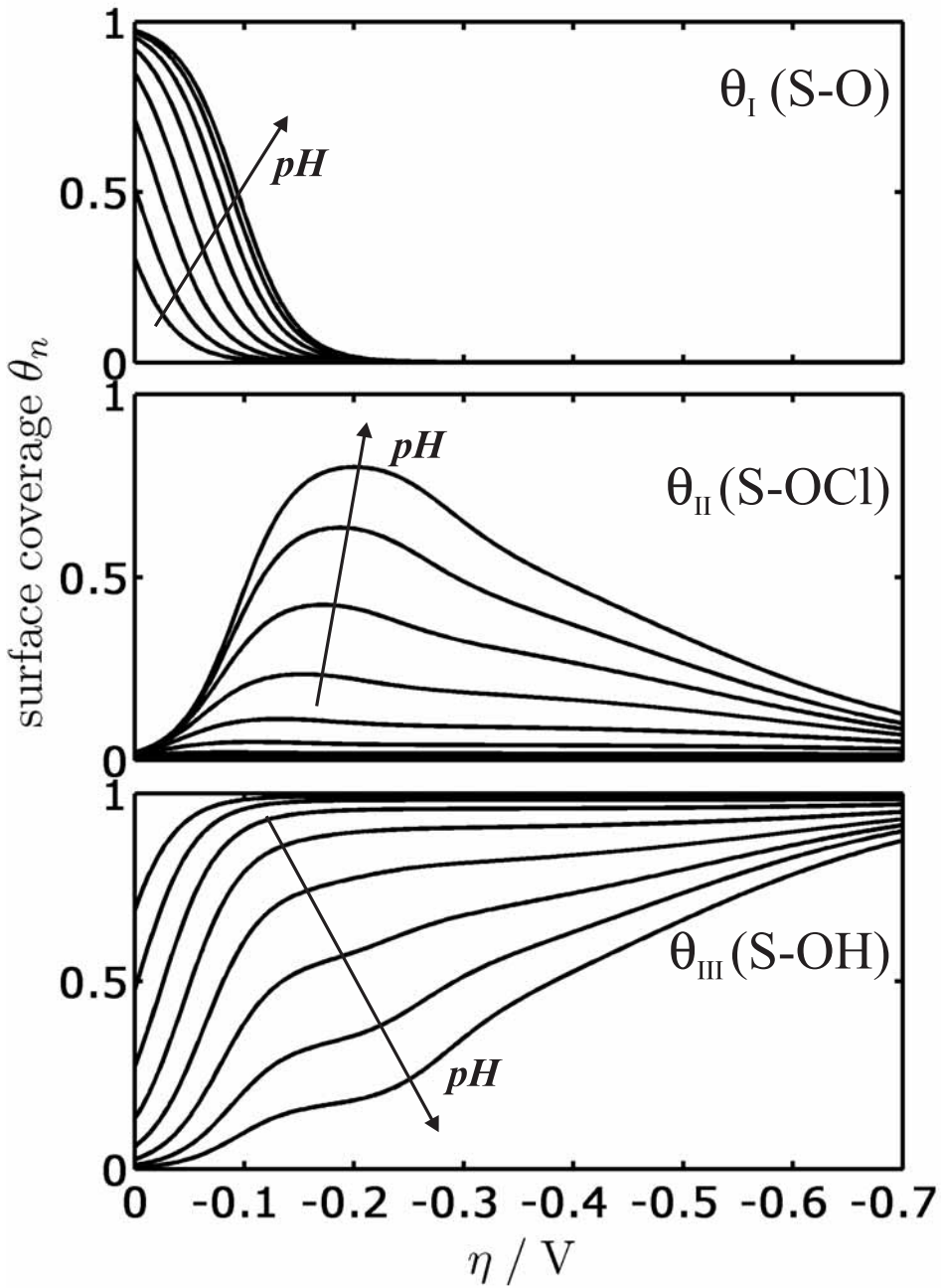
Figure 7.9: Calculated surface coverages for the different adsorbed species in the Erenburg mechanism based on the kinetic constants in Table 7.2.

7.7.3   Analysis of kinetic data

In the performed mechanistic analysis and the subsequent numerical fitting of the rate equations to the experimental data, no assumptions of rate determining steps were used. The rate constants presented in Table 7.2 together with the surface coverages of the adsorbed intermediates shown in Figure 7.9 indicates that the rate determining step for the chlorine reduction is the reduction of the adsorbed chlorine intermediate (Eq. 7.25) at low overpotentials, switching to the chemical reaction between the reduced surface site and chlorine (Eq. 7.24) at higher overpotential. Erenburg [107] determined that the reduction of the adsorbed chlorine intermediate is rate determining in the chlorine evolution reaction, corresponding well to the results found in this study.
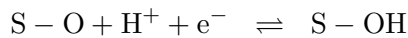
The value of the anodic transfer coefficient α, obtained by the fitting procedure, gave a relatively high value of 0.82. This result is in agreement with previously published work [29]. This high value of the transfer coefficient indicates that the electron transfer from the reduced species to the electrode is energetically favoured over the reverse transfer of electrons from the electrode to the oxidised species. This results in a asymmetry between the anodic and cathodic polarisation curves. In reality each of the electron transfer steps should have an unique transfer coefficient assigned; β_i, where i indicates the different elementary steps. This would however, substantially increase the number of fitting parameters and thus the complexity of the model without necessarily improving the fit significantly.

Using the rate constants determined and the Erenburg rate equation to predict the behaviour of the anodic evolution of chlorine, a slight dependence of the solution pH at low overpotentials is found. At higher overpotentials the curves coincides and has a Tafel slope close to 70 mV dec^{-1}. This Tafel slope is somewhat higher than the slope usually observed for chlorine evolution on RuO_2 and RTO and is possibly due to the oxide being formed electrochemically instead of the more commonly thermally prepared RuO_2. The disparity in preparation of the oxide may lead to differences in chemical as well as morphological properties of the electrode. It is well known from other studies that rough/porous electrodes may give rise to low Tafel slopes for the hydrogen evolution reaction [117].

The results from this study correspond well to earlier results from the investigation of chlorine reduction on RuO_2 single crystal electrodes [88]. It was found that the active oxide sites initially available for chlorine reduction gradually become transformed to hydroxyl groups.

7.8   Conclusions

The reduction of chlorine on electrooxidised ruthenium has been studied in order to quantitatively evaluate the effect of pH on the electrocatalytic activity of the electrode material. It was found that the activity of electrooxidised ruthenium is highly dependent on pH and that the chlorine reduction rate is highly inhibited in solutions with high H^+ concentrations. Chlorine reduction on electrooxidised ruthenium can be satisfactorily described by the Erenburg mechanism previously suggested for the chlorine evolution on RuO_2 and RTO. This involves the following sequence of steps:
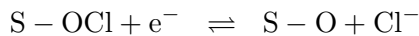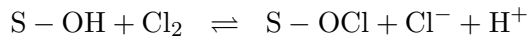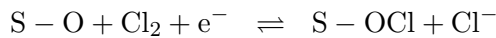
$$S - O + Cl_2 + e^- \rightleftharpoons S - OCl + Cl^-$$

$$S - OH + Cl_2 \rightleftharpoons S - OCl + Cl^- + H^+$$

$$S - OCl + e^- \rightleftharpoons S - O + Cl^-$$

$$S - O + H^+ + e^- \rightleftharpoons S - OH$$

7.9   Acknowledgements

7.10   Rate equations

Equation 7.49 is the derived equation for the total current density of the Krishtalik mechanism.

$$
i_T = \frac{
\begin{aligned}
&\big[2F k_{-1}(k_2^2 C_{Cl_2}^2 k_3 \exp(2(-1+\alpha)f\eta)k_{-1}k_4 - k_2 C_{Cl_2} k_{-3} C_{Cl^-} \exp(f\eta(3\alpha-2))k_4 k_{-1}k_3\\
&-k_2 C_{Cl_2} k_{-3} C_{Cl^-} \exp(f\eta(3\alpha-2))k_4 k_3 k_1 C_{H^+} - k_{-2} C_{Cl^-}^2 k_{-4} \exp(2\alpha f\eta)k_{-3} k_2 C_{Cl_2} k_{-1}\\
&+k_{-2}C_{Cl^-}^3 k_{-3}^2 \exp(3\alpha f\eta)k_{-4}k_{-1} + k_{-2}C_{Cl^-}^3 k_{-4} \exp(3\alpha f\eta)k_{-3}^2 k_1 C_{H^+}\big]
\end{aligned}
}{
\begin{aligned}
&\big[(k_3 \exp((-1+\alpha)f\eta)k_2 C_{Cl_2}k_{-1} + k_{-3}C_{Cl^-}^2 \exp(\alpha f\eta)k_{-1}k_{-2} + k_{-3}C_{Cl^-}^2 \exp(\alpha f\eta)k_{-2}k_1 C_{H^+}\\
&+k_{-3}C_{Cl^-}k_2 C_{Cl_2}k_{-1} + k_4 \exp(2(-1+\alpha)f\eta)k_2 C_{Cl_2}k_{-1}k_{-2}C_{Cl^-}\\
&+k_4 \exp(2(-1+\alpha)f\eta)k_2 C_{Cl_2}k_{-1}k_3 + k_4 \exp((-1+\alpha)f\eta)k_{-2}C_{Cl^-}k_1 C_{H^+}\\
&+k_4 \exp(2(-1+\alpha)f\eta)k_2 C_{Cl_2}k_{-1} + k_{-4}k_{-1}\exp(2\alpha f\eta)k_{-3}C_{Cl^-}k_1 C_{H^+}\\
&+k_{-4}k_{-1}\exp(f\eta(2\alpha-1))k_3 + k_{-4}k_{-1}\exp(2(-1+\alpha)f\eta)k_3 k_1 C_{H^+})\big(k_2 C_{Cl_2}k_{-1} - k_{-3}C_{Cl^-} - \exp(\alpha f\eta)k_{-1} - k_{-3}C_{Cl^-} - \exp(\alpha f\eta)k_1 C_{H^+}\big)\big]
\end{aligned}
}
\tag{7.49}
$$

Equation 7.50 is the derived equation for the total current density of the Erenburg mechanism.

$$
i_T = \frac{
\begin{aligned}
&2k_{-5}\big[k_1 C_{Cl_2}^2 k_2 k_3 \exp(2(-1+\alpha)f\eta) + k_1 C_{Cl_2}k_{-4}\exp(f\eta(3\alpha-2))k_3 - k_{-1}C_{Cl^-}^2 \exp(2\alpha f\eta)k_{-3}k_2 C_{Cl_2}\\
&-k_{-1}C_{Cl^-}^2 \exp(3\alpha f\eta)k_{-4} + k_3 \exp(2(-1+\alpha)f\eta)k_4 k_2 C_{Cl_2} C_{H^+} - k_{-2}C_{Cl^-} - k_{-2}C_{Cl^-}^2 C_{H^+} + k_{-3}\exp(2\alpha f\eta)k_{-4}\big]
\end{aligned}
}{
\begin{aligned}
&\big[k_5 C_{H^+}^3 + k_{-3}C_{Cl^-}^2 \exp(\alpha f\eta)k_{-2}C_{Cl^-} + k_5 C_{H^+}^2 k_1 C_{Cl_2}\exp((-1+\alpha)f\eta)k_{-2}C_{Cl^-} + k_5 C_{H^+}^2 k_{-1}C_{Cl^-}\exp(f\eta(2\alpha-1))k_4\\
&+k_5 C_{H^+}^3 + k_{-2}C_{Cl^-}k_4 \exp((-1+\alpha)f\eta)k_{-5}C_{Cl_2}k_3 \exp((-1+\alpha)f\eta) + k_{-5}k_{-4}\exp(f\eta(2\alpha-1))k_3\\
&+k_{-5}k_{-4}\exp(2\alpha f\eta)k_{-1}C_{Cl^-} + k_{-5}k_{-4}\exp(\alpha f\eta)k_{-2}C_{Cl^-} + k_{-5}k_{-3}\exp(\alpha f\eta)k_2 C_{Cl_2}k_{-1}C_{Cl^-} - \exp(2\alpha f\eta)k_{-4}\\
&+k_{-5}k_1 C_{Cl_2}^2 \exp((-1+\alpha)f\eta)k_2 + k_{-5}k_1 C_{Cl_2}\exp(f\eta(2\alpha-1))k_{-4} + k_{-5}k_2 C_{Cl_2}k_4 C_{H^+} + k_{-5}k_3 \exp(2(-1+\alpha)f\eta)k_4 C_{H^+}+\\
&+k_{-5}k_{-3}C_{Cl^-}^2 \exp(\alpha f\eta)k_{-2}C_{Cl^-} - C_{H^+}\\
&+k_{-5}k_{-1}C_{Cl^-}\exp(f\eta(2\alpha-1))k_4 C_{H^+} + k_{-5}k_{-2}C_{Cl^-} - C_{H^+} + k_4 \exp((-1+\alpha)f\eta) + k_5 C_{H^+}^2 k_3 \exp(2(-1+\alpha)f\eta)k_4\big]
\end{aligned}
}
\tag{7.50}
$$

Chapter 8

Conclusions

The work presented in this thesis can be divided into two sections. The first part, presented in chapters 2 through 4 deals with the more technological investigation and assessment of different hydrogen - chlorine fuel cell designs. The second part, chapters 5 through 7, has a more fundamental content, examining the kinetic mechanisms of the chlorine reduction reaction on various electrode surfaces in hydrochloric acid.

8.1 Fuel Cell Design Evaluation

Three low temperature fuel cell designs have been evaluated for use as a hydrogen - chlorine fuel cell for production of hydrochloric acid and electric power. The evaluated fuel cell designs consists of *a)* a conventional PEM fuel cell applying a Nafion membrane, *b)* a composite system applying an aqueous HCl electrolyte and Nafion membrane and *c)* a phosphoric acid doped PBI membrane fuel cell operating at intermediate temperatures of 150 - 175 °C. None of the investigated systems were able to demonstrate stable operation under the conditions used in this study. The main factors responsible for the observed cell instability and degradation were identified as water management, materials stability and/or retention of liquid electrolyte. These effects are discussed below.

8.1.1   Water Management

It was found that water management has a critical importance in the fuel cell designs evaluated. Both the Nafion based cell and the PBI based cell showed much higher ohmic resistances when operating on chlorine rather than oxygen. The absence of formation of water in the cell and the continuous production of hygroscopic HCl effectively dries out the Nafion membrane, causing a drastic decrease of the electrolyte conductivity. In the PBI system, the phosphoric acid is forced to liberate water, forming polyphosphoric acid in the process and thus decreasing the electrolyte conductivity. The composite Nafion - liquid electrolyte fuel cell did, as expected, not experience this resistance increase. However, the inclusion of a circulating liquid electrolyte introduced other difficulties such as electrolyte leakage and higher corrosivity.

From the results obtained in this work, it is believed that the drying effect observed cannot be fully alleviated through more sophisticated humidification of the gases. It is most probably necessary to use a proton conductor completely independent of the presence of water.

8.1.2   Materials Stability

The presence of chlorine and produced hydrogen chloride makes the fuel cell environment extremely corrosive. All the fuel cell designs evaluated showed signs of material degradation, especially the Nafion and the composite fuel cell where liquid water was present, were susceptible for high rates of corrosion. It was found that platinum catalyst are not stable in the presence of chlorine saturated aqueous HCl. The platinum is most probably dissolved as hexachloroplatinic acid. It would be advantageous to avoid any liquid water in future designs of these fuel cells to reduce the corrosivity and thus increase the stability of the system.

8.1.3   Fuel Cell Performance

The different designs had quite similar performance. At open circuit, all had voltages very close to the thermodynamical value of formation of aqueous HCl. The polarisation curves also exhibited a linear decrease in voltage at low currents, with no apparent activation controlled part as usually seen in low temperature hydrogen - oxygen fuel cells. This indicates a facile chlorine reduction

reaction which only contributes with a small part of the total voltage loss of the cell and renders highly efficient energy conversion possible.

The factor contributing to most of the voltage decrease is undoubtedly the ohmic resistance in the electrolyte, being much higher than the resistance in corresponding hydrogen-oxygen fuel cells. In this work a threefold increase of cell resistance was measured both in the Nafion and PBI based cells when switching from oxygen to chlorine operation. The nature of the composite fuel cell with a circulating electrolyte inevitably increases the electrolyte thickness and consequently causes a cell resistance increase. The developed mathematical model shows that the electrolyte resistance is responsible for the major part of the losses in this cell. Further discussions of the various fuel cells can be found in Chapters 2 and 3.

The mathematical model of the composite fuel cell further predicted an optimum electrolyte concentration of 6 mol dm^{-3} which at room temperature gave a performance of 0.6 A cm^{-2} at a cell voltage of 0.8 V. It also showed that the HCl concentration inside the gas diffusion electrodes easily reached values of concentrated HCl (12 mol dm^{-3}). It was also found that the high solubility of chlorine in hydrochloric acid minimizes the mass transport related processes in the system. More results are presented in Chapter 4.

8.2 Chlorine Reduction Kinetics

The chlorine electrode consists of two facile reactions. The well known chlorine evolution reaction has a high exchange current density and a low Tafel slope (40 mV dec^{-1}) on several catalytic materials [102], and is one of the most important reactions in todays electrochemical industry. The chlorine reduction reaction (ClRR) also shows good kinetic properties which can be utilised in electrochemical energy conversion devices. However, the knowledge and understanding of this reaction is limited. Some factors influencing this reaction have been investigated in this thesis. It is also worth commenting that, in some cases, studying the chlorine reduction reaction can be less complicated than studying the corresponding evolution reaction and the results can contribute to increasing the understanding of the chlorine evolution reaction.

8.2.1   The ClRR on Platinum

The chlorine reduction reaction on platinum was investigated with emphasis on the effect of oxidation state of the electrode. It was found that the exchange current density decreases linearly with the logarithm of the amount of surface oxide and that a step comprising adsorption of chlorine molecules with a subsequent discharge to a chloride ion and an adsorbed chlorine atom is the rate determining step. Leading to the following mechanism:

$$Cl_{2(aq)} \rightleftharpoons Cl_{2,ad}$$

$$Cl_{2(ad)} + e^- \rightarrow Cl_{ad} + Cl^-_{(aq)}$$

$$Cl_{ad} + e^- \rightleftharpoons Cl^-_{(aq)}$$
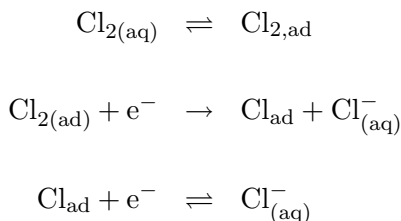
This is further discussed in Chapter 6.

8.2.2   The ClRR on Ruthenium

The chlorine reduction reaction on ruthenium was investigated for effects of oxidation state of the electrode and solution pH. It was found that the activity of the electrode towards chlorine reduction decreases with increasing amounts of oxide on the surface (Chapter 6). Furthermore, the activity of electrooxidised ruthenium towards chlorine reduction is highly dependent on pH, being strongly inhibited in solutions with high H^+ concentrations due to a hydration of the oxide (Chapter 7). The chlorine reduction on electrooxidised ruthenium was found to be adequately described by the following mechanism:

$$S - O + Cl_2 + e^- \rightleftharpoons S - OCl + Cl^-$$

$$S - OH + Cl_2 \rightleftharpoons S - OCl + Cl^- + H^+$$

$$S - OCl + e^- \rightleftharpoons S - O + Cl^-$$

$$S - O + H^+ + e^- \quad \rightleftharpoons \quad S - OH$$
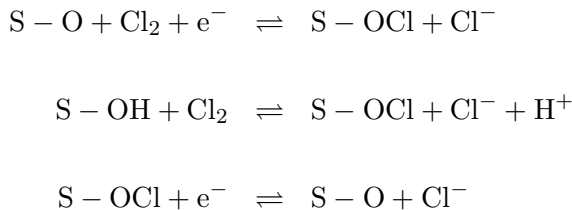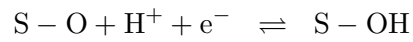
These results show that ruthenium oxides are probably not an ideal choice for chlorine reduction catalysts in fuel cells with an acidic environment. It is possible that addition of other noble metal oxides can increase the catalytic activity such as IrO_2. Further work is needed to investigate these effects.

Chapter 9

Further Work

After working with chlorine fuel cells and chlorine electrochemistry for four years it feels as if I have only scratched the surface of the knowledge and technological challenges within this field. Although I have learned a great deal during these years, it seems that more questions have been raised than answered, as it should be in the field of research. The following suggestions for further work has been divided into two categories; Technological development and more fundamental research.

9.1   Technology Development

The fuel cell designed an tested in this thesis consisted mostly of components and technology developed for oxygen fuel cells and a lot of time was used to adapt these to operation on chlorine. During the fuel cell evaluations, it became clear that the available components had critical shortcomings that need to be handled to achieve a stable fuel cell operation with high performance. A successful operation of a Nafion fuel cell on chlorine would require an extremely good humidification strategy. This would most probably include a very thin membrane and a high humidification of the hydrogen gas and possibly a higher anode pressure to force large amounts of water through the membrane to the cathode where HCl is formed. The large amounts of liquid water together with the formed HCl and chlorine would give a very corrosive environment and it is improbable that it would be possible to achieve any long term stability of this system.

The PBI system also showed problems connected with water management. Since this membrane keeps its conductivity at levels down to 5% relative humidity it is believed that developing a successful humidification management of this fuel cell would be less complicated than for the Nafion system. The absence of liquid water in this system also decreases the material stability problems due to a lower corrosivity. Studying the effects of anode and cathode humidification levels and the effect of adding small amounts of oxygen to the chlorine gas would be beneficial. It would also be interesting to dope the PBI membrane with other acids which are not as susceptible for water removal as phosphoric acid is.

A further development of the composite fuel cell would require careful construction of electrodes both able to retain the liquid electrolyte and provide a large reaction area. The extremely corrosive environment puts stringent requirements on construction materials and catalysts and work should be focused on the development of highly stable noble metal oxide catalysts such as IrO_2.

9.2   Fundamental Research

Much is known about the chlorine evolution reaction on oxide electrodes, but these catalysts are not particularly active towards the corresponding chlorine reduction reaction. Thus, a further investigation of the chlorine reduction reaction on noble metal oxides would be of interest. Single crystal experiments could provide useful information of the nature of various crystalline faces towards the reduction of chlorine and thus a further elucidation of the reaction mechanism. Differential electrochemical mass spectroscopy (DEMS), electrochemical quartz micro balance (EQCM) measurements or spectroscopic techniques like FTIR (Fourier transform infrared spectroscopy) would be useful to study the nature of the adsorbed intermediates involved. The results gained from these investigations could also further increase the knowledge of the chlorine evolution reaction.

The ideal electrolyte for a hydrogen - chlorine fuel cell would be a high temperature proton conductor which is not reliant on any presence of water. This would make operation on totally dry gases possible and would most probably reduce the corrosivity drastically. Research into new high temperature proton conductors which have conduction mechanisms independent of the presence of water would therefore be beneficial. For use in chlorine fuel cells, these would need to be stable in an atmosphere of chlorine and gaseous HCl.

Bibliography

[1] D S Scott. Fossile Fuels: "Running Out" is *not* the problem. *Int. J. Hydrogen Energy*, 30:1–7, 2005.

[2] U Bossel. *Birth of the Fuel Cell 1835-1845*. European Fuel Cell Forum, Oberrohrdorf, Switzerland, 2000.

[3] G Sandstede, E J Cairns, V S Bagotsky, and K Wiesener. *History of low temperature fuel cells, ch. 12 in: Handbook of Fuel Cells, eds. W. Vielstich, A. Lamm, H. A. Gasteiger*, volume 1. Wiley, Chichester, England, 2003.

[4] E Chen. *Fuel Cell Technology Handbook, Ch. 2, Ed: G. Hoogers*. CRC Press LLC, 2003.

[5] Dow / GM press release, 11 November, 2004.

[6] S H Langer and H P Landi. Electrogenerative Hydrogenation. *J. Am. Chem. Soc.*, 85:3043, 1963.

[7] S H Langer and H P Landi. The Nature of Electrogenerative Hydrogenation. *J. Am. Chem. Soc.*, 86:4694, 1964.

[8] S H Langer, S J Pietsch, and G P Sakellaropoulos. Electrogenerative chemical reactors. *Energy*, 4:225–233, 1979.

[9] K Sundmacher and U Hoffmann. Design and operation of a membrane reactor for electrochemical gas purification. *Chem. Eng. Sci.*, 54:2937–2945, 1999.

[10] N Furuya and H Aikawa. Comparative study of oxygen cathodes loaded with Ag and Pt catalysts in chlor-alkali membrane cells. *Electrochim. Acta*, 45:4251–4256, 2000.

[11] C G Vayenas, S Bebelis, I V Yentekakis, and S Neophytides. Non-Faradaic electrochemical modification of catalytic activity: the work function of metal electrodes in solid electrolyte cells. *Solid State Ionics*, 53-56:97–110, 1992.

[12] C G Vayenas, M M Jaksic, S Bebelis, and S Neophytides. *Modern Aspects of Electrochemistry, eds. J.O'M. Bockris, B.E. Conway, R.E. White*, volume 29. Plenum Publishing Corporation, 1996.

[13] C G Vayenas and S Bebelis. Electrochemical promotion of heterogeneous catalysis. *Catal. Today*, 51:581–594, 1999.

[14] F Forster. Über Die Wasserstoff-Chlor-Kette. *Z. Elektrochem.*, 29:64, 1923.

[15] A Schmid. Die Diffusionsgaselektrode. *Helv. Chim. Acta*, 7:370, 1924.

[16] R S Yeo, J McBreen, and S Srinivasan. Electrochemically Regenerative Hydrogen-Chlorine Energy Storage System - Electrode Kinetics and Cell Performance. *J. Electrochem. Soc.*, 126:C379, 1979.

[17] R S Yeo and J McBreen. Transport Properties of Nafion Membranes in Electrochemically Regenerative Hydrogen-Halogen Cells. *J. Electrochem. Soc.*, 126:1682–1687, 1979.

[18] R S Yeo, J McBreen, A C C Tseung, S Srinivasan, and J Mcelroy. An electrochemically regenerative hydrogen-chlorine energy storage system - electrode kinetics and cell performance. *J. Appl. Electrochem.*, 10:393, 1980.

[19] E B Anderson, E J Taylor, G Wilemski, and A Gelb. A high-performance hydrogen/chlorine fuel cell for space power applications. *J. Power Sources*, 47:321–328, 1994.

[20] A Gelb. H_2/Cl_2 Fuel Cells for Power and HCl Production - Chemical Cogeneration. *US Patent*, (5 041 197), 1991.

[21] S M A Shibli and M Noel. Platinum Iridium Bimetal Catalyst-Based Porous Carbon Electrodes for H_2-Cl_2 Fuel Cells. *Int. J. Hydrogen Energy*, 18:141–147, 1993.

[22] D L Maricle. Hydrogen/Chlorine regenerative fuel cell. *US Patent*, (4 128 701), 1978.

[23] E Anderson, E J Taylor, N R K Vilambi, and A Gelb. Preliminary Analysis of Fuel Cell Derived Technologies Applied to Energy Conservation in the Chlor-Alkali Industry. *Separation Science and Technology*, 25:1537, 1990.

[24] D T Chin, R S Yeo, J McBreen, and S Srinivasan. Electrochemically Regenerative Hydrogen-Chlorine Energy Storage System. Study of Mass and Heat Balances. *J. Electrochem. Soc.*, 126:713, 1979.

[25] E Gileadi, S Srinivasan, F J Salazano, C Braun, A Beaufrere, S Gottesfeld, L J Nuttall, and A B Laconti. Electrochemically regenerative hydrogen-chlorine energy storage system for electric utilities. *J. Power Sources*, 2:191–200, 1977.

[26] E Sandnes. Elektrokjemisk karakterisering av elektroder for bruk i H_2-Cl_2 brenselceller. Master's thesis, NTNU,Norwegian University of Science and Technology, 2000.

[27] E Sandnes and M Thomassen. Production of HCl by Fuel Cell Technology. Technical report, Department of Materials Technology, NTNU, 2000.

[28] M Thomassen, B Bøorresen, G Hagen, and R Tunold. Hydrogen Chlorine fuel cell for co-generation of electricity and HCl. *J. Appl. Electrochem.*, 33:9–13, 2003.

[29] M Thomassen, B Børresen, G Hagen, and R Tunold. Chlorine reduction on platinum and ruthenium: the effect of oxide coverage. *Electrochim. Acta*, 50:1157–1167, 2005.

[30] V M M Lobo. *Physical Science Data 41A: Handbook of electrolye solutions*, volume 41A. Elsevier , New York, 1989.

[31] A Damjanovic. *Electrochemistry in transition, from the 20th to the 21st century, O.J Murphy, S. Srinivasan, B.E Conway (eds)*, volume 41A. Elsevier , New York, 1989.

[32] S Gottesfeld and T A Zawodzinski. *Advances in Electrochemical Science and Engineering, ed. R.C Alkire*, volume 5. Wiley, Weinheim, 1997.

[33] K Ledjeff, F Mahlendorf, V Peinecke, and A Heinzel. Development of Electrode/Membrane Units for the Reversible Solid Polymer Fuel Cell (RSPFC). *Electrochim. Acta*, 40:315–319, 1995.

[34] F Seland, T Berning, B Børresen, and R Tunold. Improving the performance of high temperature PEM fuel cells based on PBI electrolyte. *Submitted to J. Power Sources*, -:–, 2005.

[35] T Mennola, M Mikkola, M Noponen, T Hottinen, and P Lund. Measurement of ohmic voltage losses in individual cells of a PEMFC stack. *J. of Power Sources*, 112:261–272, 2002.

[36] C Lagergren, G Lindbergh, and D Simonsson. Investigation of porous electrodes by current interruption - Application to molten-carbonate fuel cell cathodes. *J. Electrochem. Soc.*, 142:231–234, 1995.

[37] G Aylward and T Findlay. *SI Chemical Data*. John Wiley & Sons, New York, 3 edition, 1994.

[38] T A Zawodzinski, C Derouin, S RAdzinski, R J Sherman, V T Smith, T E Springer, and S Gottesfeld. Water-Uptake by and transport through Nafion(R) 117 membranes. *J. Electrochem. Soc.*, 140:1041–1047, 1993.

[39] Y L Ma, J S Wainright, M H Litt, and R F Savinell. Conductivity of PBI Membranes for High-Temperature Polymer Electrolyte Fuel Cells. *J. Electrochem. Soc.*, 151:A8–A16, 2004.

[40] J Cho, J Blackwell, S N Chvakun, M Litt, and Y wang. Structure of a Poly(2,5-benzimidazole)/Phosphoric Acid Complex. *J. Polymer Sci. Part B*, 42:2576–2585, 2004.

[41] B Xing and O Savadogo. The effect of acid doping on the conductivity of polybenzimidazole (PBI). *J. New Mat. Electrochem. Systems*, 2:95–101, 1999.

[42] J S Wainright, J T Wang, D Weng, R F Savinell, and M Litt. Acid-Doped Polybenzimidazoles: A New Polymer Electrolyte. *J. Electrochem. Soc.*, 142:L121, 1995.

[43] R C Weast. *Handbook of Chemistry and Physics 57th edition, ed. R. C. Weast* . CRC Press, Ohio, 1976.

[44] J H Jo and S C Yi. A computational simulation of an alkaline fuel cell. *J. Power Sources*, 84:87–106, 1999.

[45] J H Jo, S K Moon, and S C Yi. Simulation of influences of layer thicknesses in an alkaline fuel cell. *J. Appl. Electrochem.*, 30:1023–1031, 2000.

[46] D M Bernadi and M W Verbrugge. Mathematical Model of a Gas-Diffusion Electrode Bonded to a Polymer Electrolyte. *Aiche J.*, 37:1151–1163, 1991.

[47] D M Bernadi and M W Verbrugge. A Mathematical Model of the Solid Polymer Electrolyte Fuel Cell. *J. Electrochem. Soc.*, 139:2477–2491, 1992.

[48] T Berning and N Djulali. A 3D, multiphase, multicomponent model of the cathode and anode of a PEM fuel cell. *J. Electrochem. Soc.*, 150:A1589–A1598, 2003.

[49] T Berning and N Djulali. Three-dimensional computational analysis of transport phenomena in a PEM fuel cell - a parametric study. *J. Power Sources*, 124:440–452, 2003.

[50] T Berning, D M Lu, and N Djulali. Three-dimensional computational analysis of transport phenomena in a PEM fuel cell . *J. Power Sources*, 106:284–294, 2002.

[51] M Ceraolo, C Miulli, and A Pozio. Modelling static and dynamic behaviour of proton exchange membrane fuel cells on the basis of electrochemical description. *J. Power Sources*, 113:131–144, 2003.

[52] P T Nguyen, T Berning, and N Djilali. Computational model of a PEM fuel cell with serpentine gas flow channels. *J. Power Sources*, 130:149–157, 2004.

[53] T E Springer, T A Zawodzinski, M S Wilson, and S Gottesfeld. Characterization of polymer electrolyte fuel cells using AC impedance spectroscopy. *J. Electrochem. Soc.*, 143:587–599, 1996.

[54] T E Springer, M S Wilson, and S Gottesfeld. Modeling and Experimental Diagnostics in Polymer Electrolyte Fuel Cells. *J. Electrochem. Soc.*, 140:3513–3526, 1993.

[55] T E Springer, T A Zawodzinski, and S Gottesfeld. Polymer Electrolyte Fuel-Cell Model. *J. Electrochem. Soc.*, 138:2334–2342, 1991.

[56] J Newman and K E Thomas-Alyea. *Electrochemical Systems*. John Wiley & Sons, Hoboken, New Jersey, 2004.

[57] K J Vetter. *Chlorine solubilities in IUPAC solubility data series ed. A S Kertes and J W Lorimer*, volume 12. Pergamon press , Oxford, 1983.

[58] R H Perry, D W Green, and J O Maloney. *Perry's Chemical Engineers' Handbook*, volume 7. McGraw Hill , New York, 1997.

[59] Q F Li, G Xiao, H A Hjuler, R W Berg, and N J Bjerrum. Limiting Current of Oxygen Reduction on Gas Diffusion Electrodes for Phosphoric Acid Fuel Cells. *J. Electrochem. Soc.*, 141:3114–3119, 1994.

[60] A Tang and O C Sandall. Diffusion Coefficient of Chlorine in Water at 25-60 degrees C. *J. Chem. Eng. Data*, 30:189–191, 1985.

[61] K Lasch, G Hayn, L Jorissen, J Garche, and O Besenhardt. Mixed conducting catalyst support materials for the direct methanol fuel cell. *J. Power Sources*, 105:305–310, 2002.

[62] R Halseid, P J S Vie, and R Tunold. Influence of Ammonium on Conductivity and Water Content of Nafion 117 Membranes. *J. Electrochem. Soc.*, 151:A381–A388, 2004.

[63] L I Krishtalik. Kinetics and mechanism of anodic chlorine and oxygen evolution reactions on transition metal oxide electrodes. *Electrochim. Acta*, 26:329–337, 1981.

[64] S Trasatti and G Lodi. *Electrodes of conductive metal oxides part B, ed. S. Trasatti*. Elsevier, Amsterdam, 1981.

[65] T Kenjo. Influence of the Electrolyte Concentration on the Polarization Characteristics in PTFE-Bonded Raney-Nickel Hydrogen Electrodes. *J. Electrochem. Soc.*, 133:2051–2058, 1986.

[66] A Damjanovic and J O Bockris. The rate constants for oxygen dissolution on bare and oxide-covered platinum. *Electrochim. Acta*, 11:376–377, 1966.

[67] K J Vetter. *Electrochemical Kinetics: Theoretical and Experimental aspects*. Academic Press, New York, 1967.

[68] J O'M Bockris and A K N Reddy. *Modern Electrochemistry*, volume 2. Plenum, New York, 1970.

[69] T Erdey-Gruz. *Kinetics of electrode processes*. Adam Hilger Ltd, London, 1972.

[70] J Tafel. Über Die Polarisation bei Katodischer Wasserstoffentwicklung. *Z. Physik. Chem.*, 50A:641, 1905.

[71] J A V Butler. Studies in heterogeneous equilibria. Part II. The kinetic interpretation of the nernst theory of electromotive force. *Trans. Faraday Soc.*, 19:729, 1924.

[72] T Erdey-Gruz and M Volmer. Zur Theorie der Wasserstoffüberspannung. *Z. Physik. Chem.*, 150A:203, 1930.

[73] R A Marcus. Theory of Oxidation-Reduction Reactions Involving Electron Transfer. 1. *J. Chem. Phys.*, 24:966–978, 1956.

[74] V G Levich. *Advances in Electrochemistry and Electrochemical Engineering*, volume 4. 1966.

[75] H Gerischer. *Advances in Electrochemistry and Electrochemical Engineering*, volume 1. Wiley, New York, 1961.

[76] R Parsons. Electrochemical Nomenclature. *Pure Appl. Chem.*, 34:499–516, 1974.

[77] R Parsons. Electrode Reaction Orders, Transfer Coefficients and Rate Constants. Amplification of Definitions and Recommendations for Publication of Parameters. *Electrochim. Acta*, 26:1867–1874, 1981.

[78] A J Bard and L R Faulkner. *Electrochemical Methods*. John Wiley & Sons, New York, 2 edition, 2001.

[79] F T Chang and H Wick. Untersuchung über die Halogenüberspannung. *Z. Phys. Chem.*, 172:448, 1935.

[80] A Frumkin and G Tedoradze. Der Mechanismus der Ionisierung von molekularem Chlor an einer Platinelektrode. *Z. Elektrochem.*, 62:251–256, 1958.

[81] T Dickinson, R Greef, and L Wynne-Jones. The kinetics of the chlorine electrode reaction at a platinum electrode. *Electrochim. Acta*, 14:467–489, 1969.

[82] J A Harrison I R Burrows, J H Entwisle. The mechanism of oxidation of Cl^- on platinum and RuO_2/TiO_2 electrodes, and the reduction of Cl_2 on platinum. *Electrochim. Acta*, 14:467–489, 1969.

[83] L Müller and B Kaiser. Mechanism of Cathodic Chlorine Reduction at Platinum Electrodes. *Z. Phys. Chem.*, 77:1011, 1980.

[84] F B Li, A R Hillman, S D Lubetkin, and D J Roberts. Electrochemical Quartz Crystal Microbalance Studies of Potentiodynamic Electrolysis of

Aqueous Chloride Solution - Surface Processes and Evolution of H_2 and Cl_2 Gas Bubbles. *J. Electroanal. Chem.*, 335:345, 1992.

[85] S Trasatti. Electrocatalysis: understanding the success of DSA. *Electrochim. Acta*, 45:2377–2385, 2000.

[86] L Tomcsanyi, A De Battisti, G Hirschberg, K Varga, and J Liszi. The study of the electrooxidation of chloride at RuO_2/TiO_2 electrode using CV and radiotracer techniques and evaluating by electrochemical kinetic simulation methods. *Electrochim. Acta*, 44:2463–2472, 1999.

[87] F B Li, A R Hillman, and S D Lubetkin. A new approach to the mechanism of chlorine evolution: Separate examination of the kinetic steps using ac impedance on a rotating thin ring electrode. *Electrochim. Acta*, 37:2715–2723, 1992.

[88] Tadeusz Hepel, Fred H Pollak, and William E O'Grady. Chlorine evolution and reduction processes at oriented single crystal RuO_2 electrodes. *J. Electrochem. Soc.*, 133:69–75, 1986.

[89] J L Fernandèz, M R Gennero de Chialvo, and A C Chialvo. Analysis of the Volmer-Krishtalik mechanism for the chlorine electrode reaction. *Electrchemistry Communications*, 2:630–635, 2000.

[90] J L Fernandèz, M R Gennero de Chialvo, and A C Chialvo. Kinetic study of the chlorine electrode reaction on Ti/RuO_2 through the polarisation resistance Part I: experimental results and analysis of the pH effects. *Electrochim. Acta*, 47:1129–1136, 2002.

[91] J L Fernandèz, M R Gennero de Chialvo, and A C Chialvo. Kinetic study of the chlorine electrode reaction on Ti/RuO_2 through the polarisation resistance Part II: mechanistic analysis. *Electrochim. Acta*, 47:1137–1144, 2002.

[92] J L Fernandèz, M R Gennero de Chialvo, and A C Chialvo. Kinetic study of the chlorine electrode reaction on Ti/RuO_2 through the polarisation resistance Part III: proposal of a reaction mechanism. *Electrochim. Acta*, 47:1137–1144, 2002.

[93] S G Roscoe and B E Conway. State of Surface Oxide Films at Pt Anodes and Volcano Behaviour in Electrocatalysis for Anodic Cl_2 Evolution. *J. Electroanal. Chem.*, 224:163–188, 1987.

[94] L D Burke. *Electrodes of conductive metal oxides part A, ed. S. Trasatti.* Elsevier, Amsterdam, 1980.

[95] N Kameyma, H Yamamoto, and S Oko. *Proc. Imp. Acad.*, 3:41, 1927.

[96] D Pletcher, R Greef, R Peat, L M Peter, and J Robinson. *Instrumental methods in electrochemistry.* Horwood publishing limited, West Sussex, UK, 2001.

[97] V Vesovic, N Anastasijevic, and R R Adzic. Rotating-disk electrode a reexamination of some kinetic criteria with a special reference to oxygen reduction. *J. Electroanal. Chem.*, 218:53–63, 1987.

[98] S Trasatti and G Lodi. *Electrodes of conductive metal oxides part A, ed. S. Trasatti.* Elsevier, Amsterdam, 1981.

[99] H Angerstein-Kozlowska, B E Conway, and W B A Sharp. Real Condition of Electrochemically Oxidized Platinum Surfaces. 1. Resolution of Component Processes. *J. Electroanal. Chem.*, 43:9, 1973.

[100] B E Conway and S Gottesfeld. Real Condition of Oxidized Platinum Electrodes. 2. Resolution of Reversible and Irreversible Processes by Optical and Impedance Studies. *J. Chem. Soc. Faraday Trans. I*, 69:1090, 1973.

[101] B V Tilak, B E Conway, and H Angerstein-Kozlowska. Real Condition of Oxidized Pt Electrodes. 3. Kinetic Theory of Formation and Reduction of Surface Oxides. *J. Electroanal. Chem.*, 48:1–23, 1973.

[102] S Trasatti. Progress in the understanding of the mechanism of chlorine evolution at oxide electrodes. *Electrochim. Acta*, 32(3):369–382, 1987.

[103] R G Erenburg, L I Krishtalik, and V I Bystrov. Mechanism of Evolution and Ionization of Chlorine on a Ruthenium Oxide Electrode. *Elektrokhimiya*, 8:1740, 1972.

[104] R G Erenburg, L I Krishtalik, and I P Yaroshevskaya. Mechanism of chlorine evolution at a ruthenium - titanium oxide electrode. *Elektrokhimiya*, 11(7):1068–1072, 1975.

[105] R G Erenburg, L I Krishtalik, and I P Yaroshevskaya. Kinetics of chlorine evolution and ionization at ruthenium oxide and ruthenium - titanium oxide electrodes. *Elektrokhimiya*, 11(7):1072–1074, 1975.

[106] R G Erenburg, L I Krishtalik, and I P Yaroshevskaya. Liberation and ionization of chlorine on ruthenium - titanium oxide electrodes at increased current densities. *Elektrokhimiya*, 11(7):1236–1239, 1975.

[107] R G Erenburg. Mechanism of the chlorine reaction of ruthenium - titanium oxide electrodes. *Elektrokhimiya*, 20(12):1602–1607, 1984.

[108] S Trasatti. Surface-chemistry of oxides and electrocatalysis. *Croatica Chemica Acta*, 63:313–329, 1990.

[109] D Galizzio, F Tantardini, and S Trasatti. Ruthenium dioxide - new electrode material 1. Behaviour in acid solutions of inert electrolytes. *J. of Appl. Electrochem.*, 4:57–67, 1974.

[110] Hadzi-Jordanov S, H A Kozlowska, M Vukovic, and B E Conway. Reversibility and growth-behaviour of surface oxide films at ruthenium electrodes. *J. Electrochem. Soc.*, 125:1471–1480, 1979.

[111] A T Kuhn and C J Mortimer. Kinetics of chlorine evoultion and reduction on titanium-supported metal oxides especially RuO_2. *J. Electrochem. Soc.*, 120:231–234, 1973.

[112] D V Kokoulina and L V Bunakova. Oxygen evolution at the oxide electrodes RuO_2 and $RuO_2 + TiO_2$ in chloride solutions. *J. Electroanal. Chem.*, 164:377–383, 1984.

[113] N Y Bune, E N Perminova, and V V Losev. Open-circuit oxygen evolution at titanium ruthenium oxide anodes in chloride solutions. *Soviet Electrochemistry*, 22:525–528, 1986.

[114] T Arikawa, Y Murakami, and Y Takasu. Simultaneous determination of chlorine and oxygen evolving at RuO_2/Ti and RuO_2-TiO_2/Ti anodes by differential electrochemical mass spectroscopy. *Soviet Electrochemistry*, 22:525–528, 1986.

[115] L K Koopal. Mineral hydroxides: from homogeneous to heterogeneous modelling. *Electrochim. Acta*, 41:2293–2306, 1996.

[116] D A Denton, J A Harrison, and R I Knowles. Chlorine evolution and reduction on RuO_2/TiO_2 electrodes. *Electrochim. Acta*, 24:521–527, 1979.

[117] D Miousse and A Lasia. Hydrogen Evolution Reaction on RuO_2 Electrodes in Alkaline Solutions. *J. New. Mat. Electrochem. Systems*, 2:71–78, 1999.

Appendix A

Matlab files

Here are example transcripts of the two main Matlab script and function m.files used for the nonlinear curve-fitting of the developed rate equations in chapters 6 and 7.

A.1 Script file

This is the script file used for importing the experimental data into Matlab and calling the *lsqnonlin* function. `clear all; %warning off;`

```
data = csvread('Cl2_reduction.csv'); %importing data from a comma
separated file (.csv)

eta = data(:,1)'/1000; %extracting the overpotential values from the
data file and converting it to a vector

I = data(:,2)'; %extracting the current values from the data file and
converting it to a vector

opt = optimset('Diagnostics','on','Display','iter','LargeScale','on',
'maxFunEvals',10000','TolFun',1e-15,'TolX',1e-15,'maxIter',500);
```

```
x0=[0.001;1;0.001;0.001;1;1;0.001;1;0.001;1;0.5]; %inital guess of
rate constants and alpha
```

```
opt = optimset('Diagnostics','on','Display','final','LargeScale','on',
'maxFunEvals',750000,'TolFun',1e-13,'TolX',1e-13,'maxIter',50000);
```

```
[x1]=lsqcurvefit('Volmer_Krishtalik_weight',x0,eta,I,[0;0;0;0;0;0;0;0;0;0;0
,[Inf;Inf;Inf;Inf;Inf;Inf;Inf;Inf;Inf;Inf;1],opt);
```

```
eta2=[0:-0.01:-1.2];
```

```
I_new = Volmer_Krishtalik(x1,eta2);
```

```
semilogx(I,eta,'+r',I_new,eta2,'b');
```

A.2 Function file

This is the function file called by the *lsqnonlin* function. It contains the appropriate rate equations and the weighing of the fitting values.

```
function diff_weighted = Volmer_Krishtalik(x,eta,I)
% This function is called by lsqnonlin.
% x is a vector which contains the coefficients of the
% equation.
f=96485/(8.314*298); C_Cl2=0.065; C_Cl=1; C_H=0.0243;
k_1=x(1);
k_2=x(2);
k_3=x(3);
k_4=x(4);
k_5=x(5);
k_1_a=x(6);
k_2_a=x(7);
k_3_a=x(8);
k_4_a=x(9);
k_5_a=x(10);
alpha=x(11);
fit = [Insert rate equation here]
diff = fit - I;
weight = [ones(1,length(I))]./I; % Vector of weights for the error vector
diff_weighted = diff.*weight;
```